Physico-chemical Characterization and Self-assembly of Poly(2-ethyl-2-oxazoline)s in Aqueous Solutions

by

Pınar Tatar Güner

A Thesis Submitted to the
Graduate School of Sciences Engineering
in Partial Fulfillment of the Requirements for
the Degree of

Doctorate of Science
in
Material Science and Engineering

Koc University

August 2013

Koc University

Graduate School of Sciences and Engineering

This is to certify that I have examined this copy of a PhD thesis by

Pınar Tatar Güner

and have found that it is complete and satisfactory in all respects,
and that any and all revisions required by the final
examining committee have been made.

Committee Members:

_____

Adem Levent Demirel, Ph.D. (Advisor)

_____

Mehmet Sayar, Ph.D.

_____

Uğur Ünal, Ph.D.

_____

Yusuf Yağcı, Ph.D.

_____

Canan Atılgan, Ph.D.

Date: _____

ABSTRACT

Poly(2-ethyl-2-oxazoline) (PEOX) is a non-toxic, biocompatible and thermoresponsive polymer which is soluble in water at room temperature. Aqueous solutions of PEOX exhibit lower critical solution behavior and phase separate macroscopically above a cloud point temperature (T_c) which depends on several factors including polymer concentration, polymer molecular weight, ionic strength and the presence of organic additives. Despite the common use of PEOX in biomedical applications, the physico-chemical factors affecting its thermoresponsive behavior and self-assembly in aqueous solutions are yet to be understood.

In this thesis, we report on the effect of a series of sodium salts on T_c of aqueous PEOX solutions and the self-assembly of PEOX into crystalline nanofibers both above and below T_c. For 1 mg/mL aqueous PEOX-500K (molecular weight of 500,000 g/mol) solutions T_c was ~61 °C in water. The effects of 11 anions were investigated and T_c was controlled between 20 °C and 70 °C by salt addition. Kosmotropic anions decreased T_c linearly while chaotropic anions increased T_c non-linearly with salt concentration. Our results indicate that the dominant mechanism was the dehydration of PEOX for divalent kosmotropic anions (CO_3^{2-}, SO_4^{2-}, $S_2O_3^{2-}$) and direct binding for chaotropic anions (NO_3^-, I^-, ClO_4^-, SCN^-). For the remaining monovalent kosmotropic anions ($H_2PO_4^-$, F^-, Cl^-, Br^-), a combination of dehydration and surface tension mechanisms was in effect.

When aqueous PEOX solutions were kept above T_c for long times (of the order of days to weeks), PEOX self-assembled into crystalline nanofibers which

remained stable even below T_c. The addition of salts enhanced the self-assembly process. The self-assembled nanofibers were characterized by microscopic techniques, differential scanning calorimetry and X-ray diffraction. The melting temperature and the lattice constants of the crystalline PEOX nanofibers were consistent with those of other poly(2-alkyl-2-oxazoline)s (PAOX) which confirmed the successful crystallization of PEOX for the first time. A model was proposed for the crystal structure and the role of inter-molecular interactions in the self-assembly process was discussed. The self-assembly of PEOX into crystalline nanofibers was also observed below T_c, but the rate of self-assembly was even slower. The growth of aggregates as determined by dynamic light scattering indicated a nucleation and growth mechanism.

The thermoresponsive behavior of thin PEOX coatings on solid substrates was also demonstrated. Thermoresponsive PEOX coatings were given antimicrobial functionality by addition of silver nano-particles. The durability of the PEOX coatings against water adsorption was improved by sol-gel technique using tetra ethyl ortho silicate (TEOS).

ÖZET

Poli(2-etil-2-oksazolin)'in (PEOX), zehirli olmayan, biyo-uyumlu, oda sıcaklığında suda çözünebilen ve ısıl değişikliklere tepki verebilen bir polimerdir. PEOX sulu çözeltilerde alt kritik çözelti davranışı gösterir. Makroskopik faz ayrımının görüldüğü, bulutlanma sıcaklığı (T_c), polimer konsantrasyonu, polimer molekül ağırlığı, çözeltinin iyonik kuvveti ve organik katkı maddelerinin varlığı gibi birçok faktöre bağlıdır. PEOX biyomedikal uygulamalarda yaygın olarak kullanılmasına rağmen, su içindeki ısısal davranışı ve kendi kendine yapılanmasına etki eden fizikokimyasal faktörler henüz anlaşılmamıştır.

Bu tezde, seri sodium tuzlarının PEOX sulu çözeltisinin bulutlanma sıcaklığına etkisi ve PEOX'un bulutlanma sıcaklığı üstünde ve altında kendi kendine yapılanarak kristal nanofiber oluşturması sunuldu. 500,000 g/mol molekül ağırlığındaki PEOX kullanılarak hazırlanmış sulu çözeltinin T_c'si 61 °C'dir. 11 anyonun bulutlanma sıcaklığı üzerine etkisi incelenerek tuz ilavesi ile bu sıcaklığın 20°C ile 70°C arasında değiştirilebileceği bulundu. Kozmotrop anyonların konsantrasyon artışı T_c'yi doğrusal olarak azaltırken, kaotrop anyon konsantrasyonu artışının T_c'yi doğrusal olmayan bir şekilde değiştirdiği bulundu. Sonuçlarımız bu etkilere neden olan baskın mekanizmaların; iki değerlikli kozmotrop anyonlar (CO_3^{2-}, SO_4^{2-}, $S_2O_3^{2-}$) için PEOX'un dehidrasyonu ve kaotrop anyonlar (NO_3^-, I^-, ClO_4^-, SCN^-) için polimer üzerine iyonun bağlanması olduğunu gösterdi. Seride kalan bir değerlikli kosmotrop anyonlar ($H_2PO_4^-$, F^-, Cl^-, Br^-) için hem dehidrasyon hem de yüzey gerilimi mekanizmalarının etkili olduğu bulundu.

PEOX sulu çözeltileri bulutlanma sıcaklığının üzerinde uzun süre (haftalarca) bekletildiğinde, kendi kendine yapılanma ile kristal yapıda nanofiberler oluştu ve çözelti soğutulduğunda bile kararlı kaldı. Tuz ilavesi kendi kendine yapılanma sürecini hızlandırdı. Kendiliğinden yapılanan nanofiberler, mikroskobik teknikler, fark taramalı kalorimetre ve x-ışını saçılımı ölçümleri ile tanımlandı. PEOX nanofiberlerin erime sıcaklığı ve kristal örgü sabitlerinin diğer poli(2-alkil-2-oksazolin) (PAOX)'ler ile bağıntılı olması, PEOX'un ilk kez başarılı bir şekilde su içinde kristallendirildiğini doğrular niteliktedir. Kristal yapının aydınlatılması için bir model önerilerek kendi kendine yapılanma sürecindeki moleküller arası etkileşimler tartışıldı. PEOX sulu çözeltilerinin T_c altında da kendi kendine yapılanarak kristal nanofiberler oluşturduğu ancak bu sürecin T_c üzerinde yapılanmaya oranla daha yavaş olduğu bulundu. Dinamik ışık saçılımı (DLS) ile agregasyon kinetiği üzerine yapılan çalışmalar, kendiliğinden yapılanmanın çekirdeklenme ve büyüme şeklinde olduğunu gösterdi.

Bir katı yüzey üzerindeki PEOX filmlerinin de ısıya duyarlı davranış gösterdiği belirlendi. Bu filmlere gümüş nano-parçacıkları katkılanarak antibakteriyel özellik kazandırıldı. PEOX filmlerin su adsorpsiyonuna karşı kararlılığı tetraetil ortosilikat (TEOS) kullanılarak sol-jel yöntemi ile üretilmiş silikat ağı katkılanarak arttırıldı.

ACKNOWLEDGEMENTS

This thesis would not have been possible without the support of many great people. It is my pleasure to acknowledge and thank those who have contributed to my graduate studies in so many ways.

My deepest gratitude goes to my advisor, Prof. Dr. Adem Levent Demirel. Whenever I need, he always there for me with valuable suggestions; but at the same time, he gave me the freedom to make mistakes, learn from them and explore on my own. I have learned a great deal from him about scientific research but more importantly he taught me to question my results, and identify each before taking another step to achieve a true understanding of my research. I have deeply impressed from the courses “Thermo-mechanical properties of materials” and “Surface and interface properties of materials” which I took from him. His patience and also criticism gave me confidence to overcome difficulties in many tough situations and brought further motivation and ambition to my studies during the preparation of this thesis. I would like to thank him also for taking time to teach me how to present my work in the most understandable way. I am grateful to him for both professional and personal support in life in general.

I would like to express my special thanks to Dr. Annamaria Miko for valuable contribution to my studies. She was always generous to share her knowledge about many instruments and also very instructive in our discussions about crystallinity of polymers. She played a critical role to keep me focused in this tough journey and has always been supportive and helpful to overcome challenges I

faced. I deeply appreciate her belief in me and for being such a good and thoughtful friend.

I would like to thank Dr. Helmut Schlaad and Dr. Richard Hoogenboom for their close collaboration with us. They synthesized some of the polyoxazolines which I worked with during my studies.

I would like to express my gratitude to the Prof. Dr. Yusuf Yağcı. His support and comments were critical at several stages of my education. I am grateful to him for giving me the opportunity to investigate the morphologies of his specially synthesized polymers and trusting my characterizations. I am also thankful to him for sharing his experience and giving helpful advices on life.

I am indebted to my committee members, Dr. Özgür Birer and Dr. Mehmet Sayar, for helpful discussions. Dr. Birer's helpfulness and constructive criticism always made me feel welcome in his office to discuss my ideas. I feel lucky to take "Applied Spectroscopy" course from him because I have learned many things about the spectroscopy and characterization. Dr. Sayar's attitude always created a supportive environment and I am thankful to him for sharing his ideas and suggestions with me. Moreover, I have learned fundamentals of simulations and calculations about the self-assembly of polymers and filled my gaps in knowledge with intermolecular interactions in the "Intermolecular and Surface Forces" course which was given by Dr. Sayar. These two courses helped me to understand life and matter.

I would like to thank all faculty and graduate students of the Department of Chemistry for providing such a friendly environment which made me enjoy my time out of the lab. I feel lucky to be forced to give seminars each year and criticized by the staff of Chemistry Department. I appreciate them all for their suggestions and helpful discussions.

In characterization parts, I have also benefited from the resources of KUYTAM. Dr. Ugur Ünal, Dr. Birer, Dr. Barış Yağcı and Cansu Yıldırım helped me much throughout the operation of several devices.

I greatly value my past and current fellow lab members' help and friendship. Particularly, I would like to thank Dr. Sanjay Latthe for sharing his expertise in hybrid inorganic-organic systems and sol-gel chemistry and being helpful whenever I faced a technical problem with contact angle instrument. I would like to acknowledge Merve Kocakuşakoğulları for valuable contributions to my project and sincere friendship.

I would like to thank to my thesis jury members Dr. Yusuf Yağcı, Dr. Canan Atılgan, Dr. Uğur Ünal and Dr. Mehmet Sayar for having accepted to evaluate this work.

My husband, Mr. Erdin Güner, has been a constant source of love, strength and support. I am grateful to his efforts to help me to believe in myself and cultivate self-discipline to reach my goals. His continuous interest and support for my education motivated me to do my best in all those years. I am thankful to him for always holding our family together, making me feel the strength of love and being

with me through all the challenges I faced. You always knew how to put a smile on your wife's face.

I am fortunate to have sister, Mrs. Alev Tatar. Thank you all for your continuous support and caring for your little sister ☺. It is great to feel that you are always there for me whenever I need you. I am thankful to you for your unconditional support and love.

And finally, I would like to express special thanks to my parents Mr Yavuz Tatar and Mrs Zeynep Tatar for even being far away they were always morally, mentally and spiritually with me, supporting and encouraging every step of this long trip. I would like to apologize to my family for all the years of neglect, and time lost, while I explored intellectual curiosities. In the following years I hope to demonstrate that the sacrifices over these many years were not in vain.

This work is funded by Turkish Scientific and Technical Research Council (TUBITAK-109M542), and for this I am greatful. Also I would like to present my thanks to our industrial partner Arçelik A.Ş in this project for their bacterial measurements.

TABLE OF CONTENTS

LIST OF TABLES

LIST OF FIGURES

LIST OF EQUATIONS

NOMENCLATURE

AFM: Atomic Force Microscopy or Atomic Force Microscope

ATR: Attenuated total reflectance

CA: Contact Angle

CCD: Charge-coupled device

DLS: Dynamic Light Scattering

DSC: Differencial Scanning Calorimetry

E. coli: Escherichia coli

FT-IR: Fourier Transform Infrared Spectroscopy

LCST: Lower Critical Solution Temperature

NaAc: Sodium acetate

PAOX: Poly(2-alkyl-2-oxazoline)

PBOX: Poly(2-butyl-2-oxazoline)

PEOX: Poly(2-ethyl-2-oxazoline)

PIPOX: Poly(2-isopropyl-2-oxazoline)

PMOX: Poly(2-methyl-2-oxazoline)

PNIPAM: Poly(N-isopropylacrylamide)

PHOX: Poly(2-hexyl-2-oxazoline)

PPOX: Poly(2-propyl-2-oxazoline)

S. aureus: Staphylococcus aureus

SEM: Scanning Electron Microscopy or Scanning Electron Microscope

Tc: Cloud point temperature (or critical temperature)

TEOS: Tetra ethyl ortho silicate (or tetraethoxy silane)

UCST: Upper Critical Solution Temperature

UV-Vis: Ultra Violet – Visible

CHAPTER 1: INTRODUCTION

Stimuli-responsive polymers have the unique property of undergoing a reversible phase transition. This property has attracted much interest for their application in variety of applications such as adhesives, inks, coatings, and compatibilizing agents in drug delivery systems [1–5]. Thermoresponsive poly(2-alkyl-2-oxazoline)s (PAOX) form an important class of tertiary polyamides and their physical properties, such as crystallinity and solubility, depend significantly on the alkyl side chain length. Aqueous solutions of PAOX having –ethyl, -propyl, and –isopropyl alkyl side chains exhibit lower critical solution behavior in water. Hydrogen bonds between PAOX carbonyl groups and water molecules facilitate the dissolution. These interactions are disrupted by increasing temperature which results in macroscopic phase separation at a specific temperature called cloud point temperature (T_c). The mechanism leading to thermoresponsive behavior has been investigated for some PAOX and mostly acrylamide based polymers and was related to the transition in the chain conformation from coil to globule as a result of dehydration [6–10].

Poly(2-ethyl-2-oxazoline) (PEOX) is a member of PAOX family and nonionic, thermoresponsive, and biocompatible synthetic polymer, which is soluble in water and many organic solvents at room temperature [11]. PEOX has lower critical solution temperature (LCST) in water around 61 °C depending on the molecular weight [11]. Once the aqueous solution properties are better understood, it will find more extensive and valuable applications. This work investigated the aqueous solution behavior of PEOX, by changing polymer concentration, molecular weight,

and aqueous environment around the polymer with addition of different salts and varying their concentrations. Influences of these factors on T_c of the solutions were probed by dynamic light scattering (DLS) measurements. Obtained results were compared by most widely studied thermoresponsive polymer poly(N-isopropyl acrylamide) (PNIPAM).

Macroscopic phase transition at T_c is reversible with exceptions. It was previously reported that annealing of dilute aqueous solutions of poly(2-isopropyl-2-oxazoline) (PIPOX) above T_c caused irreversible formation of micron-sized aggregates [12], [13]. These aggregates are crystalline and in the form of fibers. Although thermoresponsive behavior and similar interactions are present in aqueous PEOX solutions, irreversible aggregation was not reported previously. As a part of this thesis, we have studied the formation of water insoluble crystalline aggregates of PEOX in aqueous solutions when they are kept above T_c. In addition, influence of salting-in and salting-out salts on irreversible aggregation of PEOX was explored. Thermal behavior and crystalline structure of the obtained aggregates were further investigated by differential scanning calorimetry (DSC) and x-ray diffraction (XRD) techniques. The self assembly of PIPOX above T_c was previously explained by enhancement of hydrophobic interactions in polymer rich regions, dipolar interactions and backbone solvation. Below T_c there is no macroscopic phase separation to form polymer rich regions to stimulate self assembly but irreversible aggregation of PEOX from aqueous solutions was also observed. Self assembly kinetics was followed by DLS measurements. Effect of PEOX concentration, and molecular weight on the rate of aggregation was thoroughly investigated. Aggregate morphologies were determined by atomic force

microscopy (AFM). Furthermore, thermal and structural properties of the aggregates were explored by DSC and XRD measurements.

There are very few studies in literature about the crystallinity of PAOXs in bulk [14–16]. According to the first study on crystallinity of series of PAOX carrying different linear alkyl groups on their side chain, only PEOX was found to be amorphous [14]. In more recent studies it was demonstrated that crystallization is possible only for PAOX carrying -butyl or longer alkyl groups on their side chain [15], [16]. We have studied the isothermal crystallization of bulk PAOXs with –methyl, -ethyl, -propyl, –isopropyl, -butyl, and -hexyl groups by DSC.

It is possible to deposit PEOX on surfaces to produce smart surfaces with reversibly switchable wettability by temperature. PNIPAM has been widely used in production of surfaces with reversible wettability [17–19]. Despite thermoresponsive behavior is also present in PEOX; switchable wetting of PEOX coatings has not been reported. We have produced multi-functional PEOX coatings on glass and silicon surfaces with addition of synthesized silver nano-particles (AgNPs). AgNPs were added into PEOX solutions to obtain anti-bacterial property. Since PEOX is soluble in water at ambient temperature, prepared coatings could dissolve upon water contact. Also the interaction between PEOX and substrate is only physical adsorption which results in low adhesion. To improve the adhesion of PEOX to substrates and prevention of water penetration, silica network, which was synthesized by sol-gel technique using tetraethoxy silane (TEOS) precursor, was incorporated into coating solutions. Thermoresponsive, antibacterial, and durable coatings were formed successfully on glass substrates. Static contact angle values of the coatings were determined at different

temperatures to show thermoresponsive properties of the films. Film morphologies were studied by AFM before and after water treatments to demonstrate durability of the films. Antibacterial activities were investigated against gram negative *E. coli* and gram positive *S. aureus*.

CHAPTER 2: LITERATURE REVIEW

In recent years stimuli-responsive polymers have gained much attention due to their various applications in fields such as drug delivery [20], tissue engineering [21], functional coatings [22], biosensors [23], and chromatography [24]. Stimuli-responsive polymers recognize a stimulus, and undergo drastic chemical or physical changes [25]. These polymers are also termed as smart [26], [27], intelligent [24], and environmentally sensitive [28]. Typical stimuli are chemical agents, pH, temperature, electric and magnetic fields, and mechanical stress and they can affect polymer-polymer and polymer-solvent interactions. Among them, temperature is relatively easy to control both in vitro [29] and in vivo [30] applications, thus thermoresponsive polymers form a major fraction of the stimuli responsive polymers. These polymers drastically change their physical properties usually at a critical temperature [31].

Biological polymers, such as proteins and polysaccharides, form complex architectures that are capable of many sophisticated functions such as regeneration, and sensing. Basic components of these polymers are assembled to achieve specific functions in biological systems. In contrast, the properties of the homopolymers depend on the chemical structure of the monomer unit and number of monomers. Even a small change in the chemical structure of the monomer results in significant changes in the polymer properties such as their stimuli-responsiveness. A typical example is the differences observed in solubility, crystallinity and thermoresponsiveness of the structural isomers of PNIPAM, PIPOX and P-leucine. Most studies mainly focus on polymers that show

thermoresponsive behavior in aqueous solutions, but this property is not restricted to an aqueous solvent. Water-soluble thermoresponsive polymers are of special interest because water is the solvent of living systems allowing application in the fields of biochemistry and medicine. In this review, we will only consider thermoresponsive polymers in aqueous medium.

2.1. Phase separation of thermoresponsive polymers in aqueous medium

Polymers possessing polar or ionizable groups dissolve in water. Hydrophobic molecules generally tend to aggregate in water to minimize their surface contact and associated surface energy. The arrangement of water molecules around a polymer is very complex due to the combined effects of hydrophilic and hydrophobic groups but their solubility is rather well-understood macroscopically. The phase diagram at constant pressure of aqueous polymer solutions (polymer-water binary system) is drawn by plotting the temperature of phase separation (T_c) as a function of the polymer fraction as shown in Figure 2.1.

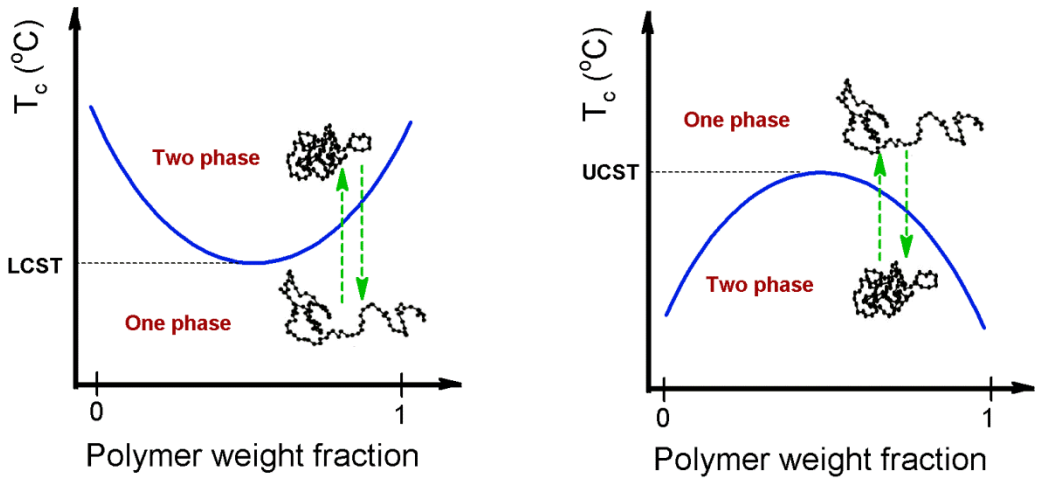

Figure 2. 1 The critical temperature–composition phase diagram with lower (left) and upper (right) critical solution temperatures. Blue curves are coexistence curves.

Polymers, which exhibit critical solution behavior in solution, display a miscibility gap in composition above or below specific temperature. In figure 2.1, blue curves are coexistence curves and denote the boundary at which two distinct phases coexist. Lower critical solution temperature (LCST) is the minimum and upper critical solution temperature (UCST) is the maximum points of coexistence curves. Within these curves, small fluctuations in composition and density will lead to phase separation. Although the solution is homogeneous at some temperature (in one phase region), a macroscopic phase separation appears when the temperature is above a critical value and two distinct phases, a polymer-rich and a solvent-rich phase, form [32]. Soluble to insoluble transition in figure 2.1, demonstrated with green arrow, is not passing through the maximum and minimum points thus temperature on coexistence curve should be denoted as critical

solution temperature or cloud point temperature (T_c). Both UCST and LCST type miscibility gaps are very common for polymer solutions. Above the UCST and below the LCST, a solute is miscible with water in all proportions. Polymers, which have a UCST become soluble in water upon heating, while LCST become insoluble with heating. Also, UCST behavior is enthalpy driven where LCST is entropy driven process [33], [34]. In LCST type phase separation, the arrangement of water molecules around a polymer is driven by negative enthalpy change due to formation of multiple interactions (bond formation enthalpy change is negative) between water and polymer at low temperatures and favors polymer dissolution. Increasing temperature weaken the interactions between polymer and water. Further increase in temperature disrupts the polymer water interactions and enthalpy change of the system become positive, due to bond breakage. It favors hydrophobic interactions between hydrophobic parts of the polymer [35]. Entropy of the system increases due to release of ordered water molecules around the polymer. Dominant hydrophobic interactions above LCST leads the polymer entropy driven collapse to minimize the surface energy [36], [37]. Gibbs free energy change (ΔG_{mix}) approaches zero and phase separation occurs [38]. UCST based on Coulomb interactions or hydrogen bonding interactions [39]. Repulsive interactions between polymer and solvent are dominant at low temperatures. Interaction parameter (χ_{ps}) between polymer and solvent increases with increasing temperature and results in dissolution. Macroscopic phase separation (soluble to insoluble or vice versa) can be explained microscopically by conformational changes of polymer chains in aqueous medium when temperature is changed. Thermal denaturation of proteins is common example for such a conformational change [40], [41].

2.2. Critical solution behavior in micro-scale

During phase separation the polymer chains, which exhibit upper critical solution behavior, undergo a transition from the insoluble to soluble state [42]. Phase transition of polymers exhibiting lower critical solution behavior, is from open coil state to contracted globule state. For a linear polymer chain in water, there has been debate in literature about coil-to-globule transition, whether hydrophobic effects and/or hydrogen bonding are dominant in aqueous solutions. Some authors explained the macromolecular contraction with the breakdown of polymer-water hydrogen bonding interactions [43], [44] whereas others attribute the chain collapse to hydrophobic interactions between polymer chains [8], [10], [36]. A third group of authors reported that the critical solution behavior of the thermoresponsive polymers was associated with changes in both hydrogen bonding and hydrophobic interactions within the interacting polymer water system [7], [9], [45]. According to last group the first step of the phase separation is the disruption of the relatively strong hydrogen bonds formed around the polymer chain and water molecules and this step is followed by collapse of the polymer chain into a hydrophobic globule. Contraction of polymer chains take place since hydrogen bonding between polymer and water becomes weaker and breaks as the temperature is raised. Hydrophobic interactions are responsible for the aggregation and the resulting precipitation of the polymer.

2.3. Thermodynamics of polymer solutions, which have LCST in water

Specific interactions between solute and solvent are required for the occurrence of the phase transition, which result in change in values for the enthalpy, ΔH_m, and the entropy, ΔS_m, of mixing [46]. Water molecules make hydrogen bonds with the hydrophilic part of the polymer, and also forms ordered structures upon the hydrogen bonds between themselves around the hydrophobic part of the polymer [47]. In dissolution of polymer in water at low temperatures, formation of hydration shell around the polymer gives negative enthalpy of mixing [48]. Increasing temperature cause change in ΔH_m, and ΔS_m as a result of breaking hydrogen bonds and water molecules excluded into the bulk. Then hydrophobic groups interact with each other between the same and different polymer chains leading to aggregation. Conformational movements of the chains are suppressed and both ΔH_m, and ΔS_m increases. Increase in enthalpy (δH) and entropy (δS) are dominant during phase separation and can be expressed in the following Gibbs free energy of mixing equation

$$\Delta G_m(T) = \Delta H_m(T_0) + \delta H(T) - T\left[\Delta S_m(T_0) + \delta S(T)\right]$$

Equation 2. 1

As a consequence, the sum of the second and third terms on the right-hand-side of equation increases monotonically with increasing T and $\Delta G_m(T)$ approaches to 0 [38]. This predicts that, as the temperature is raised, the system becomes increasingly unstable and phase separation takes place above a critical temperature [49]. Despite the phase transition is a classical subject, many

theoretical studies, mainly using extensions of Flory-Huggins Theory (considers the entropy of mixing, ΔS_m and interaction energy contribution ΔH_m to the Gibbs free energy of mixing, ΔG_m [46] have been reported mostly about poly(N-isopropylacrylamide) (PNIPAM) gels [8], [50], [51].

2.4. Common thermoresponsive polymers, which exhibit UCST and/or LCST in water

There are three main types of thermoresponsive polymers; the first present a UCST while the second present an LCST, and third group exhibit both LCST and UCST together. Some polymers are known to exhibit a UCST in water under relatively extreme conditions. One example is poly(ethylene oxide), (PEO) that shows a loop-shaped miscibility gap with UCST>LCST [52], [53]. The center of the loop is located around 200 °C. Another example is Poly(vinyl methyl ether) (PVME), exhibits two UCST miscibility gaps in the low and high concentration regions around -15 and -25 °C respectively [54], [55]. Some polymers exhibit upper critical solution behaviors in mild conditions (in the temperature range of 0 to 100 °C) contain zwitterionic polymers, polyelectrolytes and carboxylic polymers. The examples of these polymers are poly-3-dimethyl(methacryloyloxyethyl) ammonium propane sulfonate (PDMAPS) [56], blockcopolymer consisting of PEO and poly(2-vinylpyridine) (P2VP) [57], and poly(acrylic acid) [58].

The most widely studied thermoresponsive polymer system which exhibits LCST is poly(N-substituted acrylamide)s. *N*-substituted polyacrylamides have attracted much interest due to their unique thermal response in aqueous medium [59]. The phase transition temperature of this series of *N*-substituted

polyacrylamide derivatives differs strictly depending on the chemical structure of the side chains [60]. Their ability to exhibit lower critical solution behavior in aqueous solution has attracted much attention. Thermoreversible response of such species is established in aqueous media and has been attributed to the two-stage mechanism: individual chains collapse in a coil-to-globule transition prior to aggregation of the resultant globules [61]. LCST of a polymer is found to be dependent on molecular weight and architecture [62], [63]. Another important class of polymer exhibiting lower critical solution behavior in water is polyoxazolines but they are discussed in detail in section 2.6.

2.5. Poly(N-isopropylacrylamide), PNIPAM

The most extensively studied thermoresponsive polymer in the family of poly (*N*-substituted acrylamides) is PNIPAM. Chemical structure of the polymer can be seen in figure 2.2.

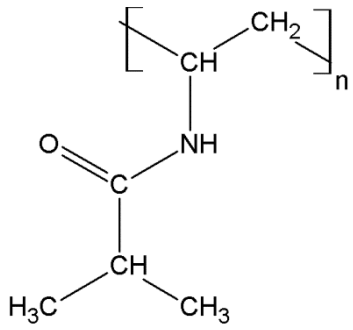

Figure 2. 2 Chemical structure of PNIPAM

At low temperature, PNIPAM is soluble in water as random coils since the amide side chains form hydrogen bonds with water molecules. At the same time, the poor interaction of hydrophobic isopropyl side chains with surrounding water molecules results in polymer-polymer attraction [6]. At low temperatures the solvent-polymer interaction is stronger than the polymer-polymer interaction, thus PNIPAM remains soluble. At elevated temperature, hydrogen bonding and polar interactions are disrupted. As a result, the polymer-polymer interaction becomes stronger than the solvent-polymer interaction as temperature is increased, leading to the formation of insoluble globular polymer precipitates. The polymer phase separation is driven by the entropy increase upon the release of structured water molecules surrounding the hydrophobic groups [6]. The LCST at which the phase separation takes place is ~32 °C for PNIPAM, which is close to the human body temperature [59], [64], [65]. PNIPAM samples, obtained from conventional radical polymerizations, have broad polydispersities. Since high and low molecular weight fraction may mask the LCST of bulk PNIPAM, precise investigation of lower critical solution behavior in water requires low polydispersity values. Different synthesis methods, to observe PNIPAM with low polydispersities were already reported [66–70]. However, the effect of molecular weight on the LCST of PNIPAM is not yet clear. The LCST of PNIPAM have been reported to be directly dependent [43], inversely dependent [71] or independent [10], [41], [59] of the molecular weight. There have been extensive studies regarding the different effects such as polymer concentration, cosolvent, pressure, presence of salts and surfactants on T_c. It was demonstrated that T_c decreases gradually with increasing PNIPAM concentration [71]. Similarly, methanol and ethanol additions were shown to decrease T_c [72]. Study about pressure effects on aggregation behavior of PNIPAM showed that aggregation of the polymer in aqueous solution could be prevented by increase in

pressure up to 50 MPa [73]. Maximum was observed at 50 MPa in T_c vs. pressure graph and was attributed to the existence of some factors other than hydrophobic interaction acting on the aggregation of polymer chains. Detailed investigation of the effects of different salts on T_c of aqueous PNIPAM solutions showed that decrease in T_c directly related with the Hoffmeister series of anions [43]. Effects of surfactant sodium dodecyl sulfate concentration on collapsed PNIPAM molecules (above T_c of the solution) was studied by small angle neutron scattering (SANS) and demonstrated that addition of small quantity of surfactant can resolubilize the precipitated polymer and increase the T_c [74].

2.6. Poly(2-alkyl-2-oxazoline)s, PAOXs

Although acrylamide based polymers were widely studied, polyoxazolines - structural isomers of poly(N-substituted acrylamide)s- have recently gained attention [13], [75], [76]. They are referred to as poly(N-acyl ethylene imine)s and considered as pseudopeptides because of the structural relation to polypeptides [14], [77]. The general formula of the polymer in figure 2.3 clearly demonstrates that they can be classified as tertiary polyamides.

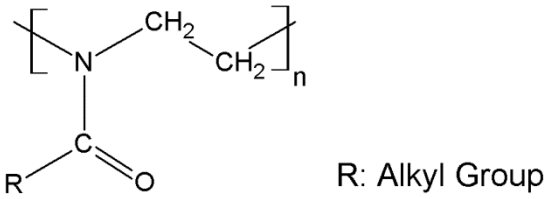

Figure 2. 3 Chemical structure of poly(2-alkyl-2-oxazoline)s

In the 1960s different groups independently reported the cationic ring opening polymerization (CROP) of 2-oxazolines [78–81]. Several reviews can be found in literature about polymerization of 2-oxazolines in detail [82–86]. Despite the usage of poly(2-oxazoline)s in adhesive and coating formulations [2], [3], in drug delivery applications [87] and as dispersants [1], there were nearly no study in the 1980s and 1990s due to their long polymerization times [88]. Recent developments in polymer technology, especially the usage of microwave reactors in polymerization reactions, maintained living character to the polymerization of 2-substituted oxazolines and also accelerated the polymerization reaction significantly [89–91]. Living and controlled polymerization techniques provided the possibility for the preparation of polymers with defined composition, narrow molar mass distribution and also allow the creation of different architectures such as linear, star-shaped, and graft copolymers [69], [70], [92], [93]. Despite a lot of research has been done on poly(2-alkyl-2-oxazoline)s to obtain smart materials like nonviral gene carriers [94], biocompatible hydrogels [95] and antimicrobial agents [96], properties of homopolymers have not been clarified yet.

It is possible to obtain water soluble, water insoluble, hard and soft materials from polymerization of a variety of 2-oxazoline monomers using living polymerization method. Physical properties of poly(2-oxazoline)s such as crystallinity and solubility depend significantly on the type of alkyl side chains [14], [97]. Poly(2-methyl-2-oxazoline) is soluble in water and does not exhibit lower critical solution behavior. However poly(2-ethyl-2-oxazoline) have LCST in water around 60 to 65 °C depending on the molecular weight [11]. It was reported that poly(2-n-propyl-2-oxazoline) also have cloud point at 24 ºC in aqueous solution [98]. Decrease in cloud point temperature from 60 to 24 ºC is a result of increasing

carbon atom number in the alkyl side chain. This is expected because hydrophobic character of the polymer is increasing, thus further increase in carbon atom number in alkyl group caused insolubility in water. Similarly crystallinity of the polymers was also related to the size of the alkyl side chain. The earliest systematic investigation on the crystalline structure of PAOXs reported that except PEOX, all polyoxazolines were crystalline and d spacings along alkyl groups increased linearly with alkyl side chain length [14]. It was demonstrated that crystallinity is only present for the polymers with longer side chains (-butyl, -pentyl, -hexyl, -nonyl etc.) [15] and these polymers are not soluble in water.

2.7. Characteristics of poly(2-isopropyl-2-oxazoline) (PIPOX)

Poly(2-isopropyl-2-oxazoline) (PIPOX), which possess an isopropyl group in the side chain, is the only polymer which is both crystalline and soluble in water at room temperature [98]. Aqueous solutions have critical solution behavior in water and have LCST around 37 ºC, which is close to human body temperature [13], [99]. PIPOX is the structural isomer of polyleucine and PNIPAM. Chemical formulas of the PIPOX, PNIPAM, and polyleucine are shown in figure 2.4.

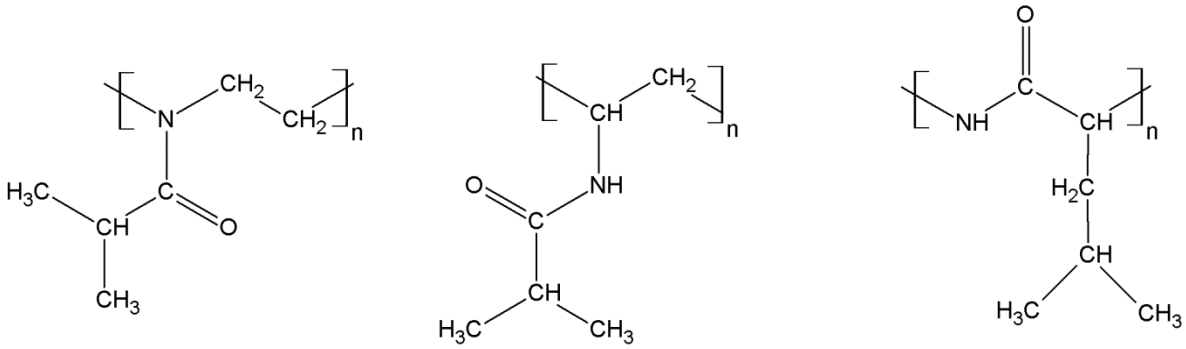

Figure 2. 4 Chemical structure of a) PIPOX, b) PNIPAM, and c) polyleucine

Polyleucine is a crystalline polypeptide and includes amide groups in its backbone and has entirely nonpolar side chain. PNIPAM has a nonpolar backbone and contains amide groups in its side chain. It is an amorphous polymer and has LCST in water around 32 ºC as mentioned before. In PIPOX, one end of the amide moiety is on the backbone and bears isopropyl group in side chain. PIPOX combines the advantageous properties of its structural isomers. It can be crystallized like polyleucine and also exhibit lower critical solution behavior in water like PNIPAM. PIPOX was first introduced by Kobayashi, Uyama and Kataoka [100–102]. Studies related to poly(2-oxazoline)s, especially PIPOX, focused on synthesis and characterization [15], [75], [90], [91], [103], [104]. However, there are also many studies about the LCST modulation of PIPOX aqueous solutions, because this is an important parameter in the determination of polymer usage in biological applications. It was demonstrated that LCST of polyoxazolines can be tuned by; copolymerization [47], [76], [98], [105], molecular weight of the polymer [106] and end group modification [101], [106–108], varying solvent composition

[109], [110], and also addition of salts to the aqueous solution [111]. Copolymerization of variety of oxazoline monomers with different hydrophobic and hydrophilic co-monomers allow us to prepare well defined copolymers with finely tunable LCST [76], [98], [105], [112]. Demixing and remixing kinetics studies of aqueous PIPOX solutions clearly proved that cloud point temperatures decreases with increasing molecular weight [106]. It was also shown that this typical behavior is in contrast with PNIPAM, where T_c independent of molecular weight of PNIPAM. The higher cloud point temperatures of shorter polymers can be ascribed to the stronger influence of the end groups. In general end groups are either methyl or hydroxyl. Methyl groups can be easily hydrated and hydroxyl group is hydrophilic already. It was shown that LCST in water strongly depends on the polarity of the terminal group of the chain [106]. Introduction of hydrophobic groups decreases LCST while hydrophilic ones increase it [101], [107], [108], [113]. It would be expected that decreasing polarity of the water improves the solubility of polymer and increase the cloud point temperature. However, addition of less hydrophilic ethanol to the PIPOX aqueous solutions caused opposite effect. This decrease was explained with the hydration of ethanol molecules. Ethanol molecules in water preferably surrounded by water molecules and decrease the hydration of PIPOX. Decrease in hydration of polymer results in decrease in cloud point temperature [109], [110]. It was reported that the cloud point temperature of poly(2-oxazoline)s changed with the addition of salts [11], [111]. Change in T_c was related to the hydrophillicity of the polymer, but no systematical investigation was performed. For more hydrophilic PEOX, T_c was tuned over almost the whole temperature range of liquid water under atmospheric conditions while T_c was varied to a lesser extend for PIPOX.

2.8. Influence of salts on cloud point temperatures of polyoxazolines and PNIPAM aqueous solutions

The effect of ion types on LCST of thermoresponsive polymers was generally explained by Hofmeister series. The effects of these changes were first worked out by Franz Hofmeister, who studied the effect of ions on the solubility of proteins [114]. The ability of salts to precipitate certain proteins from an aqueous solution follows a recurring trend now known as the Hofmeister series. This behavior is more pronounced for anions than cations. The typical order of the anion series is:

$$CO_3^{2-} \rangle SO_4^{2-} \rangle S_2O_3^{2-} \rangle H_2PO_4^- \rangle F^- \rangle Cl^- \rangle Br^- \approx NO_3^- \rangle I^- \rangle ClO_4^- \rangle SCN^-$$

According to Hofmeister series, anions can be categorized into two general groups based upon the physical behavior of polymer solutions in their presence [115–117]. Basically, species to the left are called kosmotropes, which are strongly hydrated anions, and have been shown to salt polymers out of the solution. On the other hand, species to the right are called chaotropes and are known to increase the solubility of polymers in solution. Kosmotrope and chaotrope terms were originally used to describe the ability of ions to make or break bulk water structure respectively, and also thought to be the explanation of mechanism of the effect. It has been shown that influence of particular salt on structure of water in bulk solution plays a role in the Hofmeister effect [118–120]. In contrast to the role of ions on water structure, it has been demonstrated that direct interactions between ions and macromolecules can be key to understand Hofmeister series [121]. Recent theories include polarizability of the ions and specific ion binding together

[122], [123]. Since, bulk water structure, except the first hydration shell of the polymer, is not affected by the nature of salt present in aqueous solution of polymers, the influence of salts of Hofmeister series on polymer solubility should be explained considering ion-macromolecule and ion-first hydration shell water interactions together. Changes in the critical temperature of PNIPAM with added salts were recently explained with a model [124]. Three different mechanisms were used together for the clarification of interactions of Hofmeister anions with PNIPAM in aqueous solutions. Dehydration and surface tension mechanisms were used to explain decrease in the solubility of polymer, while direct binding mechanism was employed to describe increase in the polymer solubility. In the dehydration mechanism, polarizations of water molecules in the first hydration shell of the polymer in the presence of anions cause dehydration and decrease the solubility of polymer and lower the T_c. Surface tension mechanism explains the salting out of the polymer and decrease in T_c due to the increase in free energy of alkyl/water interface with increase in surface tension of solution in the presence of salts. In the third mechanism, salting in effect was explained with improvement of hydration of the polymer via direct ion binding. The change in mechanism from a polarization effect to a surface tension and direct ion binding effect was proposed as the indicator of the division between kosmotropic and chaotropic behavior. Since few studies were published about the influence of salts on T_c of polyoxazoline aqueous solutions, the fundamental thermodynamic understanding is still missing at the molecular level. We have studied all of the sodium salts of Hofmeister anion series given above to understand their influence on cloud point temperature of PEOX aqueous solution. Observations and detailed discussions are presented in Chapter 4.

2.9. Reversibility of phase separation of thermoresponsive polymers in aqueous medium and unexpected behavior of PIPOX

The coil to globule transition is important for understanding structure – property relationship of thermoresponsive polymer materials. The transition at cloud point temperature is usually reversible with hysteresis. Hysteresis in the heating / cooling cycles of polymer – water systems, which exhibit lower critical solution behavior, has been ascribed to delay of hydration of formed globules during cooling. Hysteresis happens due to limited diffusion of water into dense hydrophobic phase [125], [126]. Although PNIPAM is the most widely known and studied thermoresponsive polymer, thermal solubility transition of aqueous solutions show strong hysteresis like majority of thermoresponsive *N*-substituted poly(acrylamide)s and poly(methacrylamide)s [127]. This behavior is attributed to the formation of intermolecular and intramolecular hydrogen bonds in the collapsed state [128], [129]. Therefore many studies focus on finding alternative polymers with reversible phase transition without hysteresis. Polyoxazolines are better alternatives to PNIPAM because they exhibit a reversible, concentration dependent phase transition and do not show significant hysteresis [108]. However, it was reported that long term annealing of dilute PIPOX aqueous solutions, above the cloud point temperature of the solution, caused irreversible formation of micron-sized aggregate particles consisting of nanofibers [13]. Intermolecular hydrogen bridges were proposed to explain self-assembly driven aggregation. Subsequent study after this work clearly demonstrated that formed aggregates are crystalline [12]. Crystallization investigations of polyoxazolines, carrying different alkyl side chains, in bulk are essential for clarifying such a self-assembly driven aggregation mechanism.

2.10. Crystallization of polyoxazolines in bulk

The understanding of crystallization and melting in bulk polymers is a main issue in polymer physics. It is well known that a semi-crystalline polymer will crystallize when cooled from the melt or heated from the amorphous state in the temperature region between glass transition temperature (T_g) and melting temperature (T_m) [130]. The bulk crystal structures of series of polyoxazolines were investigated in very few studies. In the first study, series of polyoxazolines, carrying different alkyl side chains, were synthesized and their crystallinities were investigated with wide angle x-ray diffraction technique [14]. Fibers were prepared by extrusion of polymers and oriented by stretching in silicon oil bath below the melting points. It was shown that all polyoxazolines, bearing –methyl, –propyl, –butyl, –pentyl, –hexyl, –heptyl, –undecanoyl side chains, are crystalline. Only –ethyl substituted one was found to be amorphous. Largest d spacings are shown to be quite regular with the change in number of carbon atoms in the side chain and indicates similar mode of packing. Similar regularity was also observed for the melting points of polyoxazolines. Melting points decreased with increasing alkyl chain length of polyoxazolines, whose number of carbon atoms in the alkyl group is greater than 3. Such regularity was not observed for smaller alkyl chain length polyoxazolines and this was attributed to a structural change. Thermal properties of series of polyoxazolines were investigated in another study by DSC [15]. Glass transition temperatures were only observed for polyoxazolines having 1-5 carbon atoms in the side chains and decreased linearly with increasing alkyl chain length. Endothermic transitions due to the melting of crystalline polymers were observed for the polymers with -pentyl and longer alkyl side chains and explained by side-chain crystallization. Thermal, mechanical and surface properties of

polyoxazolines, carrying linear alkyl side-chains, were investigated and crystallinities of the polymers were found to be relevant with the previously reported data [16]. It was shown that melting temperatures for polyoxazolines having 4-9 carbon atoms in the side chain were nearly constant around 150 °C and independent of the length of the side-chain. The glass transitions of amorphous shorter alkyl side chain polyoxazolines were shown to decrease with increasing number of carbon atoms in side chains. We have studied isothermal crystallization of a series of polyoxazolines carrying different alkyl groups as side chain to understand the self-assembly driven aggregation mechanism of PAOX in water. Observations about the effect of alkyl side chain length on crystallization behavior are presented in chapter 7.

2.11. Crystallization of polyoxazolines in aqueous medium

Self-assembly driven crystallization of PIPOX in aqueous solutions above T_c was briefly mentioned in section 2.9. PIPOX were found to crystallize upon isothermal treatment in aqueous solutions above the T_c [12], [13]. Driving mechanism for self assembly was proposed, which involve non-specific hydrophobic interactions, oriented dipolar interactions, and backbone solvation together. Since hydrophobic interaction strength increases with increasing temperature and induce some order, it cannot explain such an ordered aggregation [131]. According to the proposed mechanism, nonspecific hydrophobic interactions become dominant above the cloud point temperature and bring hydrophobic isopropyl groups together. The close distance between the chains allows the amide dipoles of PIPOX to interact and align. One end of the amide dipole is on

the backbone of the PIPOX so backbone solvation also contributes to the mobility of polymer and leads the system to form well-defined crystals. The crystal structure and melting temperature of the crystalline PIPOX fibers formed in water above the T_c were consistent with the PIPOX crystals produced isothermally in bulk. Similarly PIPOX crystallization in water above the T_c was directly monitored by wide angle X-Ray scattering (WAXS) measurements [132]. Observed diffraction patterns of crystalline powders revealed the same crystalline reflections and intensity with the previously published data. Sharpness of the peaks increased with time sigmoidally and was interpreted as the sign of typical nucleation and growth type crystallization mechanism. Crystallization studies in aqueous medium were extended by the same group to thermoresponsive poly(2-alkyl-2-oxazoline)s other than PIPOX [133]. In this study temperature dependent phase separation of poly(2-isobutyl-2-oxazoline) and poly(2-nonyl-2-oxazoline) showed upper critical solution behavior in the presence of ethanol. Annealing of these polymer solutions below T_c caused crystallization. It indicates that crystallization of PIPOX in aqueous solution above the phase separation temperature is not specific to polymer and solvent system. Crystallization behavior and resemblance in the aggregate morphologies were attributed to the structural similarities. Also, such an aggregation was investigated in aqueous solution of polyoxazolines carrying glucose units in the side chain [134]. For this specific case, driving force for the self assembly was found to be hydrogen bonding between the sugar moiety and amide groups of the polymer backbone. Furthermore, mechanism of the heat induced phase separation and crystallization of PIPOX in water above T_c was investigated via vibrational spectroscopy [135]. It was demonstrated that formation of polymer rich phase via heat induced phase separation initiated change of polymer chains mostly in trans-conformation. Dipolar interactions between polymer chains were promoted in this

conformation and facilitate nucleation and crystallization of PIPOX. Neither the thermodynamic factors affecting the self-assembly process nor its mechanism is yet well-understood. Despite thermoresponsive behavior and similar interactions are also present in aqueous PEOX, and PPOX solutions, irreversible formation of fibers and aggregation were not studied before. Crystallization behavior of these polymers in aqueous solutions should be studied, in order to extend and generalize the concept of crystallization in phase-separated aqueous polymer solutions. For this purpose we have studied the aggregation of PEOX in aqueous solutions above T_c with and without salt additions. Observations about the influence of salts on crystallization kinetics and characterization of self-assembled aggregates are presented in chapter 5.

2.12. Thermoreversible surface wettability

It is well known that surface wettability is governed by surface chemistry and morphology [136–138]. Smart surfaces that respond to external stimuli such as pH, and temperature are of interest in many studies such as chromatography, biosensing, drug delivery, and optical devices. [4]. Temperature can trigger conformational changes from extended to collapsed structure of thermosensitive polymers, and hence it is considered a promising external stimulus to easily alter the surface wettability. Preparation of thermoresponsive surfaces can be done by directly coating polymers on solid substrates as thin films or by monolayer polymer brushes. Polymer brushes are prepared by attaching polymer molecules from one end to a surface by covalent bonding or physical adsorption [139] and were shown to be used as stimuli-responsive surfaces [140]. The most widely studied

temperature controlled films are built from PNIPAM [17], [141], [142]. PNIPAM chains present a widespread hydrogen bonding network between the amide groups and water molecules. Above T_c PNIPAM films undergo a phase transition, from a hydrated swollen state to a collapsed morphology (solvent is forced out) [143], [144]. Surface attached stimuli-responsive polymers do not aggregate to form a separate phase, but the conformational transition from the hydrophilic to hydrophobic state gives the surface with regulated hydrophobicity. In an exemplary study, PNIPAM was synthesized with carboxyl functionalized end group, then grafted to glass substrates via two different methods, and surface properties were investigated as a function of temperature [141]. They clearly demonstrated that prepared terminal and multipoint grafted surfaces possess temperature responsive surface properties around 24 °C. Extents of increase in hydrophobic character with increasing temperature for terminal graft surfaces were found to be greater than that for multipoint graft surfaces and associated with the graft conformations. Similarly, effects of graft configurations on thermoresponsive wettability changes were investigated on three different types of PNIPAM-grafted surfaces [17]. It was shown that, surface wettability changes in response to temperature change strongly depends on graft architecture and density. The effect of cross-linked structure on thermoresponsive wettability was investigated with PNIPAM-hydrogel modified surfaces [142]. The three-dimensional network structure showed strong influence on release of hydrophobic particles due to temperature changes. Since another method to prepare thermoresponsive surfaces is directly coating polymers on solid substrates, plasma polymerization was used to deposit PNIPAM chains on different surfaces [145]. AFM modulation measurement was performed on PNIPAM coated samples as a function of temperature and sharp change in response signal was found at 28.5 °C, which attributed to the phase separation

temperature of PNIPAM. Polyoxazolines are suitable candidates for thermoresponsive surface applications because they are soluble in water at low temperatures and show phase separation in aqueous solutions above critical temperatures varying very wide temperature range. Although they have similar properties to PNIPAM, heat-induced wetting properties of polyoxazolines on surfaces have not been reported previously. We have studied the preparation of thermoresponsive surfaces using PEOX. Silver nano-particles and silica network were also added to achieve multifunctional smart coating design. Results on switching of surface wettability due to thermally activated swelling transitions, antibacterial activity of the coatings, and stability of coatings on surfaces are shown in chapter 8.

CHAPTER 3: MATERIALS AND METHODS

3.1. Chemicals

Poly(2-ethyl-2-oxazoline) (PEOX) (M_w ~ 50,000g/mol and 500,000g/mol), and poly(N-isopropylacrylamide) (PNIPAM) (M_w ~ 23000 g/mol) were purchased from Aldrich. PEOX polymers of M_w 5,000g/mol and 200,000g/mol were obtained from Alfa Aesar. All of the polymers were used without any purification. Poly(2-isopropyl-2-oxazoline) (PIPOX) (M_w ~ 6,800 g/mol), having polydispersity index (PDI) of 1.08, was synthesized by Dr. Helmut Schlaad. Poly(2-methyl-2-oxazoline) (PMOX) (M_w ~ 17,000 g/mol), poly(2-propyl-2-oxazoline) (PPOX) (M_w ~ 22,600 g/mol), poly(2-butyl-2-oxazoline) (PBOX) (M_w ~ 7,600 g/mol), and poly(2-hexyl-2-oxazoline) (PHOX) (M_w ~ 9,300 g/mol), having PDI values in between 1.1 and 1.2 were synthesized by Dr. Richard Hoogenboom.

Distilled ~18.2 MΩ water (DI-H_2O) was produced using Milli-Q filtration system (Millipore Corporation, USA). Prime quality silicon (100) wafers were purchased from Ultrasil Corporation (USA). Analytical grade sodium carbonate (Na_2CO_3), sodium sulfate (Na_2SO_4), sodium dihydrogen phosphate (NaH_2PO_4), sodium chloride (NaCl), sodium acetate (CH_3COONa), and sodium nitrate ($NaNO_3$) were purchased from Merck. Other analytical grade sodium salts, which are sodium thiosulfate ($Na_2S_2O_3$), sodium fluoride (NaF), sodium bromide (NaBr), sodium iodate (NaI), sodium perchlorate monohydrate ($NaClO_4.H_2O$), and sodium thiocyanate (NaSCN), were purchased from Aldrich.

3.2. Instruments

3.2.1. Dynamic Light Scattering (DLS)

Dynamic light scattering is a technique for measuring diameters of particles. When particles are dissolved in liquid medium they undergo Brownian motion due to the bombardment by the solvent molecules surrounding them. According to the Brownian motion theory smaller particles move quickly than large particles. They kicked further by the solvent molecules and move rapidly. When a small particle is illuminated by a laser, the particle will scatter light in all directions. If a screen is held close to the particle, the screen will be illuminated by the scattered light. The screen would now show a speckle pattern as shown in figure 3.1.

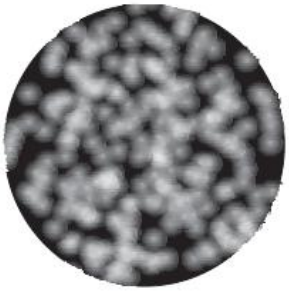

Figure 3. 1. Speckle pattern of screen consists of dark and bright areas [146]

The bright areas are where the light scattered by particles arrive at the screen and interferes constructively and dark areas are where interference is destructive.

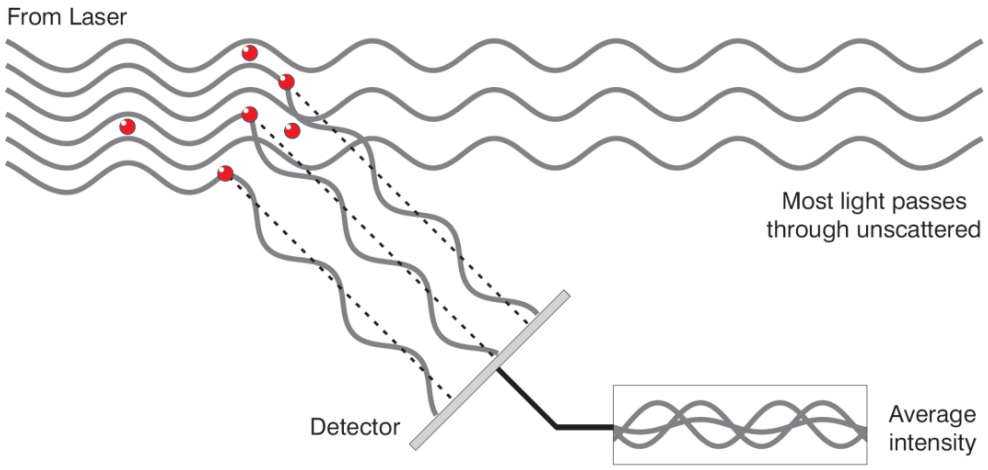

Figure 3. 2. Representation of propagated waves when the light interacts with the particles [146]

Figure 3.2 represents the propagated waves, when laser light interacts with the particles. As the particles move around the scattered light intensity appears to fluctuate due to diffusion. Intensity of light fluctuates in time is correlated with the diffusion coefficient (D) using Stokes-Einstein relation. [147]

$$D = \frac{k_B T}{6\pi\eta a}$$

Equation 3. 1

where k_B is the Boltzman constant, T is the temperature , η is the viscosity of the medium and a is the diameter of the particles. The fluctuation in scattered intensity is examined with a digital correlator which measures similarity between two signals over a period of time. At short time intervals the correlation is high

since the particles do not have a chance to change their position significantly. When the time delays become longer, correlation decays exponentially and eventually reach zero. The smaller particles diffuse faster than the larger particles, so the correlation function decays much faster for smaller particles as shown in figure 3.3.

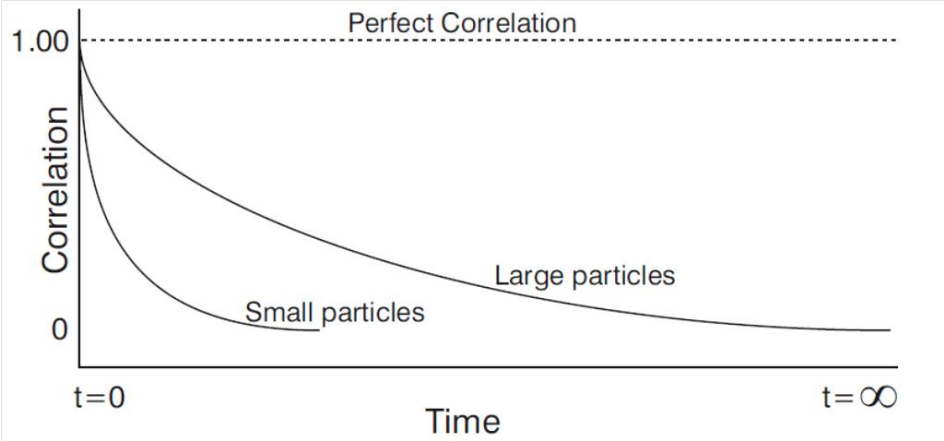

Figure 3. 3. Typical correlation function against time for small and large particles [146]

The graph shows the correlation function for large and small particles. The rate of decay for the correlation function is related with particle size. Correlation data is analyzed through autocorrelation function. The second order autocorrelation curve is generated from the intensity trace is:

$$g^2(q;\tau) = \frac{\langle I(t)I(t+\tau)\rangle}{\langle I(t)\rangle^2}$$ [148]

Equation 3. 2

where $g^2(q;\tau)$ is the autocorrelation function, q is the wave vector, τ is delay time and I is the intensity. If the sample is monodisperse then the decay is a single exponential. The Siegert equation relates second-order autocorrelation function with the first-order autocorrelation function $g^1(q;\tau)$

$$g^2(q;\tau) = 1 + \beta\left[g^1(q;\tau)\right]^2 \text{ [148]}$$

Equation 3. 3

Parameter β is the correction factor depends on geometry and alignment of the laser beam in the set-up. Once autocorrelation function is generated, different approaches can be used to determine size of particles. For monodisperse population simplest approach is to treat function as a single exponential decay as follows

$$g^1(q;\tau) = \exp(-\Gamma\tau) \text{ [148]}$$

Equation 3. 4

where Γ is the decay rate. The translational diffusion coefficient D_t may be derived at a single angle or at a range of angles depending on the wave vector q.

$$\Gamma = q^2 D_t \text{ with } q = \frac{4\pi n_0}{\lambda}\sin\left(\frac{\theta}{2}\right) \text{[148]}$$

Equation 3. 5

where λ is the incident laser wavelength, n_0 is the refractive indice of the sample and θ is angle at which the detector is located with respect to the sample cell. The software basically uses decay rate algorithms and extracts the different size classes to produce an intensity distribution graph as shown in figure 3.4.

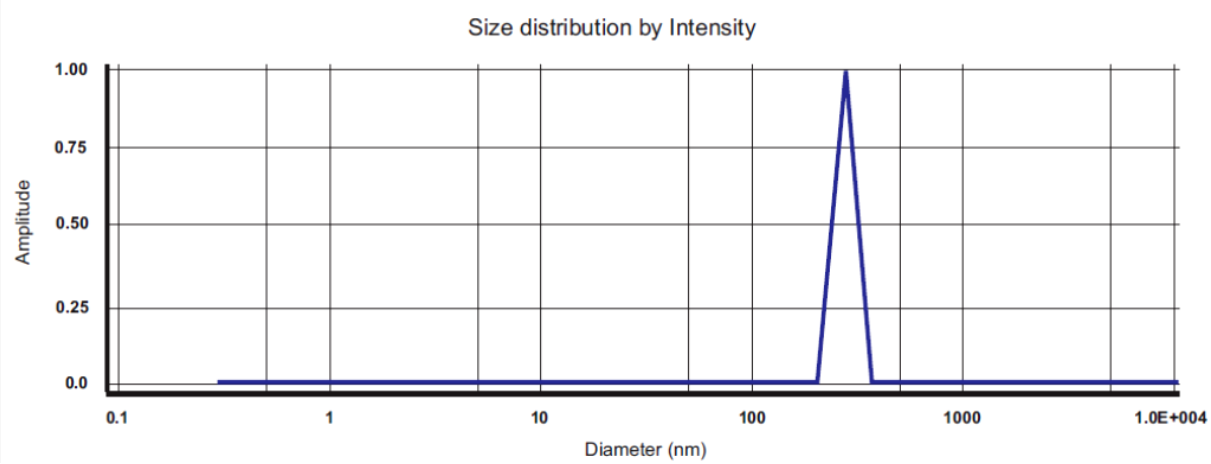

Figure 3. 4. Typical intensity distribution graph [146]

The x axis shows a distribution of size classes and y axis represents the relative intensity of the scattered light. Maxima of the curve can be used as an average size of the particles. In this thesis, Malvern Zetasizer Nano S DLS instrument was used. A 633 nm red laser illuminates the solution and a detector measures the intensity of the scattered light at an angle of 173° [146]. This is known as backscatter detection. In this angle the incident beam does not have to travel through the entire sample and reduces multiple scattering. The light will pass through a shorter path length therefore concentrated samples can be measured. Contaminants such as dust particles are larger compared to sample size. Since larger particles mainly scatter in forward direction, backscatter detection also reduces the effect of contaminants on measurements.

Behavior of polyoxazoline aqueous solutions has been studied extensively by DLS. This technique was used to detect cloud point temperature of aqueous PEOX solutions and also following kinetics of self-assembled fibers. The detectable size range of the instrument is 0.6 nm – 6000 nm therefore particle size out of this range was appeared as 0. During the DLS measurements viscosities of aqueous PEOX solutions were used. Viscosities of solutions were determined by micro-viscometer.

3.2.2. Viscosity measurements

Viscosity is a material property of fluids and defined as resistance of fluid against flow. In a fluid, shear stress is proportional to shear rate and viscosity is the proportionality constant. Viscosities of solutions were determined by Anton Paar AMVn micro-viscometer. A spherical steel ball with a density of 7.85 mg/ml was used for analyzing dynamic viscosities of PEOX solutions. The viscosity was determined by measuring the time that a falling ball spends between two marks in an inclined capillary column. The inclination angle of the capillary could be changed. In the present study, the measurements were done at an angle of 30°. Depending on the concentration of the solutions and the resulting viscosity values, different capillary sizes and different ball sizes were used. The dynamic viscosities of the polyoxazoline solutions were calculated by device using the calibration constant $K_1(\alpha)$ of the measuring system, the rolling time t_1 and the difference in density $\Delta\rho$ between the ball and the sample according to

$$\eta = K_1(\alpha) \times t_1 \times (\rho_k - \rho_s)$$

Equation 3. 6

where η is dynamic viscosity of sample [mPa.s], K1(α) is measuring system calibration constant [mPa.cm^3 /g], t_1 is rolling time, ρ_k is ball density [g/cm^3] (steel ball= 7.85 g/cm^3) and ρ_s is density of sample to be measured (g/cm^3) [149]. Calculated dynamic viscosity values were used in DLS measurements as sample viscosities instead of using water itself.

3.2.3. Ultraviolet-Visible Absorption Spectroscopy

In the UV-Visible range, the molecules absorb light and undergo electronic transitions to higher energy levels. Aqueous PEOX solutions do not have any significant absorption band in UV-Vis spectral region (400 – 900 nm). We have instead used UV-Vis Absorption Spectroscopy as a measure of aggregation and turbidity in the solutions. As aggregates form in the solution by heating due to phase separation the solution gets turbid, the incoming light (intensity I_o) is scattered more and the intensity of light reaching the detector (I) is decreased.

$$A = -\log \frac{I}{I_0}$$

Equation 3. 7

UV-Vis spectra of PEOX aqueous solutions were recorded at different temperatures using PG T80 UV/Vis Spectrometer. Before each measurement, background was taken with water. To analyze critical solution behavior of PEOX aqueous solutions, absorbance change (as base line increase) was investigated at a specified wavelength as a function of temperature.

3.2.4. Fourier Transform Infrared Spectroscopy (FT-IR)

Formation of self-assembled fibers is generally explained by the establishment of intermolecular hydrogen bridges, as observed for collagen [150], and polyoxazoline based lipopolymers [151]. FT-IR spectrum of both self-assembled PEOX fibers and pristine polymer were examined to find an evidence for H-bridges. Nicolet is10 FTIR Spectrometer was used at room temperature with a set up consisting of Mid-infrared Ever-Glo (9600-50 cm^{-1}) and Tungsten/halogen as light source, deuterated triglycine sulfate (DTGS) and liquid-nitrogen-cooled mercury cadmium telluride (MCT) as detector and diamond ATR as a sample holder. Before taking measurement, background was recorded to eliminate the humidity and CO_2 contributions from air.

3.2.5. Optical Microscopy

A Leica DMLM optical microscope was used to observe self-assembled PEOX fibers formed in aqueous solutions. The samples were prepared by solvent casting. The image from an optical microscope was captured by CCD camera to generate micrographs.

3.2.6. Scanning Electron Microscopy (SEM)

Zeis EVO LS15 Scanning electron microscope (SEM) was used to examine microscopic detail of self-assembled fibers on surfaces like light microscope. Basically the image is produced by scanning an extremely small focused beam of electrons (adjustable down to a few nm in diameter) across the surface of a

specimen in an array of picture points (pixels). High-energy electron bombardment of the specimen causes signals to be emitted at each pixel. These are collected and their intensities are used to produce images of the specimen by modulating the brightness of equivalent pixels on a TV monitor. Better resolution, greater depth of field and ability to carry out X-ray microanalysis are three distinct advantages of it. SEM examination was needed in order to provide fiber thickness information which is not available with light microscope.

3.2.7. Atomic Force Microscopy (AFM)

AFM is one type of scanning probe microscopes used to image surface morphology and surface forces. AFM measurements have high vertical resolution on the order of fractions of nanometer. Thus atomic-scale defects, molecular structures and perfectly ordered atomic structures can be observed via AFM. The standard AFM contains a microscopic tip attached to a cantilever spring, a piezoelectric cylinder, laser and a photodiode detector (Figure 3.5).

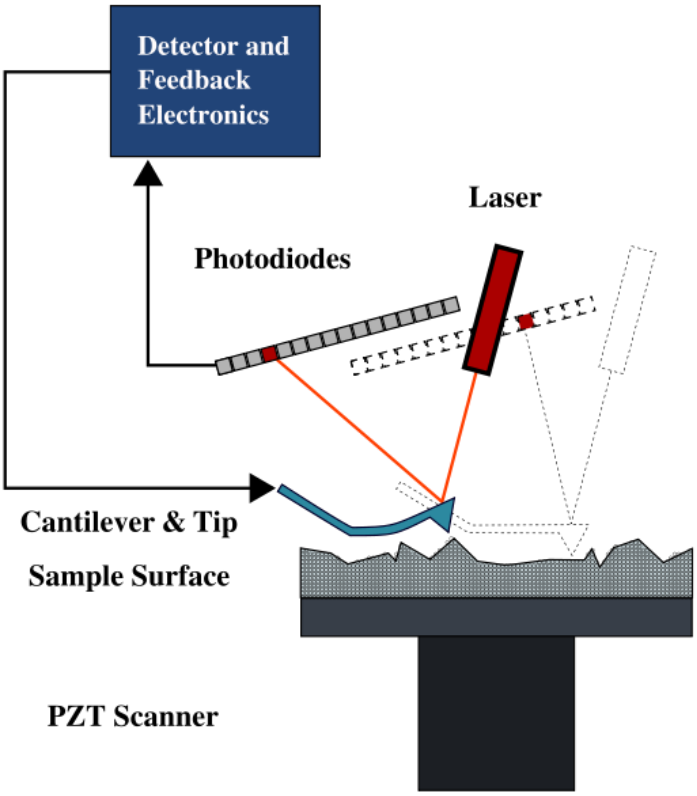

Figure 3. 5. Typical components of AFM and working principle [152]

The working principle is based on measurement of deflection of the cantilevers as a response to external forces. In order to detect this bending a laser beam is focused on the back of the cantilever. Laser beam is reflected from this position towards a position sensitive photodetector. The position of the reflected beam changes depending on the cantilever deflection. The photodetector converts this change to an electrical signal and surface structure is obtained from the alteration of vibration amplitude of the cantilever. The main types of imaging modes are; contact mode, non-contact mode and tapping mode. In thesis studies atomic force

microscope was used to examine microscopic details of self-assembled fibers and surface morphology of hybrid thermoresponsive films. Experiments were carried out by Solver microscope P47 (NT-MDT) with silicon cantilevers having different k values and surfaces were scanned at room temperature using tapping mode.

3.2.8. Differential Scanning Calorimetry (DSC)

DSC measures the temperatures and heat flows associated with transitions in materials as a function of time and temperature in a controlled atmosphere. These measurements provide quantitative and qualitative information about physical and chemical changes that involve endothermic or exothermic processes, or changes in heat capacity. In a DSC the difference in heat flow to the sample and a reference at the same temperature, is recorded as a function of temperature. The reference is an inert material such as aluminum pan. The temperature of both the sample and reference are increased at a constant rate. Since the DSC is at constant pressure, heat flow is equivalent to enthalpy changes:

$$\left(\frac{dq}{dt}\right)_p = \frac{dH}{dt}$$

Equation 3. 8

Here heat flow is dH/dt. The heat flow difference between the sample and the reference is:

$$\Delta\frac{dH}{dt} = \left(\frac{dH}{dt}\right)_{sample} - \left(\frac{dH}{dt}\right)_{reference}$$

Equation 3. 9

And can be either positive or negative. The calorimeter consists of a sample holder and a reference holder as shown in Figure 3.6.

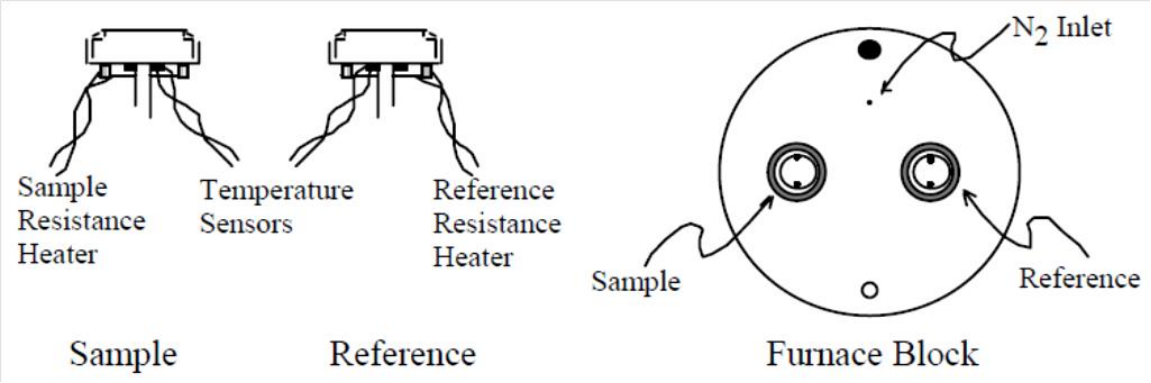

Figure 3. 6. DSC sample and reference holders

Under each holder are resistance heaters and temperature sensors. Currents are applied to the two heaters to increase the temperature at the selected rate. The difference in the power to the two holders, necessary to maintain the holders at the same temperature, is used to calculate ΔdH/dt. A flow of nitrogen gas is maintained over the samples to create a reproducible and dry atmosphere. The nitrogen atmosphere also eliminates air oxidation of the samples at high temperatures. TGA/DSC Q200 DSC instrument with cooling system was used to understand the thermal characteristics of self-assembled fibers and pure polymers.

3.2.9. Powder X-ray Diffraction (XRD)

Polymers are in many forms. They can be crystalline, microcrystalline or amorphous. In a single polymer, these three forms, depending on how the polymer was made and processed, could be together. The atoms in a crystal are arranged in a periodic array and can diffract light. Both neutron and X-ray wavelengths are comparable with inter-atomic distances and thus is an excellent probe for this length scale. W. L. Bragg explained this result by modeling the crystal as a set of discrete parallel planes separated by a constant parameter d. (figure 3.7).

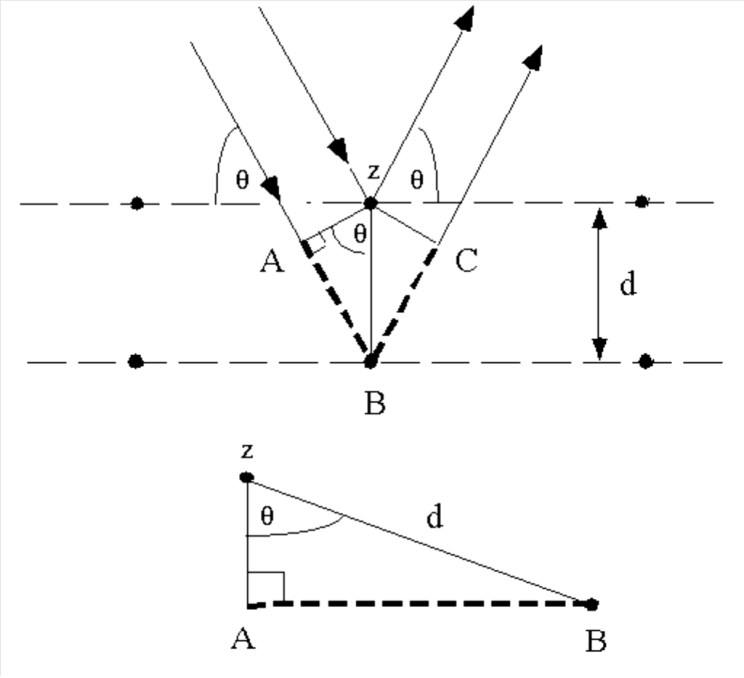

Figure 3. 7. Bragg Diffraction of two beams with identical wavelength and phase.

It was proposed that the incident X-ray radiation would produce a Bragg peak if their reflections off the various planes interfered constructively. Constructive

interference occurs only when nλ = AB + BC. The path difference between two waves undergoing constructive interference is given by $2d\sin\theta$, where θ is the scattering angle. This leads to Bragg's law, which describes the condition for constructive interference from successive crystallographic planes of the crystalline lattice:

$$2d\sin\theta = n\lambda$$

Equation 3. 10

In thesis studies self-assembled PEOX fibers formed in aqueous solutions were investigated with Bruker D2 Phaser X-ray Diffractometer. Also peak positions were calculated from the proposed model crystal structure in monoclinic unit cell with Materials Studio. It is a comprehensive materials modeling and simulation application, which allows scientists to design and analyze models of structures.

3.2.10. Contact angle measurements

The surface tension of solids, especially polymers with a low surface free energy cannot be measured directly. The general method is estimating the solid surface tension from that of the contacting liquid [148]. If we consider a liquid drop resting on a solid surface as shown in Figure 3.8, the drop is in equilibrium by balancing three forces, namely, the interfacial tensions between solid and liquid, *SL*; between solid and vapor, *SV*; and between liquid and vapor, *LV*. The contact angle, θ, is the angle formed by a liquid drop at the three-phase boundary where a liquid, gas and solid intersect.

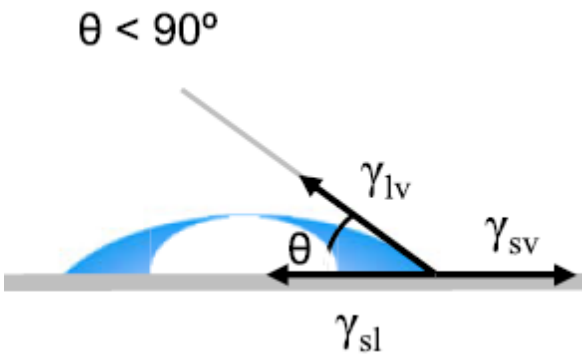

Figure 3. 8. Two-dimensional representation of a drop on a surface describing interfacial tensions as forces balanced along the x axis which results in Young's equation.

T. Young was the first to describe contact angle equilibrium, in 1804 [151], [153] . The vectorial summation of forces at the three-phase intersection point gives vectorial equilibrium for a drop of a liquid resting on a solid surface to balance three forces (interfacial tensions).

$$\gamma_{sv} = \gamma_{sl} + \gamma_{lv} \cos\theta$$

Equation 3. 11

where γ_{lv}, γ_{sv} and γ_{sl} represent the liquid-vapor, solid-vapor, and solid-liquid interfacial tensions respectively, and θ is the contact angle. Ideally, the shape of a liquid droplet is determined by the surface tension of the liquid. In a pure liquid, each molecule in the bulk is pulled equally in every direction by neighboring liquid molecules, resulting in a net force of zero. However, the molecules exposed at the surface do not have neighboring molecules in all directions to provide a balanced

net force. Instead, they are pulled inward by the neighboring molecules (figure 3.9) creating an internal pressure.

Figure 3. 9. Surface tension is caused by the unbalanced forces of liquid molecules at the surface

As a result, the liquid contracts its surface area to maintain the lowest surface free energy. Low values of θ indicate that the liquid spreads, or wets well, while high values indicate poor wetting. If the angle θ is less than 90° the liquid is said to wet the solid, with a contact angle of zero representing complete wetting. If it is greater than 90° it is said to be non-wetting. Two different approaches are commonly used to measure contact angles of non-porous solids, optical tensiometry (goniometry) and force tensiometry. Analysis of the shape of a drop of test liquid placed on a solid is the basis for optical tensiometry. Contact angle can be accessed directly by measuring the angle formed between the solid and the tangent to the drop surface. The primary focus of contact angle studies is the most direct measure of wetting. In thesis studies DataPhysics Instruments, Contact Angle System OCA20 was used to check the presence of thermoresponsive behavior on surfaces. Images of the droplets on the surfaces were recorded with integrated CCD camera to the set-up. Water contact angle values were calculated with SCA20 uEye 4.1.11 software by analyzing images.

CHAPTER 4: THERMORESPONSIVE BEHAVIOR OF POLY(2-ETHYL-2-OXAZOLINE)S IN AQUEOUS SOLUTIONS

4.1. Overview

Polymers which exhibit good solubility in aqueous solutions at low temperatures, but separate from the solvent above a certain temperature, called the cloud point temperature (T_c), have received much interest in recent years. Drastic changes in the solubility and other physicochemical properties as a function of temperature make them attractive for smart material applications. Therefore, precise modulation of T_c of the polymer is important for designing "smart" polymeric materials. Many studies were reported in the literature about the effect of hydrophobicity, ionization, and additives on the phase separation of aqueous poly(N-isopropylacrylamide) solutions with temperature, the best-known and extensively studied thermoresponsive polymer [36], [154–158]. Poly(2-isopropyl-2-oxazoline) (PIPOX), which is structural isomer of PNIPAM, recently gained attention. (PIPOX), which possess an isopropyl group in the side chain, is the only polymer which is both crystalline and soluble in water at room temperature [98]. Aqueous solutions have critical solution behavior in water and have LCST around 37 ºC, which is close to human body temperature [13], [99]. There are many studies in literature about PIPOX. They are mainly focused on synthesis and characterization [15], [75], [90], [91], [103], [104]. However, there are also many studies about the effect of LCST modulation of PIPOX aqueous solutions. It was

demonstrated that LCST of polyoxazolines can be tuned by; copolymerization [47], [76], [98], [105], molecular weight of the polymer [106] and end group modification [101], [106–108], varying solvent composition [109], [110], and also changing ionic strength of the aqueous solution [111]. Similarly, in a light scattering investigation of water solutions the second virial coefficient of PEOX was found to decrease with increasing temperature, indicating LCST behavior due to hydrogen bonding [102]. In another study it has been reported that aqueous PEOX solutions have a cloud point temperature around 62 – 65 °C depending on the molecular weight and NaCl addition caused decrease in the cloud point temperatures while tetrabutyl ammonium bromide increased it [11]. Aqueous solution behavior of polyoxazolines, carrying different alkyl side chains, were investigated recently in the presence of various salts [111]. It was reported that addition of NaCl to PIPOX, PPOX, and PEOX aqueous solutions caused decrease in cloud point temperature [102]. It was demonstrated that responses of the polymers to the salts depended significantly on their side chain. For most hydrophilic PEOX, Tc in water was tuned in a very large temperature range.

LCST can be tuned simply by addition of salts to the aqueous solutions. In many cases, the influence of the ions follows the Hofmeister series [114]. The ability of anions to influence polymer properties is more pronounced than cations [116]. The anion series is as follows:

$$CO_3^{2-} \rangle SO_4^{2-} \rangle S_2O_3^{2-} \rangle H_2PO_4^- \rangle F^- \rangle Cl^- \rangle Br^- \approx NO_3^- \rangle I^- \rangle ClO_4^- \rangle SCN^-$$

Basically, species to the left of Br^- are called kosmotropes, which are strongly hydrated anions, and have been shown to salt polymers out of the solution. On the

other hand, species to the right are called chaotropes and are known to increase the solubility of polymers in solution [159]. Despite the wide range of studies on water soluble macromolecules that follow this series, an underlying molecular level description of the mechanism is still far from complete.

Three different mechanisms were proposed to explain the effect of Hofmeister anions on the T_c of aqueous PNIPAM solutions [124]. These mechanisms were related with the interaction of anions with the water molecules bonded to polymer, increase in free energy of alkyl/water interface with addition of anions, and direct binding of anions to the polymer. The effect of series of Hofmeister salts on T_c of aqueous PEOX solutions has not been studied before. In this part of the thesis aqueous solution behavior of PEOXs were investigated as a function of temperature. In section 4.3.1 methods for cloud point determinations are presented. The influence of molecular weight of the PEOX on LCST is presented in section 4.3.2. To understand the effect of anions on polymer – polymer and polymer – water interactions, aqueous environment around the PEOX was studied with addition of sodium salts of Hofmeister anion series and by variation of salt concentration of solutions in section 4.3.3. Obtained results were explained with the mechanisms previously proposed for PNIPAM in section 4.4. Comparison of the results of PNIPAM and PEOX aqueous solutions are presented in section 4.4. Our results indicate that the dominant mechanism in T_c modulation of aqueous PEOX solutions is the dehydration of PEOX chains for divalent kosmotropic anions and direct ion binding for chaotropic anions. For monovalent kosmotropic anions, combination of dehydration and surface tension mechanisms were proposed. Weaker dependence on T_c with kosmotropic ion concentration was found for PNIPAM and attributed to the different chemical structure of the polymer.

4.2. Experimental details

Dynamic light scattering (DLS) was used to probe the aggregation process of PEOX solutions as a function of temperature. PEOX having 500,000 g/mol, 200,000 g/mol, 50,000 g/mol and 5,000 g/mol molecular weight were chosen for cloud point temperature determination. Solution concentrations were kept constant at 1 mg/ml. The duration of each measurement was 10 seconds and 3 measurements were taken for each temperature. Each of 3 measurements is an arithmetic mean of 10 measurements. Equilibration time at the set temperatures was 3 minutes. During these studies, temperatures of the aqueous solutions were varied between 20 to 70 °C. The hydrodynamic diameter of particles was determined according to intensity distribution. The detectable size range of the instrument is 0.6 nm – 6000 nm therefore particle size out of this range was appeared as 0. During the DLS measurements viscosities of aqueous PEOX solutions at different temperatures were used. Aggregate sizes were plotted against temperature and critical temperatures (cloud point temperatures) were determined by linear fits at the transition.

As another method of T_c determination, absorbances of 1 mg/ml aqueous PEOX solutions were also investigated at different temperatures (20 to 70 °C) by UV-Vis spectroscopy. Before each measurement, background was taken with water. Then, the prepared solution was put into glass cuvette (path length = 1 cm). The cuvette was placed in the sample holder of the instrument and measurements were done while changing temperature. Equilibration time for each temperature was chosen as 3 min. Phase separation causes significant decrease in transmitted intensity (I_1) due to scattering of light. The temperature at which

absorbance ($A = -\log\left(\frac{I_1}{I_0}\right)$) increased sharply, was assigned as the cloud point temperature. To analyze kinetics of aggregation, absorbance change (as base line increase) was investigated at a specified wavelength of 600 nm as a function of temperature.

To understand the effect of anions on polymer – polymer and polymer – water interactions, aqueous environment around the PEOX was studied with addition of sodium salts of Hofmeister anion series (Na_2CO_3, Na_2SO_4, $Na_2S_2O_3$, NaH_2PO_4, NaF, NaCl, NaBr, $NaNO_3$, NaI, $NaClO_4$, and NaSCN). In addition, salt concentrations were varied in between 0 to 1 M to investigate the effect of salt concentration on T_c.

4.3. Results

4.3.1. Determination of cloud point temperatures of aqueous Poly(2-ethyl-2-oxazoline solutions

In DLS studies homogenous solutions were heated in the temperature range from 20 to 70°C with 1°C increments and sizes of the aggregates were recorded. The obtained data points were plotted as particle size versus temperature and the value of T_c was approximated through linear fits at the transition region (Figure 4.1).

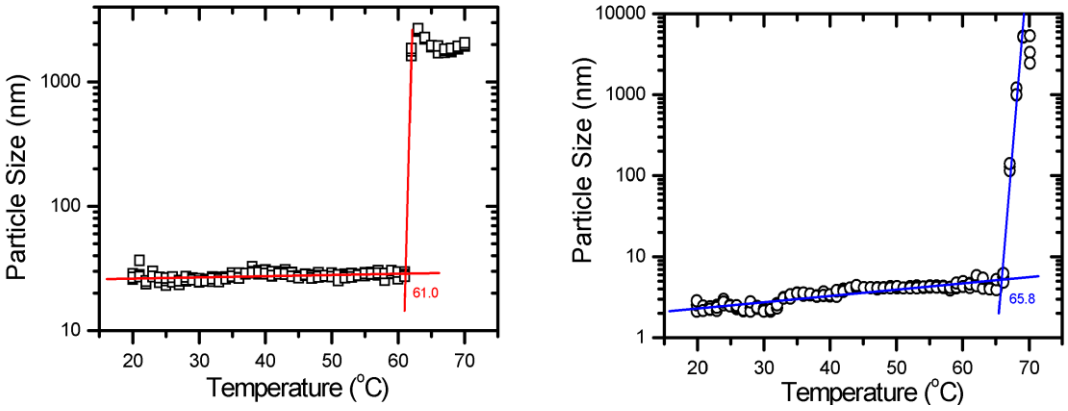

Figure 4.1. DLS data of 1mg/ml aqueous solutions of a) PEOX – 500K and b) PEOX – 5K.

As seen clearly in Figure 4.1, particle size increased sharply at a certain temperature. The cloud point temperature was determined by the intersection of linear fits to the data points before and after the transition. Cloud point temperatures were approximated as 61.0 °C and 65.8 °C for PEOX-500K and PEOX-5K, respectively.

To confirm the T_c values by another method, absorbance of the solutions were measured at visible wavelengths. The phase separation was probed by the intensity of the transmitted light in the range of 400 nm to 900 nm as the turbidity of the solution changed with temperature.

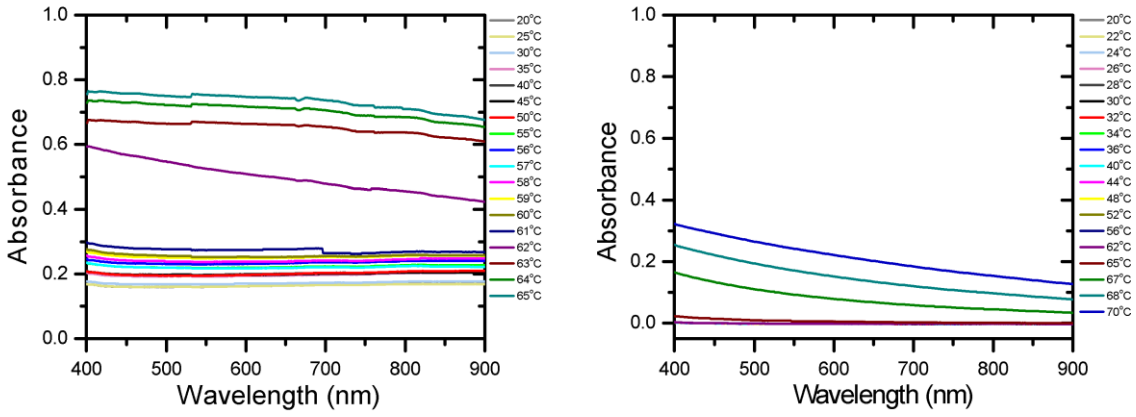

(a) (b)

Figure 4. 2. Temperature dependent change of the UV-Visible absorbance between 400-900 nm for 1.0 mg/ml a) PEOX – 500K and b) PEOX – 5K solutions recorded at temperature range between 20 °C – 70 °C

Figure 4.2 shows the change in absorbance values of polymer solutions as a function of temperature. Absorption values were nearly constant up to a certain temperature after which significant increase in absorbance was observed. Since polyoxazolines do not show any characteristic absorbance peak in the range of 400-900 nm, absorbance changes were due to scattering of the light from the phase separated large domains (aggregates) which decreased the intensity of the transmitted light. We plot absorbance as in absorption spectroscopy as defined by “write the formula”. Figure 4.3 shows the absorbance as a function of temperature at wavelength of 600 nm for the data of Figure 4.2.

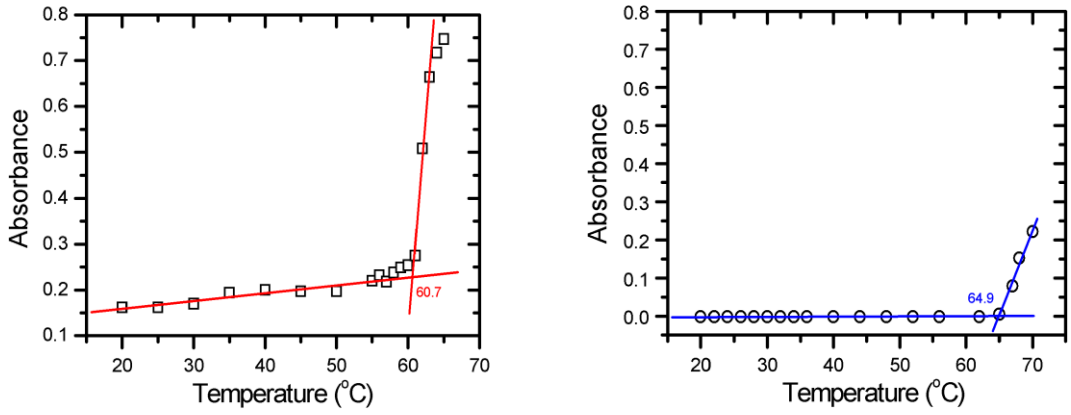

(a) (b)

Figure 4. 3. Turbidity curves as determined by absorbance at 600 nm showing the phase separation of a) PEOX – 500K and b) PEOX – 5K solutions having concentrations of 1 mg/ml. .

T_c values were approximated by linear fits at the transition as 60.7 °C for PEOX-500K and 64.9 °C for PEOX-5K solutions, respectively. The cloud point temperatures of solutions determined by DLS (figure 4.1) and by absorbance at visible wavelengths (figure 4.3) are in agreement with each other. Further measurements were carried out by DLS, because of its better sensitivity and better detection limit down to nanometer sizes.

4.3.2. Effect of M_w of PEOX on cloud point temperature of aqueous solutions

T_c values of polymer solutions were determined by DLS measurements. A homogenous solution of polymer in water was heated in the temperature range

from 20 to 70°C with 1 °C increments. The particle sizes were plotted against temperature and the value of T_c for each specific concentration was then approximated through linear fits (see exemplary graph in figure 4.1). Next the values for T_c against the concentration of polymers were recorded. Finally concentration and temperature for the lowest point of the curves were assigned as LCST (figure 4.4).

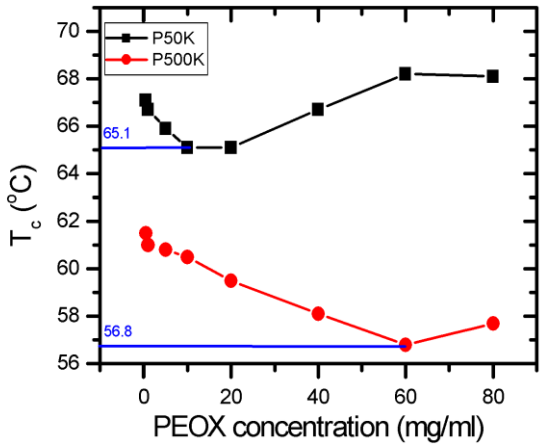

Figure 4. 4 T_c values of (black squares) PEOX-50K and (red dots) PEOX-500K

As the molecular weight of the polymer increases, LCST decreases. The obtained values for the LCST and critical concentration for both measured PEOX-500K and PEOX-50K are 60 mg/ml and 56.8 °C, 20 mg/ml and 65.1°C respectively. To understand the effect of molecular weight on T_c, we have also studied with PEOX-200K and PEOX-5K. Their concentrations were kept constant at 1 mg/ml, and cloud point temperatures were determined by DLS as mentioned previously. Then these temperatures were graphed as a function of PEOX molecular weight (figure 4.5).

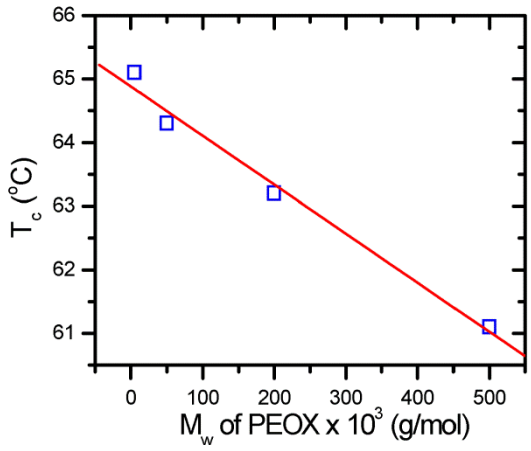

Figure 4. 5 T_c as a function of PEOX molecular weight

In Figure 4.5, T_c vs. PEOX molecular weight graph is shown. Red line is linear fit to data. It is clearly seen that, T_c decreases with increasing molecular weight. The higher cloud points of shorter polymers can be ascribed to the stronger influence of the end groups.

4.3.3. Effect of salts on cloud point temperature of aqueous PEOX solutions

To establish a more detailed insight into the effect of salts on the solution behavior of PAOXs, the solubility behavior of PEOX in the presence of sodium salts of Hofmeister anion series was investigated by DLS measurements. Electrolytes have been used as additives because they interact more strongly with water and with polymers compared to nonelectrolytes. The ions affect the hydration of the PEOX chains and change the T_c of the solutions significantly. 1

mg/ml PEOX solutions were prepared in water. Various sodium salts (Na_2CO_3, Na_2SO_4, $Na_2S_2O_3$, NaH_2PO_4, NaF, NaCl, NaBr, $NaNO_3$, NaI, $NaClO_4$, and NaSCN) were added at salt concentrations varying between 0 to 1 M. Homogenous solutions were heated in the temperature range from 20 °C to 70 °C with 1 °C increments in DLS. The obtained data points from aqueous PEOX-500K solutions containing 0.2 M NaSCN (triangles) and 0.2 M Na_2CO_3 (circles) were plotted as a function of temperature in Figure 4.5 (b).

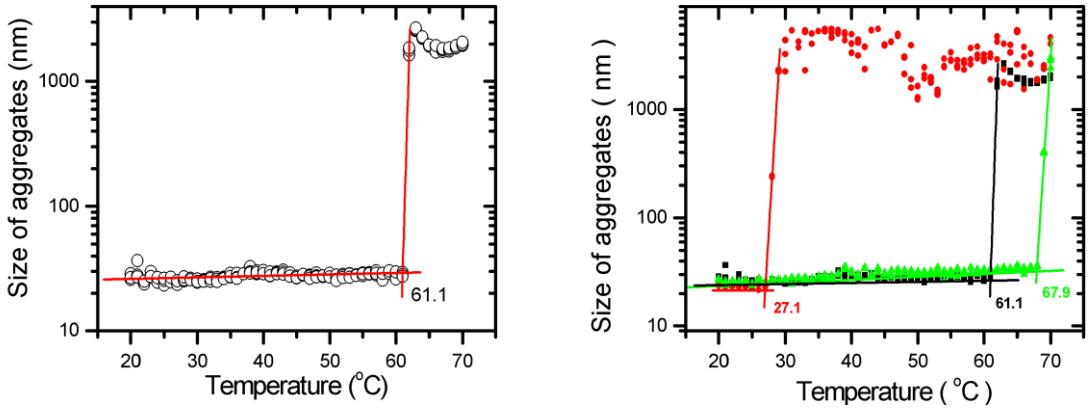

(a) (b)

Figure 4. 6. Cloud point temperatures of 1 mg/mL aqueous PEOX-500K solutions as determined by DLS a) in water, b) in water (black squares), in 0.2M Na_2CO_3 (red circles), and in 0.2 M NaSCN (green triangles).

T_c for solutions, which were prepared in water, 0.2 M Na_2CO_3 and 0.2 M NaSCN, were approximated through linear fits as 61.1, 27.1 and 67.9 °C, respectively. Addition of kosmotropic Na_2CO_3 to the solution decreased the cloud point temperature while the chaotropic NaSCN increased it. To understand the mechanism by which the salt affects T_c, salt concentrations were varied. Figure 4.6

shows the change in T_c values of 1 mg/ml PEOX-500K solutions as a function of salt concentration.

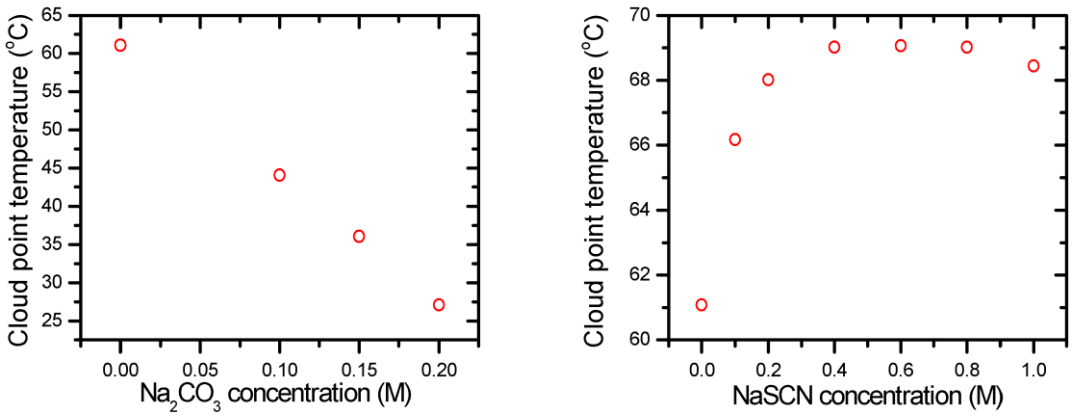

(a) **(b)**

Figure 4. 7. Cloud point temperatures of 1 mg/ml PEOX in a) Na_2CO_3 and b) NaSCN solutions

Linear decrease in cloud point temperature with increasing salt concentration was observed for Na_2CO_3. Cloud point temperature increased slightly and non-linearly with addition of NaSCN indicating that different mechanisms were responsible for the two salts. The initial increase in the case of NaSCN was followed by decrease at larger salt concentrations.

Changes in T_c of aqueous PEOX solutions in the presence of other sodium salts, Hofmeister anion series, were also investigated.

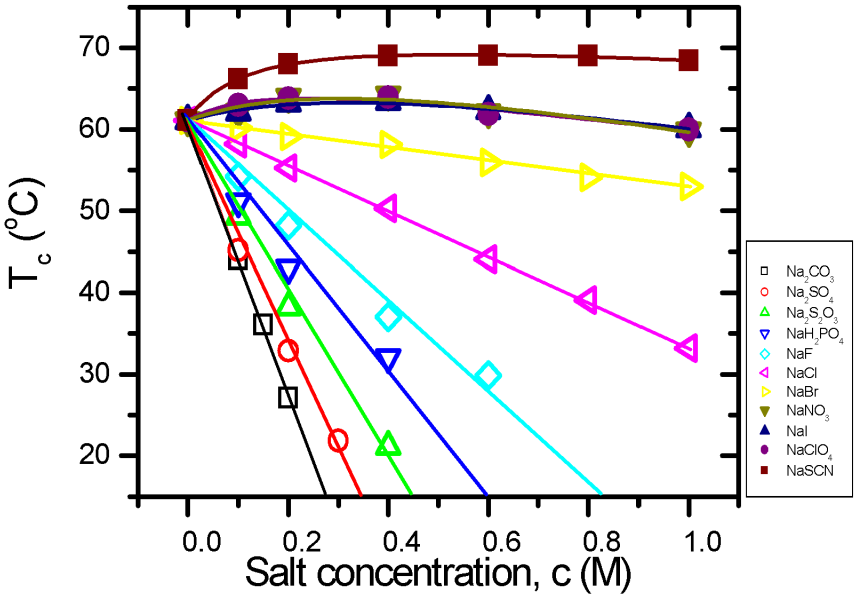

Figure 4. 8. The change of Tc of 1 mg/ml aqueous PEOX-500K solutions with the concentration of various sodium salts. For kosmotropic anions, the solid lines are linear fits to the data (open symbols). For chaotropic anions, the solid lines are binding isotherm fits to the data (closed symbols).

Figure 4.8 shows the effect of series of Hofmeister anions on T_c of aqueous PEOX-500K solutions. In the presence of kosmotropic anions T_c decreased linearly with increasing salt concentrations. T_c changes non-linearly in the presence of chaotropic anions. Initial increases of T_c's in dilute salt solutions are followed by decreases in concentrated salt solutions. Solid lines and curves are linear and nonlinear fits to the data points and equation parameters were discussed in the following section.

4.4. Discussions

It was found that T_c decreases as the molecular weight of the polymer increases. LCST values for PEOX-500K and 50K are 56.8 and 65.1 °C respectively. It has been previously shown that LCST value for PEOX-500K and 50K are 61 and 63 °C, respectively, according to visual observations [11]. Differences can be caused by the used techniques for LCST determination. It is well known that the higher molecular weight species will undergo the phase transition at smaller temperatures, which leads solution into thermodynamically unstable region [64] . It was shown that LCST in water strongly depends on the polarity of the terminal group of the chain [106]. Introduction of hydrophobic groups decreases LCST while hydrophilic ones increase it [101], [107], [108], [113]. For polymers, which have same end-caps in their backbone end, increasing molecular weight cause decrease in effect of end groups on T_c.

Changes in the cloud point temperature of PNIPAM with added salts were recently explained with a model [124]. Three different mechanisms, which are dehydration, surface tension and direct ion binding, were introduced for the interaction of Hofmeister anions with PNIPAM in aqueous solutions.

In the dehydration mechanism polarization of water molecules around the polymer (hydrogen bonded to polymer) in the presence of salts cause dehydration and decrease its solubility. In figure 4.9 interactions were shown for PEOX and PNIPAM together.

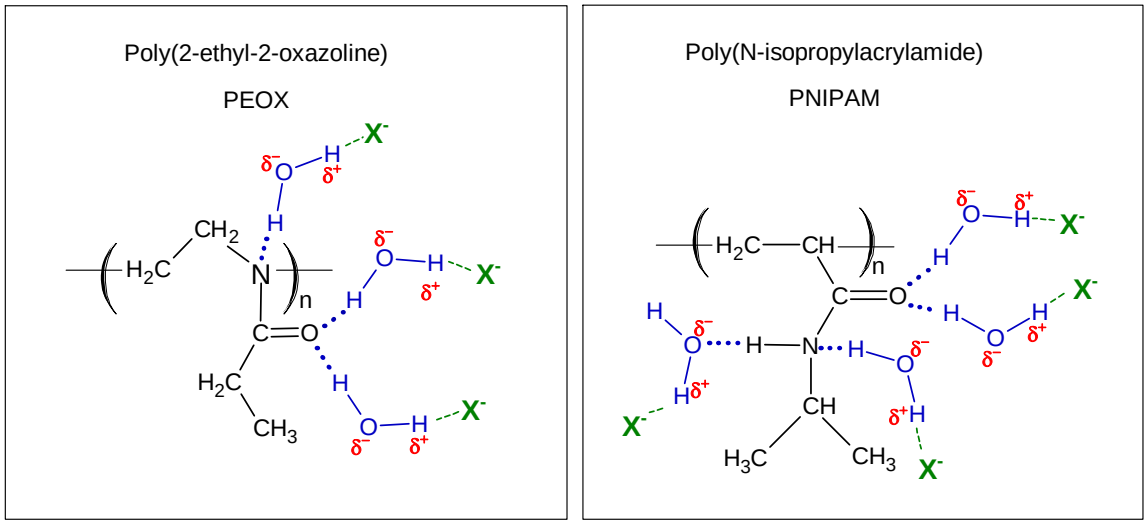

Figure 4. 9. Polarization of water molecules around PEOX and PNIPAM

With addition of ions surface tension at the hydrophobic/aqueous interface will increase. As a result, polymer will try to minimize its surface area to decrease the energy of the system by contraction. It will salt polymer out of the solution and decrease the cloud point temperature (figure 4.10).

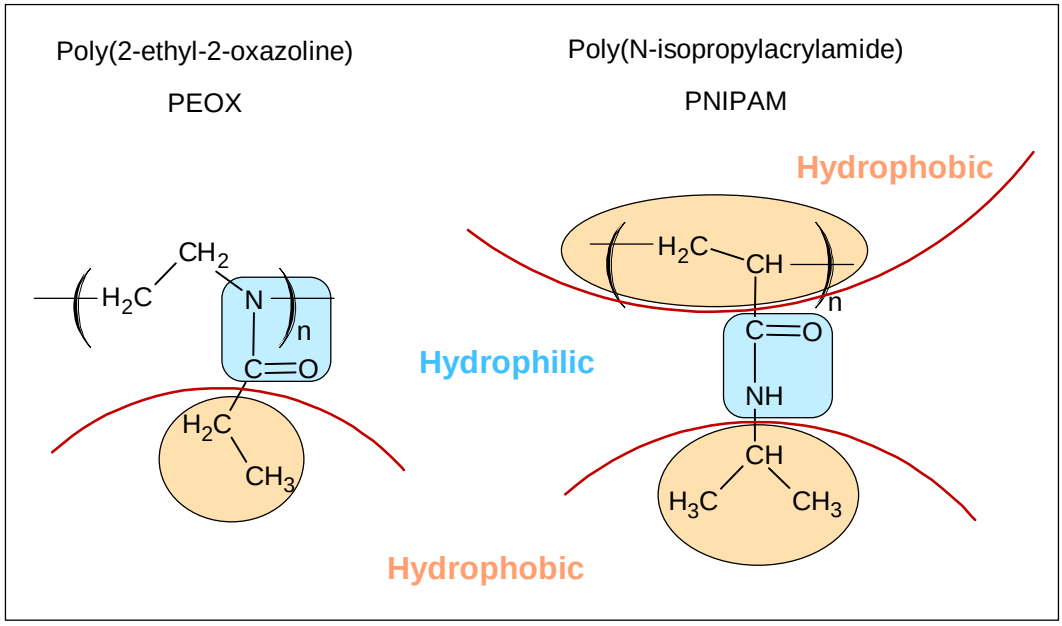

Figure 4. 10. Surface tension of water at the hydrophobic/aqueous interface of PEOX and PNIPAM

Improvement of hydration by direct ion binding increases the solubility and the critical temperature (figure 4.11).

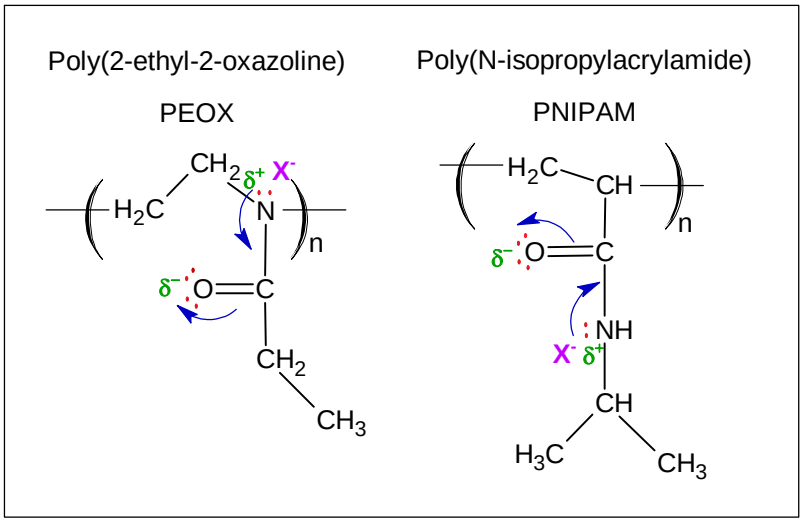

Figure 4. 11 Improvement of hydration by direct ion binding

Polarization of water molecules around the polymer in the presence of salts and surface tension of water at the polymer/water interface vary linearly with salt concentration. This mechanism applies to both kosmotropic and chaotropic salts. Salting in effect due to direct ion binding to the polymer is considered as saturation phenomenon and modeled with Langmuir binding isotherm.

In figure 4.8 solid lines for open symbols (kosmotropic anions) are fit to the following linear equation (Give numbers to equations):

$$T_c = T_c^0 + c.s$$

Equation 4. 1

where T_c is the critical temperature of the solution in the presence of salts and the constant T_c^0 is the T_c of 1 mg/ml aqueous solution of PEOX-500K and its value is 61.1 °C. c is the salt concentration and s term represents the slope of the linear decreases. Their fitting parameters were given in Table 4.1.

Table 4. 1 Fitting parameters of kosmotropic anions for T_c versus c curve in figure 4.7

Anions	Slope, s (°C/M)
CO_3^{2-}	-169.0
SO_4^{2-}	-135.7
$S_2O_3^{2-}$	-103.4
$H_2PO_4^-$	-77.2
F^-	-55.5
Cl^-	-27.8
Br^-	-8.3

The slope of the linear fits decreases in the order of $CO_3^{2-} > SO_4^{2-} > S_2O_3^{2-} > H_2PO_4^- > F^- > Cl^- > Br^-$. This order is in agreement with the order of Hofmeister anions.

In figure 4.8 solid curves for the closed symbol data are fit to an equation containing salting out and salting in parameters together. Perturbations in critical temperatures of polymer by addition of chaotropic salts were expressed by an equation:

$$T_c = T_c^0 + c.s + A.\left(\frac{K_C}{1+K_C}\right)$$

Equation 4. 2

First two terms are same with Equation 4.1 and responsible from salting – out contribution. Salting – in effect due to direct ion binding to the polymer was considered as saturation phenomenon and modeled with the Langmuir adsorption isotherm (third term in Equation 4.2). Here K_c represents the binding constants of anions and A is maximum shift in cloud point temperature due to direct ion binding. Fitting parameters were tabulated in Table 4.2.

Table 4. 2 Fitting parameters of chaotropic anions for T_c versus c curve in figure 4.7

Anions	Slope, s (°C/M)	A (°C)	K_c (M^{-1})
NO_3^-	-7.2	8.6	4.0
I^-	-10.1	13.0	2.2
ClO_4^-	-7.6	7.5	6.3
SCN^-	-3.5	12.3	8.0

In dilute salt condition, direct anion binding mechanism dominates and T_c increases up to a plateau A. Further increase in salt concentrations causes decrease in T_c due to dominating salting – out contribution of dehydration and surface tension mechanisms. As a result initial increase in T_c and further decrease cause a peak in the curve where maximum points are close to “A” value in Equation 4.2.

Dehydration and surface tension mechanisms may contribute to the linear decrease in T_c. Electron distribution in the hydrogen bonds changes with addition of kosmotropic salts to the polymer solution. Attractions of water molecules by

anions cause breakage of hydrogen bond between polymer and water and salts polymer out of solution. As a result T_c decreases. It is well known that surface tension of salt containing solutions increases linearly with increasing salt concentrations [160]. Free energy of the alkyl/water interface also increases in dissolved polymer solutions. This triggers aggregation of polymer to minimize surface area of the interface and decreases T_c of the solution. Contributions of dehydration and surface tension mechanisms were investigated by relating the fitted slope (s) in Equation 4.2 with the hydration entropy ($\Delta S_{hydration}$) and surface tension increment ($\Delta\sigma$) of anions in figure 4.12.

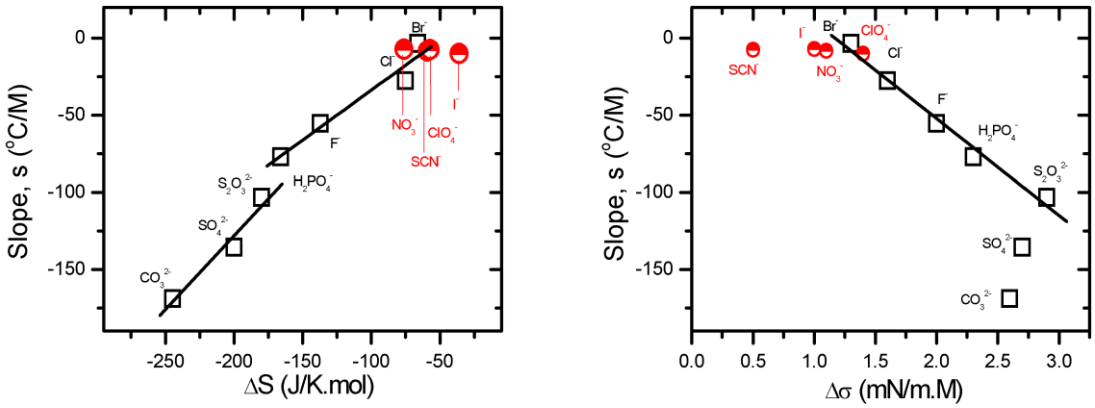

Figure 4. 12. Slope s in Equation 4.2 as a function of a) hydration entropy ($\Delta S_{hydration}$) and b) surface tension increment ($\Delta\sigma$) of anions. Open squares represents kosmotropes and half filled red circles for chaotropes.

Solid lines in Figure 4.12 a) are linear fits to the data. Sharper increases in slopes were observed for divalent anions as expected. It may be related with the stronger interactions between divalent anions and water. For these three anions

dehydration mechanism should be dominant. Change of the slope from divalent to monovalent anions may be explained also by increase in contribution of surface tension mechanism. Solid line is a linear fit to the data for anions Br^-, Cl^-, F^-, $H_2PO_4^-$ in figure 4.12(b). Decrease in the slope from CO_3^{2-} to $S_2O_3^{2-}$ caused increase in surface tension increment Δσ. Values of Δσ for CO_3^{2-}, SO_4^{2-} and $S_2O_3^{2-}$ anions are nearly same with each other but their slopes are very different. It suggests that dehydration contribution of the salting – out effect is dominant for CO_3^{2-} to SO_4^{2} anions. However this inverse relationship is not valid for the other kosmotropes. Δσ values are decreasing with decreasing slopes of kosmotropic anions. Therefore surface tension mechanism plays an important role in decreasing their solubilities. The slope "s" did not show any correlation with hydration entropy and surface tension increments for chaotropic anions. It indicates that direct ion binding is the dominant mechanism for chaotropic anions. The values of $\Delta S_{hydration}$ and Δσ were obtained from literature [124] and tabulated in table 4.3.

Table 4. 3 Hydration entropy ($\Delta S_{hydration}$) and surface tension increment ($\Delta\sigma$) values used for the analysis

Anion	$\Delta S_{hydration}$ (J/K.mol)	$\Delta\sigma$ (mN/m.M)
CO_3^{2-}	-245	2.6
SO_4^{2-}	-200	2.7
$S_2O_3^{2-}$	-180	2.9
$H_2PO_4^-$	-166	2.3
F^-	-137	2.0
Cl^-	-75	1.6
Br^-	-59	1.3
NO_3^-	-76	1.1
I^-	-36	1.0
ClO_4^-	-57	1.4
SCN^-	-66	0.5

Similar behavior has also been observed for the 1mg/ml aqueous solutions of different molecular weight PEOX samples and widely studied thermoresponsive polymer PNIPAM as shown in Figure 4.13.

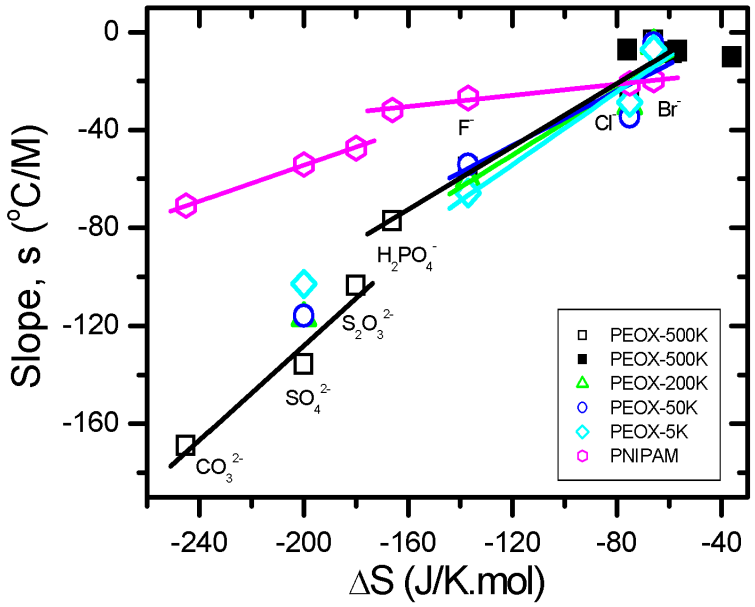

Figure 4. 13. The plot of slope, s as a function $\Delta S_{hydration}$ for 1mg/ml different molecular weights PEOX and PNIPAM (open images) solutions. Closed squares for chaotropic anions of PEOX-500K

Black solid lines in figure 4.13 are fits to the slopes of divalent and monovalent anions of PEOX-500K. For the divalent anions, fitted line is sharper than monovalent anions as mentioned before. Linear fits for the monovalent anions of different molecular weight PEOX samples are close to each other. Therefore it can be concluded that similar mechanisms are responsible for the thermoresponsive behavior. Pink solid lines are linear fits for the divalent and monovalent anions of PNIPAM solutions. The data of PNIPAM also showed similar behavior with PEOX samples. PNIPAM showed weaker dependence on $\Delta S_{hydration}$ compared to PEOX samples. It may be referred to its different chemical structure. Basically PNIPAM

can make more hydrogen bonds with water per monomer compared to PEOX. PNIPAM has secondary amides in its structure, and behave as hydrogen donor and acceptor thus requires more ions for dehydration.

4.5. Conclusions

T_c of solutions were determined by DLS and also confirmed by absorbance measurements at visible wavelengths. It was demonstrated that both techniques gave similar results. Increase in PEOX concentration caused decrease in T_c to a minimum, which was defined as LCST, and further increase caused increase in T_c. Increased molecular weight of PEOX caused decrease in LCST and increase in critical concentration. In addition, T_c was probed for 1 mg/ml different molecular weight PEOX solutions. T_c was found to be decreasing linearly with increasing molecular weight. The higher cloud points of shorter polymers were attributed to the stronger influence of the end groups.

Influences of Hofmeister anions on T_c of aqueous PEOX solutions were investigated as a part of this thesis and published recently [161]. Contribution of different mechanisms in T_c change for the Hofmeister anion series were identified mainly for PEOX aqueous solutions. For divalent kosmotropic anions the dominant mechanism was proposed as the dehydration of PEOX chains. For monovalent kosmotropic anions a combination of dehydration and surface tension mechanisms was responsible for the change of T_c. Similar behaviors were also observed for different molecular weight PEOX and PNIPAM solutions. Weaker dependence on hydration entropy was found for PNIPAM and attributed to the chemical structure difference. The s values for chaotropic anions did not show any correlation with

hydration entropy and surface tension increments. It indicates that direct ion binding is the dominant mechanism for chaotropic anions.

CHAPTER 5: SELF ASSEMBLY OF PEOX ABOVE CLOUD POINT TEMPERATURE IN AQUEOUS SOLUTIONS

5.1. Overview

In self-assembly process, ordered structures spontaneously form from disordered components with minimal human or machine intervention [162]. Molecular self-assembly is driven by non-covalent interactions such as electrostatic, dipolar, Van der Waals and hydrogen bonding. The water mediated interactions are especially important for living systems because most of the biomolecules including peptides and proteins self-assemble themselves in aqueous environment to form well-defined functional structures. Compared to complexity of protein molecules, polypeptides and synthetic polymers act as simple model systems to understand the self-assembly mechanisms. Poly(2-isopropyl-2-oxazoline) (PIPOX) is the structural isomer of polypeptide “polyleucine” and also thermoresponsive polymer PNIPAM [163]. Polyleucine is a crystallizable, water insoluble polypeptide. On the other hand, PNIPAM is a water soluble amorphous polymer and exhibit lower critical solution behavior around 31 °C depending on its molecular weight [6]. PIPOX is soluble in water at room temperature. It is thermoresponsive like PNIPAM, but at the same time it can crystallize like polyleucine [75]. LCST value of PIPOX is close to human body temperature (~ 38 °C) and can be varied between 10 to 70 °C by changing molecular weight [102], concentration of polymer in solution [100], end group modification [112], copolymerization [105], [112], [76], and by addition of salts [100], [111]. Typically,

lower critical solution behavior is reversible with small hysteresis between heating and cooling cycles. However, it was reported that annealing dilute aqueous solutions of PIPOX above its cloud point temperature cause irreversible formation of micron-sized coagulate particles[13]. In similar conditions PNIPAM did not form any kind of coagulate above its T_c. Formation of these particles was explained in a subsequent study by self-assembly into crystalline structures which was driven by both hydrophobic and dipolar interactions [12]. Increase in the mobility of backbone by solvation of PIPOX dipoles was also proposed to contribute to crystallization process. As such, self-assembly of PIPOX in aqueous solutions is reminiscent of self-assembly of polypeptides and proteins. Furthermore, PIPOX crystallization in hot water was directly monitored by wide angle X-Ray scattering (WAXS) measurements [132]. The sharpness of the peaks increased sigmoidally with time. This was interpreted as the sign of typical nucleation and growth type crystallization mechanism. Neither the thermodynamic factors affecting the self-assembly process nor its mechanism is yet well-understood. Also, the generality of the self-assembly process for polyoxazolines other than PIPOX was not known.

First studies about the crystallinity of polyoxazolines carrying linear alkyl groups showed that poly(2-ethyl-2-oxazoline) (PEOX) was not crystallizable in bulk [14], [81]. In a more recent study, polyoxazolines with short alkyl side chains (methyl, ethyl and propyl) were found to be amorphous [15]. Although similar interactions are present in other polyoxazolines carrying shorter alkyl side chains and they exhibit thermoresponsive behavior, crystallization in bulk or self-assembly in aqueous solutions above the T_c have not previously been observed.

This chapter reports on the self-assembly of PEOX in aqueous solutions above its critical temperature. The effect of model salting-in (sodium acetate) and salting-out (sodium isocyanate) salts on self-assembly kinetics and mechanism were also presented. Irreversible formation of PEOX fibers in water and in the presence of salt solutions were observed for the first time in aqueous solutions above the cloud point temperature. Morphology investigations of self-assembled structures were carried out by optical microscopy, and scanning electron microscopy (SEM). Microscopic results are shown in section 5.3.1. Thermal properties of the self-assembled fibers and pristine PEOX, for comparison, were studied with differential scanning calorimetry (DSC) and observed heating curves are presented in section 5.3.2. The crystallinities of the self-assembled fibers were analyzed by powder X-ray diffraction (XRD) technique and reported in section 5.3.3. In discussion section, the effect of salts on self-assembly kinetics and the comparison of measured spacings between polymer chains with the previously reported data [14] are presented. A structural model was proposed for the self-assembled crystalline fibers.

5.2. Experimental Details

For self-assembly studies PEOX (Mw ~ 500,000 g/mol) was chosen because of its lower T_c. Polymer concentration in water was kept constant at 1 mg/ml during all studies. The effect of salting-in (sodium thiocyanate, NaSCN) and salting-out (sodium acetate, NaAc) salts were investigated by preparing polymer solutions in 0.2 M salt solutions. DLS technique was used to understand the aggregation kinetic during self-assembly process as described previously. Optical microscope

was used to observe the aggregates in aqueous solutions. The samples were prepared on solid substrates by solvent casting for microscopy measurements. 200 µl of a solution, which is containing self-assembled fibers, were taken by a micropipette, dropped onto glass slides or silicon wafers and then solvent was evaporated in vacuum at room temperature to observe self-assembled fibers under microscope. The image from optical microscope was captured by CCD camera. SEM was used to examine self-assembled fibers in detail. DSC was used to understand the thermal characteristics of self-assembled aggregates and pure polymers. Self-assembled aggregates were freeze dried for DSC and XRD investigations. Measurements were performed by using aluminum hermetic pans and lids. The heating/cooling rate was kept constant at 10 ºC/min under nitrogen flow of 50 mL/min. PEOX fibers, formed above T_c in aqueous solutions, were investigated by powder x-ray diffraction measurements. Peak positions were calculated for the model crystal structure having monoclinic unit cell by Materials Studio. The initial structure was then refined such that the calculated XRD peaks by software replicated the experimental XRD data.

5.3. Results

5.3.1. Self-assembled PEOX fibers in aqueous solutions

1 mg/ml PEOX solution was prepared in water and cloud point temperature (T_c) of the solution was determined as 61 °C by DLS as described in Chapter 4. When PEOX solution was kept at 70 °C, which is above the T_c, for several weeks, aggregates were formed in solution. When solution was cooled to room temperature, aggregates were not dissolved. It indicates irreversible aggregation. Aggregates were placed on to silicon substrates and investigated by optical

microscope to observe their morphologies. In figure 5.1 room temperature photographs of the a) freshly prepared PEOX aqueous solution, and b) formed aggregates after 45 day annealing at 70 °C are presented. Also optical micrograph of the aggregates is shown in figure 5.1.c.

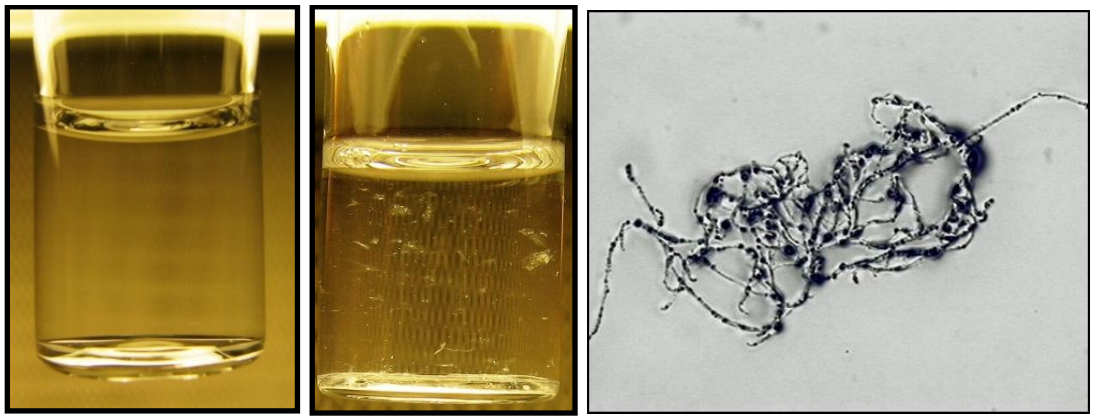

(a) **(b)** **(c)**

Figure 5. 1 Pictures of PEOX solutions a) after preparation, b) after keeping the solution at 70 °C for 45 days. c) optical micrograph of the aggregates in solution of (b).

Aggregates were formed of entangled fibers having average diameter of 3.8 ± 0.8 μm. The formation rate of these aggregates was slow and required weeks to be visible by naked eye. Consequently, amount of obtained aggregates was not enough for further analysis. Increasing the concentration of PEOX solution to 10 mg/ml decreased the cloud point slightly by 1 °C but did not increase the aggregation rate. In concentrated solutions, entanglements of the chains and slower relaxations prevented the self-assembly into well defined shapes.

When 1 mg/ml aqueous PEOX solution was prepared in 0.2 M NaAc solution, 6 °C decrease in cloud point temperature was observed. Addition of salting-out constituent to the polymer solution increased the aggregation rate. Aggregates were visible to the naked eye within a week. Annealed PEOX aqueous solution in the presence of NaAc was cooled back to room temperature and photographed (figure 5.2 a). Aggregates were placed on to a silicon substrate and investigated by optical microscope (figure 5.2 b). In addition, annealed PEOX-NaAc solution was spin coated on a silicon substrate and morphology of the aggregates were further investigated by SEM (figure 5.2 c).

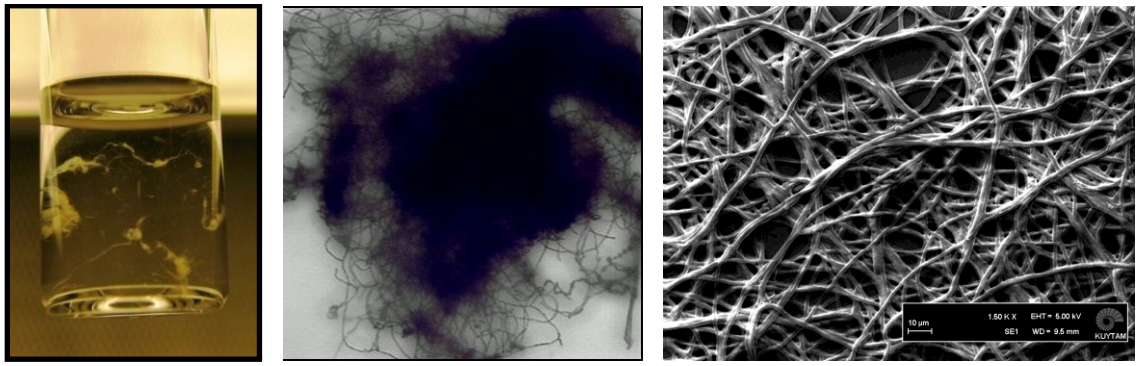

(a) **(b)** **(c)**

Figure 5. 2 Picture of PEOX solution in 0.2 M NaAc after keeping the solution at 70 °C for 7 days. b) Optical micrograph of the aggregates in solution of (a). c) SEM image of the spin coated aggregates on silicon surface.

Aggregates were denser compared to those in pure water and formed of entangled fibers as seen at the perimeter of the aggregate in optical micrograph. SEM image in figure 5.2 shows that fibers have an average diameter of 2.7 ± 0.5 µm and maintained their shape in the dry state when spin coated on solid

substrate. Fibers formed both in pure water and in the presence of NaAc when the solutions were kept above T_c. This means fiber formation was not due to salting-out of the polymer in NaAc solution. Experiments were repeated for the PEOX solution, which was prepared in 0.2 M NaSCN solution, to check that self-assembly process also works in the presence of salting-in anion SCN^-. T_c of the polymer solution increased slightly to 68 °C. When this solution was kept at 70 °C, aggregates were formed and were visible to the naked eye after few weeks. Photograph, which was recorded at room temperature, and optical micrograph of the aggregates are presented in figure 5.3.

(a) **(b)**

Figure 5. 3 Picture of PEOX solution in 0.2 M NaSCN when the solution was kept at 70 °C for 20 days. b) Optical micrograph of the aggregates in solution in (a).

When the amount of aggregates were compared after a certain time interval for PEOX solutions in pure water, 0.2 M NaAc and 0.2 M NaSCN, the rate of aggregation was slowest in pure water. Addition of salting-in (NaSCN) and salting-out (NaAc) salts enhanced the rate of aggregation. Optical micrograph in figure 5.3 clearly shows that the morphology of the aggregates in the presence of NaSCN was similar to those formed in pure water and in the presence of NaAc. They are in the form of entangled fibers having an average diameter of 2.9 ± 0.6 μm. The observation of PEOX fibers both in pure water and in the presence of salting-out or salting-in anions indicate that the ions are not the main driving force in fiber formation above T_c, but contribute to kinetic of fiber formation.

5.3.2. Thermal analysis of self-assembled fibers formed in 0.2 M aqueous NaAc solution

Since the aggregation rate of PEOX in pure water was very slow and amount of aggregates was not enough for further analysis, the freeze-dried aggregates of PEOX from 0.2 M aqueous NaAc solution were analyzed by DSC. Before freeze drying, all aggregates were washed several times by water to remove salts from the aggregates. During this process the aggregates did not dissolve in water. Figure 5.4 shows the first heating curve of freeze dried fibers.

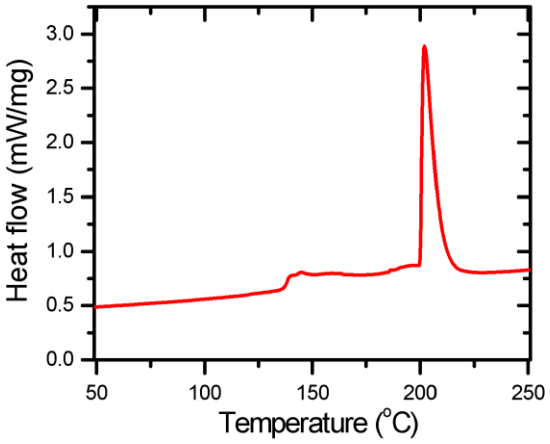

Figure 5. 4 DSC first heating curve of PEOX fibers formed in 0.2M NaAc solution at 70 °C.

The DSC analysis of the fibers showed an intense endothermic peak at 201 ^{o}C in the heating curve which we attribute to the melting of PEOX crystals. A small endothermic peak also appeared around 150 ^{o}C which may be due to the not well organized polymer crystals. Thermal analysis of NaAc was also performed and did not show any endothermic peak in temperature range between 0 ^{o}C to 250 ^{o}C.

5.3.3. X-ray diffraction analysis of PEOX fibers

The freeze-dried aggregates from PEOX solutions in aqueous NaAc and NaSCN were further analyzed by X-ray diffraction (XRD). Figure 5.5 shows the XRD data of the self-assembled fibers.

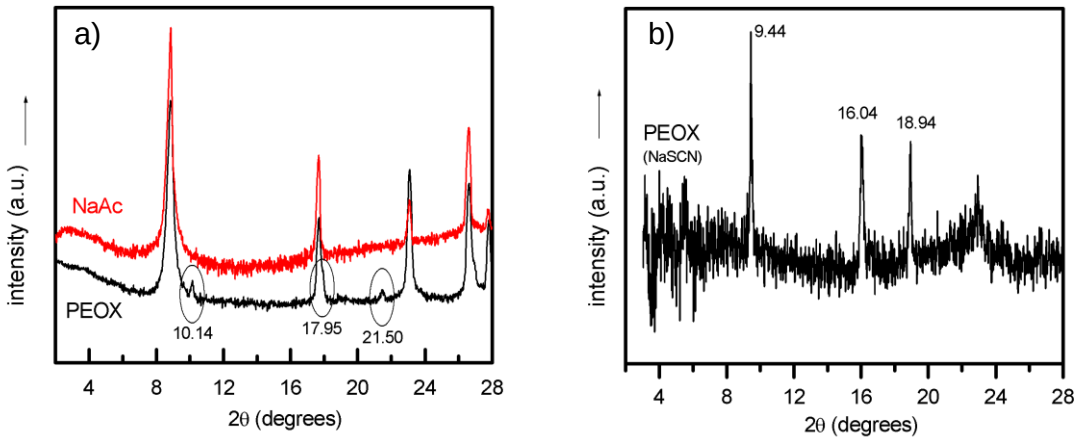

Figure 5. 5 a) XRD data of the PEOX fibers formed in NaAc "black curve" and NaAc "red curve". b) XRD data of the PEOX fibers formed in NaSCN

Figure 5.5.a shows the XRD data of PEOX fibers formed in NaAc solution (black curve) together with NaAc (red curve). Although the fibers were washed several times by water, it is clearly seen that XRD data was dominated by NaAc peaks. It should be noted that crystalline peaks of NaAc and PEOX are very close to each other. Three peaks of PEOX fibers were identified at 2θ values of 10.14°, 17.95° and 21.50°. Corresponding distance between the crystalline planes (d values) are 0.871 nm, 0,494 nm and 0.413 nm respectively. The PEOX fibers formed in NaSCN solution were also analyzed by XRD after washing and freeze drying (figure 5.5 b). NaSCN did not have any crystalline peaks in 2θ range of 4°-30°. Crystalline peaks of PEOX fibers formed in NaSCN solution were clearly observed because of the well-separation from NaSCN peaks. The measured 2θ values for PEOX peaks are 9.44°, 16.04°, and 18.94°. Corresponding d values are 0.938 nm, 0.552 nm, and 0.468 nm.

5.4. Discussions

Transition from one-phase to two-phase state was reversible for aqueous PEOX solution independent of the amount and type of salts as long as the solution was not kept above T_c for more than a day. PEOX aggregates formed both with and without salts, when the solutions were kept above T_c for several days to weeks. PEOX aggregates maintained their structure when solutions were cooled down to room temperature or washed several times by water to remove excess salt. The formation rate of aggregates in water was rather slow and required weeks to be visible by naked eye. Addition of salting-in (NaSCN) and salting-out (NaAc) salts enhanced the rate of aggregation. The difference between the annealing temperature and T_c of the solutions seems to contribute to the rate of aggregation. Optical microscopy and SEM images confirmed that all aggregates are in the form of fibers having average diameter between 2 to 4 μm. PEOX aggregates formed in NaAc containing solution showed an intense endothermic peak at 201 °C. We attributed this endothermic transition to melting of PEOX crystals. Crystallization of fibers from NaAc and NaSCN were further investigated by XRD. In the case of NaAc, the crystalline peak positions of PEOX crystals were found to be very close to NaAc peaks. Despite the fibers were washed several times by water to remove salts from the system, crystal peaks of PEOX were dominated by NaAc. On the other hand, crystalline peaks of NaSCN and PEOX were well separated from each other. Peak positions were calculated from the proposed model crystal structure. This initial structure was then refined such that the calculated XRD peaks by software replicated the experimental XRD data. Figure 5.6 shows the proposed model crystal structure in monoclinic unit cell together with the calculated peak

positions and XRD data of PEOX fibers obtained from NaSCN containing solutions.

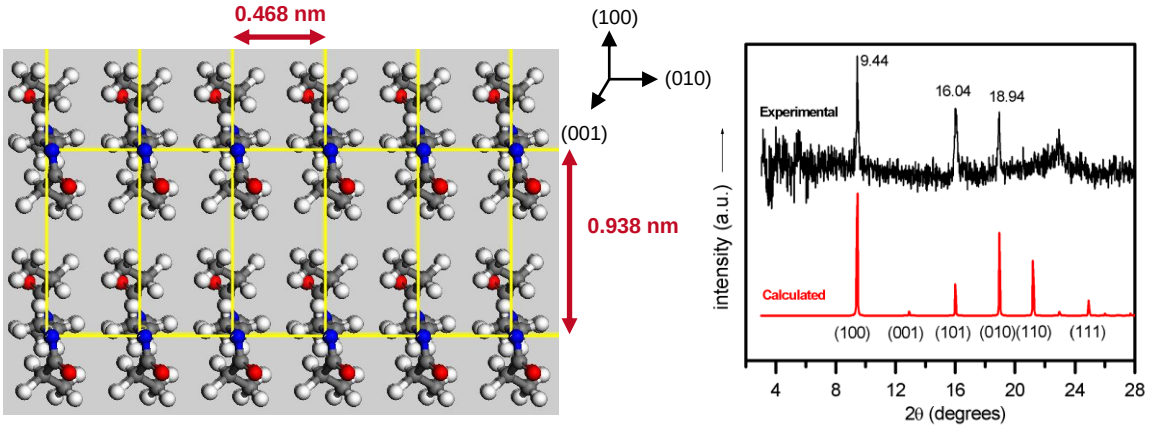

Figure 5. 6 a) Structural model, b) XRD data of PEOX fibers formed in NaSCN "black curve" and calculated XRD according to the structural model "red curve".

Polymer backbone is oriented along [001] direction. Side chains are alternately aligned up and down along [100] direction. Strong amide dipoles are directed along [010] direction. The calculated peak positions and experimentally observed XRD peaks are consistent with each other. The micron size PEOX fibers are expected to be formed by fusion of nanofibers, similar to PIPOX. Crystallization mechanism of PIPOX was explained previously, which involves both non-specific hydrophobic interactions and oriented dipolar interactions [12]. At elevated temperatures, phase separation occurs due to rapture of hydrogen bonds between polymer and water and dominating hydrophobic interactions. In this condition non-specific hydrophobic interactions bring isopropyl side groups together in aqueous medium.

This allows the amide dipoles of the PIPOX to interact and align. It is well known that polyoxazolines have stiff backbones due to strong amide dipole whose nitrogen is on the polymer backbone. Solvation of amide dipoles increases the backbone mobility and contributes to alignment of dipoles. The direction of fastest crystallization was determined as [010] direction which corresponds to alignment direction of carbonyl dipoles [12]. Since amide dipoles interact with each other much stronger for shorter alkyl side chains, conformational relaxations needed to achieve equilibrium crystal structure are hindered. Because of this reason PEOX crystallization was found to be slower compared to PIPOX. In the presence of water molecules, the hydration of the amide dipole introduces backbone flexibility which leads to crystallization of PEOX in water above T_c. The displacement of the d_{100} values with the change in number of carbons in the side chain was shown to be quite regular previously [14]. Measured d_{100} values of PEOX were compared with the previously reported data in figure 5.7.

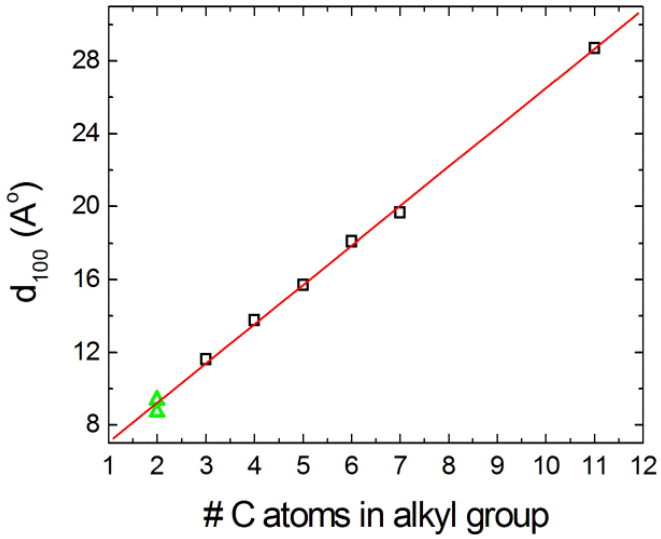

Figure 5. 7 Lattice constant d_{100} of polyoxazolines carrying linear alkyl side chains. n-propyl and longer side chains from Ref. 81 (squares) and PEOX fibers formed in aqueous solutions (triangles). Red line is a linear fit to the squares.

Black squares belong to the d_{100} spacing of polyoxazolines carrying alkyl side chains longer than ethyl and were taken from the previously reported data [81]. Green triangles represent the d_{100} spacing of PEOX fibers formed in aqueous solutions and red line is a linear fit to the black squares. The d_{100} spacing (along the side chains) of PEOX fibers are consistent with d_{100} spacing of longer side chain poly(alkyl oxazoline)s. Lattice constant of crystalline polyoxazolines decreasing linearly with decreasing alkyl chain length. This is expected because they can pack more closely in the case of shorter alkyl side chains. Melting peak of the PEOX crystals was also compared with the longer alkyl side chain polyoxazolines in figure 5.8.

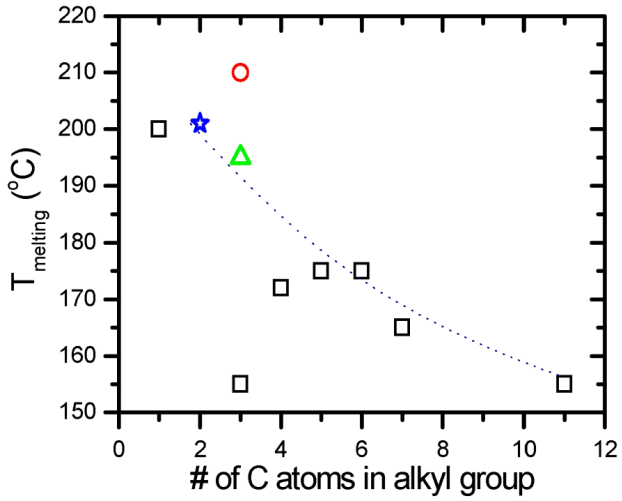

Figure 5. 8 T_m of polyoxazolines carrying linear alkyl side chains. n-propyl and longer alkyl side chains from Ref. 81 (squares). Red circle is for isopropyl side chain and from Ref. 81. Green triangle is for isopropyl side chain from Ref. 12. Blue star is for PEOX-500K fibers formed in 0.2 M NaAc aqueous solution. The dashed curve is to guide to eye.

Melting temperature (T_m) of PEOX fibers is shown as blue star in the graph. Black squares belong to T_m of series of polyoxazolines and taken from the earliest bulk crystallization study [81]. Red circle was also taken from the same literature and demonstrates the melting point of PIPOX. Green triangle also shows T_m of PIPOX, but the value was taken from the more recent study [12]. The dashed curve is just guide to eye. It is clearly seen that observed melting temperature is in agreement with the previously reported values for longer side chain polyoxazolines. T_m of crystalline polyoxazolines increases with decreasing alkyl side chain length thus indicates the difficulty in crystallizing polyoxazolines with shorter side chains. We attributed this behavior to different polymer chain

mobilities. In the case of short alkyl side chains, polymers interacting through amide dipoles cannot relax and change their orientation easily to achieve equilibrium crystal structure.

5.5. Conclusions

Self-assembled crystalline PEOX fibers were observed for the first time in aqueous solutions after keeping the solution above T_c for several days to weeks. The self assembly mechanism of PEOX in hot aqueous solutions was explained similar to the previously reported mechanism for PIPOX crystallization [12]. The fiber formation above T_c happened both in pure water and in the presence of salting-in (SCN^-) and salting-out (CH_3COO^-) ions therefore it is not due to salting-out effect. The DSC analysis of the fibers formed in 0.2 M NaAc solution showed an intense endothermic peak at 201 °C in the heating curve which we attribute to the melting of PEOX crystals. The measured melting temperature of the PEOX crystals were consistent with previously reported data on polyoxazolines having longer alkyl side chains. Increase in T_m value with decrease in side chain length was attributed to the difficult crystallization due to strong dipolar interactions. Crystallinity of PEOX fibers were confirmed by XRD analysis. Model crystal structure was proposed similar to previously reported model for PIPOX [12]. According to this model, d_{100} spacing is the distance between the side chains of different PEOX chains. Measured d_{100} values of PEOX were compared with the previously reported data [14], and found to be decreasing linearly with increasing alkyl side chain length. This indicates that polyoxazolines can pack closer with decreasing number of carbon atoms in the alkyl group.

CHAPTER 6: SELF-ASSEMBLY OF PEOX BELOW THE CLOUD POINT TEMPERATURE IN AQUEOUS SOLUTIONS

6.1. Overview

Structural order over many length scales can be created in self-assembled materials by the presence of several molecular interactions including Coulombic forces, dipolar interactions, hydrogen bonding and Van der Waals forces [164]. Self-assembly occurs from nano-scale to micro-scale and includes meso-phase formation, adsorption or crystallization [165].

Crystallization of PIPOX above the T_c of the aqueous solution was already reported in literature [12]. In Chapter 5, we showed that PEOX also forms water insoluble crystalline fibers when dilute aqueous solutions are kept above the cloud point temperature and this can be enhanced by the addition of salts [166]. The self-assembly of polymers above T_c can be explained by formation of polymer rich regions due to phase separation and increasing polymer-polymer interactions in these regions. As will be described in this chapter, self-assembly of PEOX in aqueous solutions was also observed below T_c.

This part of the thesis contains the results of systematic studies on self-assembly of PEOX into fibers below the cloud point temperature. We have studied on self-assembly kinetics by monitoring the size of the aggregates as a function of time. Observations are shown in section 6.3.1. Influences of polymer concentration and molecular weight on self-assembly kinetics are demonstrated in sections 6.3.2

and 6.3.3, respectively. Morphologies of the self-assembled aggregates were investigated by AFM and the results are shown in 6.3.4. In section 6.3.5, crystallinity of the aggregates is presented. In discussion part comparison of measured d_{100} values with the previously reported data in literature is presented. Also crystallization kinetics was analyzed and interpreted by Avrami exponents. Self-assembly mechanism of PEOX in aqueous solutions below T_c was compared to the previously reported mechanism for PEOX crystallization above T_c.

6.2. Experimental Details

Different molecular weight (5K, 50K, 200K and 500K) PEOX polymers were used for the investigation of self-assembly of PEOX aqueous solutions at 30 °C, which is lower than T_c for all molecular weights. PEOX solutions were prepared in deionized water (resistivity at 25 °C is 18.0 MΩ.cm), and the solutions were kept in temperature controlled water bath at 30°C. Size distribution profiles of aggregates in aqueous solutions were studied with DLS as mentioned before. The duration of each measurement was 10 seconds and 100 measurements were recorded for statistical investigations. For AFM measurements, solutions containing coagulates were spin coated on silicon substrates at 2000rpm for 90s. AFM measurements were carried out using silicon cantilevers. Coagulates on the surfaces were scanned at room temperature in tapping mode. Crystallinity of self-assembled aggregates was investigated by X-ray diffraction after freeze drying.

6.3. Results

6.3.1. Self-assembly kinetics of PEOXs below the cloud point temperature

Self-assembly kinetics of 1 mg/ml different molecular weight PEOX aqueous solutions were investigated via DLS measurements at 30 °C. Cloud point temperatures of 1 mg/ml PEOX-5K, 50K, 200K and 500K solutions are 65.2, 64.3, 63.2, and 61.1 °C respectively. The difference between annealing temperature (T_a) and cloud point temperatures (T_c) were denoted as ΔT. These differences are 35.2, 34.3, 33.2, and 31.1 °C. It is clearly seen that annealing temperature is much below the T_c of all PEOX samples. 1 mg/ml homogeneous PEOX-500K solution was prepared and aggregation stages were followed. Figure 6.1. a) shows the aggregate size distribution of the solution, at different times, as a function of number of measurements. In figure 6.1. b), same data is shown, after sorting them in an increasing manner.

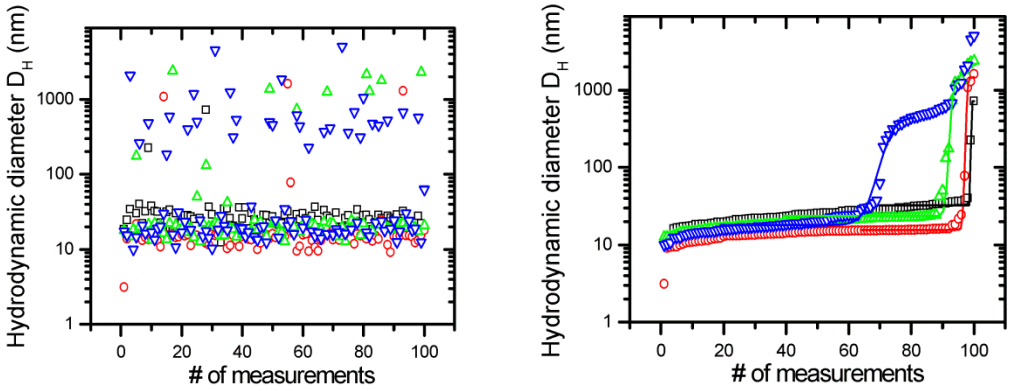

Figure 6. 1 a) Size distribution of PEOX-500K in 1 mg/ml aqueous solution at different times as a function of measurement number b) Sorted size distribution data of PEOX-500K at different times as a function of measurement number. For both graph recorded data at day 1, day 7, day 13, and day 41 are shown as black squares, red circles, green triangles, and blue inverse triangles, respectively. Curves are sigmoidal fit to the data points.

It is clearly seen that freshly prepared PEOX-500K solution shows unimodal size distribution. The evolution of self-assembled aggregates with time increased the hydrodynamic diameter of some particles in solution. When obtained size data was sorted in ascending manner, two plateaus was obtained as seen in figure 6.1.b). It indicates the change of unimodal size distribution to bimodal one. Sigmoidal curves were fitted to the data points. Obtained inflection points were subtracted from the total number of 100 measurements and interpreted as percent aggregation. On the first day of the measurement inflection point is very close to 100, indicating no aggregation. The position of inflection point decreased due to growth of self-assembled structures in the solution. In figure 6.2 percent

aggregation of 1 mg/ml PEOX-500K in aqueous solution is shown as a function of time.

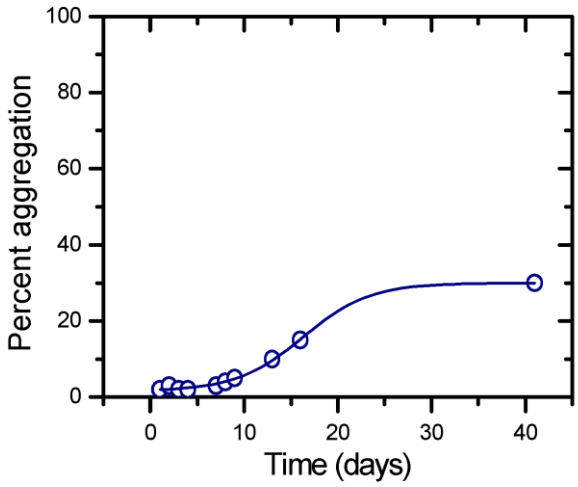

Figure 6. 2 Percent aggregation as a function of time for 1 mg/ml PEOX-500K solution. The solid line is a sigmoidal curve fit to the data points.

Very small initiation period around 5 days is detected before self-assembly. This period is followed by growth of aggregate number resulting in a sigmoidal shape growth curve. The self assembly is finished by a plateau that represents the end of aggregation.

6.3.2. Effect of concentration of PEOX on self-assembly kinetics below the cloud point temperature

PEOX-500K solution concentration was changed between 0.1 to 10 mg/ml to understand its influence on self assembly process. Self-assembly kinetics of these solutions is shown in figure 6.3 as percent aggregation vs. time.

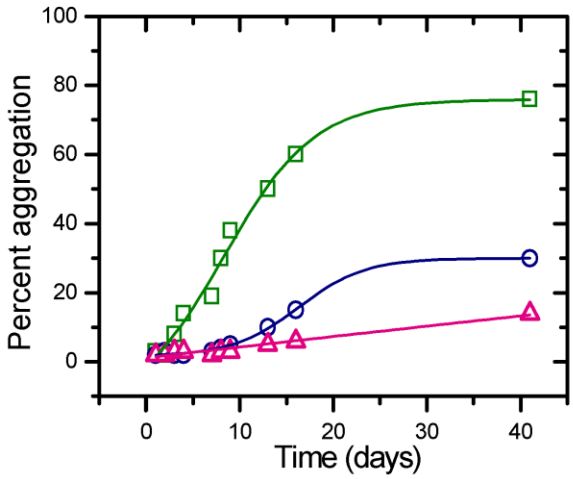

Figure 6. 3 Percent aggregations as a function of time for 0.1 (green squares), 1.0 (blue circles) and 10 (pink triangles) mg/ml PEOX-500K solutions. Curves are sigmoidal fits to data points.

Solid curves on the graph are sigmoidal fit to the experimental data. Inflection point is decreased with increasing PEOX concentration. It indicates aggregation rate is faster in diluted sample. In the case of precipitation of substances from their solutions, increase in solute concentration favors precipitation. Contrarily, dilution caused increase in self-assembly rate of PEOX. The reason behind this behavior could be explained by the increase in chain freedom to achieve equilibrium structures. Moreover, the difference between upper and lower plateau of the sigmoid shape isotherms increased with decreasing PEOX concentration. Since rate of self-assembly is faster for dilute PEOX solution, amount of aggregates after same annealing time is more.

6.3.3. Influence of molecular weight of the PEOX on self assembly kinetics below the cloud point temperature

Effect of molecular weight of the polymer on self-assembly kinetics was also investigated using 1 mg/ml solutions of different molecular weight PEOX. At this concentration, self assembly of PEOX having molecular weight of 500K was quite slow. Percent aggregations were monitored as a function of time for different molecular weight PEOX solutions and results are shown in figure 6.4. a).

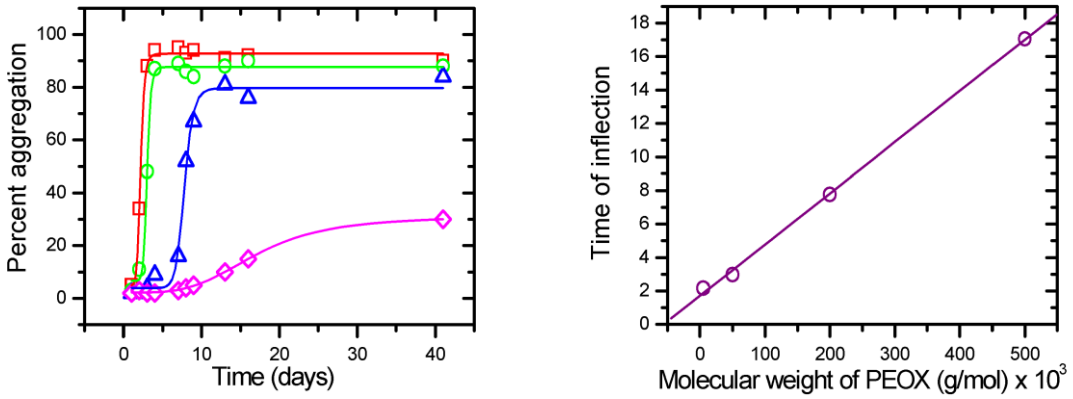

(a) (b)

Figure 6. 4 a) Percent aggregation as a function of time for 1 mg/ml PEOX 5K (red squares), 50K (green circles), 200K (blue triangles) and 500K (pink rhombohedrons) solutions. Curves are sigmoidal fits to data points. b) Time of inflection points as a function of molecular weight of the PEOX. Purple line is linear fit to data points.

In figure 6.4. a) percent aggregations kinetics was compared as a function of molecular weight. Curves are sigmoid type fits to data points. Figure 6.4. b) shows the time of inflection points of sigmoid curves as a function of molecular weight of

the PEOX. When the molecular weight of the PEOX was increased in solution, inflection points shifted to shorter times. This indicates that self-assembly is faster for lower molecular weight PEOX polymers. Upper plateau of the isotherms were changed from 20% to 95% with decreasing molecular weight. As a result of faster aggregation, amount of aggregates are more for shorter PEOX samples. During these studies polymer concentrations were kept constant at 1 mg/ml. Because of difference in molecular weight of PEOX samples, numbers of polymer chains in solutions were different. For PEOX 500K the concentration is 2 x 10^{-6} M so there is less number of chains in solution and for PEOX 50K it is 2 x 10^{-5} M. Thus, aggregation kinetics of PEOX solutions having same number of chains was compared in figure 6.5.

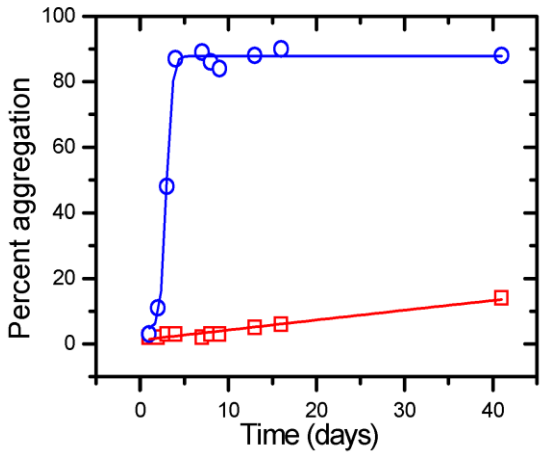

Figure 6. 5 Percent aggregations of solutions both have 2 x 10^{-5} M PEOX 500K (red squares) and 50K (blue circles) as a function of time. Sigmoid shape curves are fit to the data.

In Figure 6.5 percent aggregations of 2 x 10^{-5} M PEOX-500K and PEOX-50K aqueous solutions are shown as a function of time. Curves are sigmoid type fit to

data points. Inflection point of the curve shifted to shorter time for PEOX-50K solution compared to PEOX-500K. It indicates that rate of aggregation is faster for shorter PEOX sample. Also increase in difference between upper and lower plateaus with decreasing molecular weight was observed. This behavior can be attributed to relaxation of entanglements in small size polymers and also increase in mobility of the chains to form self-assembled aggregates.

6.3.4. Morphological investigations of self-assembled aggregates

Solutions having aggregates of different molecular weight PEOX, were coated on silicon substrates at day 16 and investigated by AFM to observe their morphologies. All measurements were carried out in ambient temperature and in tapping mode. Figure 6.6 shows typical height images of the aggregates.

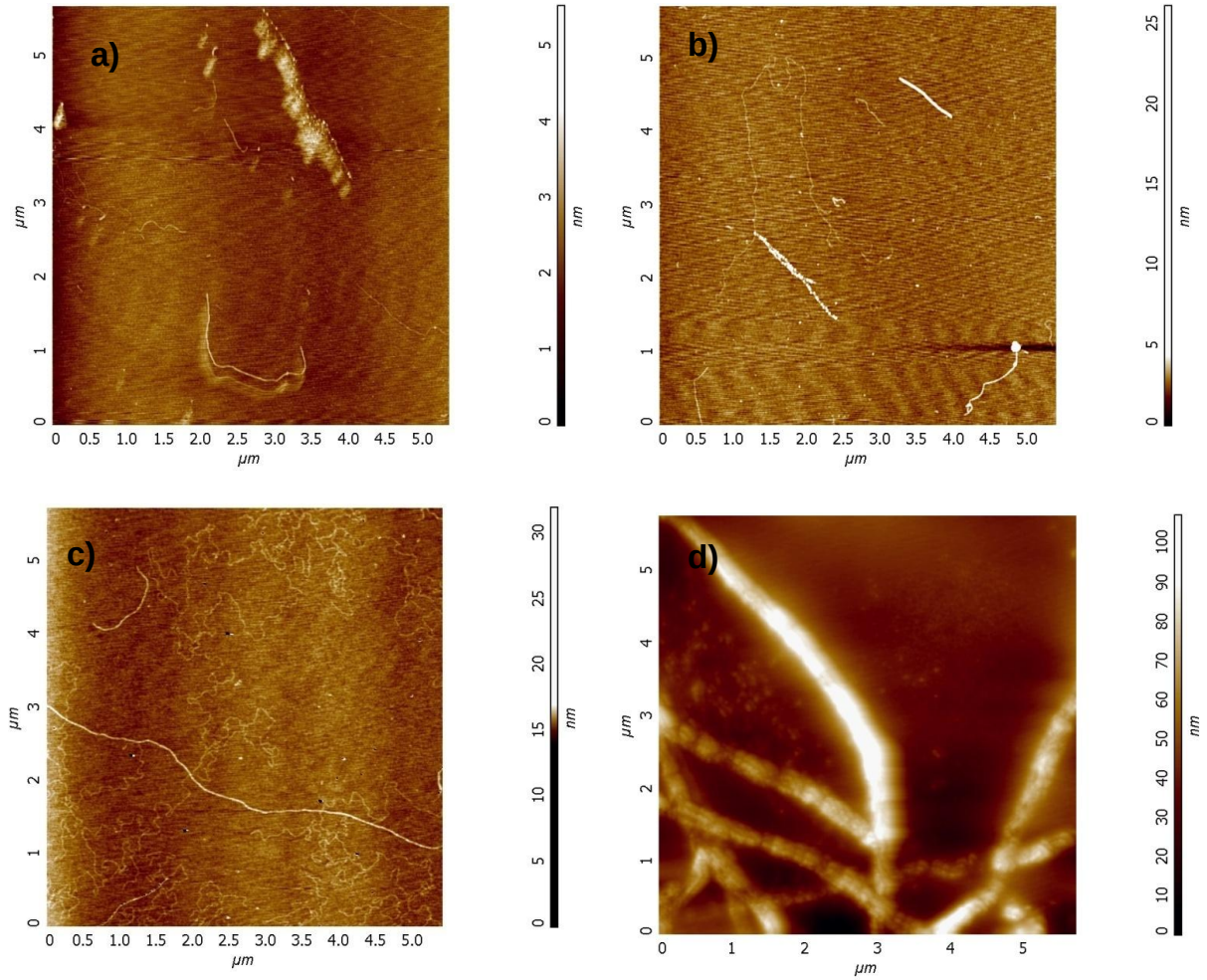

Figure 6. 6 AFM micrographs of self-assembled aggregates in 1 mg/ml a) PEOX-5K, b) PEOX-50K, c) PEOX-200K and d) PEOX-500K solutions

Figure 6.6 shows the 5 µm x 5 µm scanned height image of aggregates which were formed in 1 mg/ml of different molecular weight PEOX aqueous solutions at 30 °C. All of the AFM images confirmed that obtained aggregates are in the form of fibers. The thickness of the fiber in a) is in the order of 4 nm and length is in few microns. The thickness of the fibers was increased to 5 to 10 nm when molecular weight of the PEOX was increased to 50K in b). Further increase in molecular

weight of the polymer caused increase in thickness of the obtained fibers. Thickness of the long fiber in c) is around 17 nm and shiny fiber thickness in d) is around 100 nm. Heights of the fibers are very small compared to the width and length of them but they are increasing with increasing molecular weight.

6.3.5. X-ray diffraction analysis of PEOX fibers

The freeze-dried aggregates from 1 mg/ml PEOX-500K aqueous solution were further analyzed by X-ray diffraction (XRD). Figure 6.7 shows the XRD data of fibers.

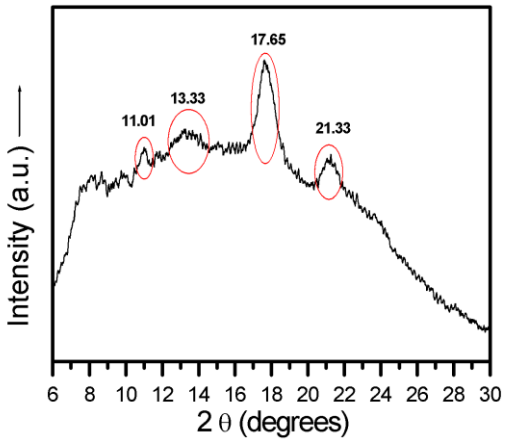

Figure 6. 7 XRD data of the PEOX fibers formed in aqueous solution.

Four peaks of PEOX fibers were identified at 2θ values of 11.01°, 13.33°, 17.65°, and 21.31°. Corresponding d values are 0.803 nm, 0,664 nm, 0.502 nm, and 0.417 nm, respectively. Crystalline fibers, formed in NaAc and NaSCN containing aqueous solutions above T_c, were also investigated with XRD and results are shown in chapter 5. It was found that d values are close to each other.

It indicates that crystal structures are similar. Small differences in d values could be explained with the incorporation of salts in crystal structures. In addition, peaks are sharper in the presence of salts and attributed to the better crystallization. Amorphous part seen in XRD data is attributed to the presence of non-crystallized PEOX molecules.

6.4. Discussions

PEOX aggregates were observed, when the solutions were kept below T_c for few days to several weeks. A sigmoidal growth isotherms were observed, which are characteristic of nucleation and growth processes and an inherent property of polymer crystallization [167]. Avrami equation was used to evaluate the aggregation kinetics based on nucleation and growth process.

$$1-\lambda(t)=1-\exp(-kt^n)$$

Equation 6. 1

Where λ(t) is the fraction transformed at time (t), k corresponds to rate constant and n is Avrami exponent. This exponent is not unique, and represents the dimension of nucleation and growth processes. n = 2 correspond to one-dimensional growth, n = 3 for two dimensional growth and n = 4 for three dimensional growth [167]. log(-ln(1 – λ(t))) was plotted for different concentration and molecular weights of PEOXs as a function of log t as shown in figure 6.8 to determine the exponents.

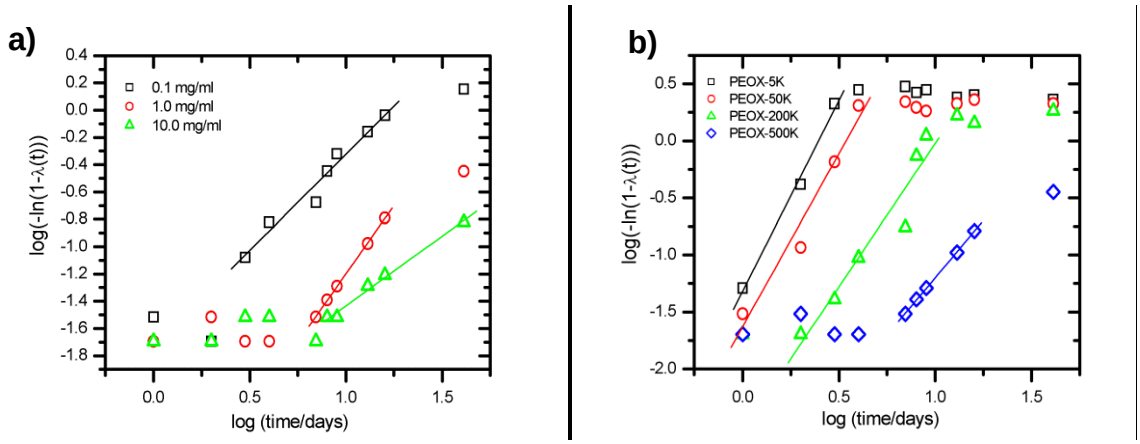

Figure 6. 8 Avrami equation fits of aggregation kinetics of a) PEOX-500K at different concentrations and b) PEOX with different molecular weights at 1 mg/ml concentrations.

Avrami exponents (n) were calculated from the slopes of linear fits and are listed in table 6.1 and 6.2.

Table 6. 1 The Avrami exponents (n) as a function of PEOX-500K concentration

PEOX-500K concentration (mg/ml)	Avrami exponent (n)
0.1	1.8
1.0	2.0
10.0	1.0

Table 6. 2 The Avrami exponents (n) as a function of molecular weight of PEOX for 1 mg/ml concentration

Molecular weight of PEOX (g/mol x 1000)	Avrami exponent (n)
5	3.3
50	3.0
200	2.5
500	2.0

An exponent 2.0 to 2.5 indicates the fibrillar growth. Exponents were found to be 3.0 to 3.3 for smaller molecular weight PEOXs and much diluted solution of the PEOX-500K. This corresponds to two dimensional growths. The Avrami exponent decreases with increasing concentration of polymer solution and also decreasing with increasing molecular weight of the polymer. This indicates that aggregation rate of diluted PEOX solution is faster than concentrated one. In common aggregation processes, increase in solute concentration in solution cause faster aggregation due to the increase in colliding possibility of substances to make strong interactions. However, self-assembly is cannot be considered as simple aggregation. Substances should interact with weaker interactions compared to aggregation to move and orient themselves to achieve more ordered structures. In concentrated solutions, mobilities of the polymer chains are hindered due to crowd in the solution. As a result, self-assembly rate decreases. In addition, aggregation showed significant dependence on molecular weight of the polymer and increase in molecular weight resulted decrease in aggregation rate. Relaxation of chain entanglements results in enhancement of polymer-polymer interactions to form ordered structures in the case of shorter polymer chains.

Self-assembled aggregates of PEOX-500K in water below T_c was found to be crystalline similar to those obtained from aqueous solutions above T_c in the presence of NaAc and NaSCN. Observed peak positions and corresponding d values are close to each other. This indicates that all self-assembled fibers have similar crystal structures. The d_{100} values with the change in number of carbons in the side chain was shown to be quite regular previously by Morton Litt and discussed previously in chapter 5 [14]. In a more recent study, PIPOX was crystallized in bulk isothermally and also in water above T_c [12]. Observations of identical endothermic peaks in the DSC scans and the same crystalline peaks in XRD for both self assembled aggregates of PIPOX and isothermally crystallized PIPOX were shown to be the confirmation of same crystalline structure. We could not crystallize PEOX in bulk isothermally but by considering the case in PIPOX, calculated d_{100} value was compared with the previously reported data [14] for longer alkyl side chain polyoxazolines in figure 6.9.

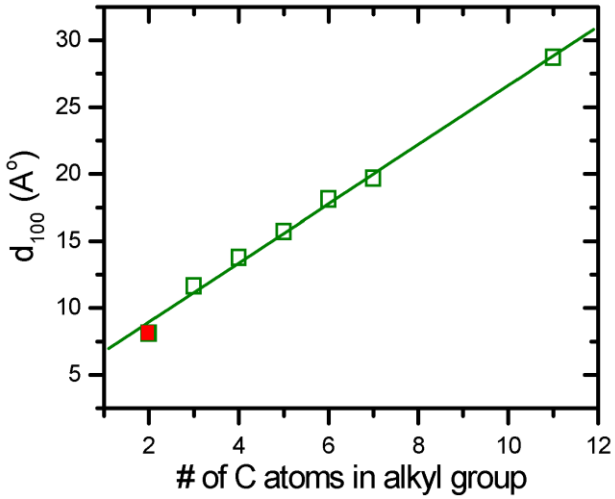

Figure 6. 9 Lattice constant d_{100} of polyoxazolines carrying longer linear alkyl side chains (open squares) and closed red square belongs to PEOX fibers, gren line is a linear fit to open squares.

In figure 6.9 green open squares belongs to the d_{100} spacing of polyoxazolines carrying longer alkyl side chains and taken from the previously reported data [14] as described previously. Red closed square represent the d_{100} spacing of PEOX fibers and green line is a linear fit to the green squares. The XRD peaks of obtained PEOX fibers are consistent with d_{100} spacing (along side chains) of longer side chain poly(alkyl oxazoline)s. Lattice constant of crystalline polyoxazolines decreasing linearly with decreasing alkyl chain length as expected because they can pack more closely in the case of shorter alkyl side chains.

It is complicated to explain crystallization below T_c. Why homogeneous solution phase disintegrates. In the case of crystallization in solution, the behavior of the system during nucleation is less understood. Two-step nucleation pathway was

proposed recently in literature [168]. First concentration fluctuations occur in homogeneous polymer solution and create regions of higher polymer concentration with a limited lifetime. In this stage nucleus is formed which exceeds a critical threshold size. The rate at which such nuclei form depends on the free energy cost needed to form a critical nucleus of new phase. Gibbs free energy of mixing, ΔG^{mix} , has the following form:

$$\Delta G^{mix} = \Delta H^{mix} - T\Delta S^{mix}$$ [130]

Equation 6. 2

For ideal mixing $\Delta S^{mix} = R(X_A \ln X_A + X_B \ln X_B)$, where X_A and X_B are the molar fractions of components A and B in the mixture and $X_A + X_B = 1$. However the enthalpy of mixing may be written as $\Delta H^{mix} = \beta X_A X_B$, where β is an interaction parameter. According to this interaction parameter, sign of the ΔG^{mix} term changes. Demixing occurs and creates new phases in the system. These sites have probability to start phase separation process and any particular fluctuation in concentration can trigger nucleation. Then, these nuclei grow and produce structured crystalline clusters.

6.5. Conclusions

PEOX formed fiber type aggregates when aqueous solutions kept long time at 30 °C, which is far below the T_c of the solution. Self-assembly kinetics of PEOXs in aqueous solutions was studied by following aggregation stages as a function of polymer concentration and molecular weight via DLS measurements. According to the experimental results it can be concluded that dilution and molecular weight decrease cause increase in aggregation rate. Aggregation process followed sigmoidal growth which indicates nucleation and growth mechanism. Avrami equation was used to evaluate the aggregation kinetics based on nucleation and growth process. Results showed that the Avrami exponent decreases (nucleation rate decreases too) with increasing concentration of polymer solution and also increasing molecular weight of the polymer. Surface topologies of the aggregates were investigated with AFM. Dimensions of obtained fibers differ from each other in the same solution and also very different when compared with polymers, which have different molecular weights. Thicknesses of the aggregates were found to be increasing with increasing molecular weight of the polymer. Crystallinities of the self-assembled aggregates were further investigated with X-Ray diffraction (XRD) technique. The crystalline peak positions of PEOX-500K fibers formed in aqueous solution below T_c were found to be very close to PEOX-500 peaks, which were formed above T_c and also in agreement with the previously reported data in the literature. Therefore similar interactions should be responsible for crystallization of PEOX both below and above T_c.

CHAPTER 7: BULK CRYSTALLIZATION OF POLY(2-ALKYL-2-OXAZOLINE)S

7.1. Overview

Physical properties of polyoxazolines, such as crystallinity and solubility, depend significantly on the alkyl side chain length [14], [97]. There are very few studies in literature about the crystallinity of the polyoxazolines in bulk [14–16]. According to the first study on crystallinity of different poly(2-alkyl oxazoline)s, carrying linear alkyl groups from –methyl to –dodecanoyl on their side chain, only -ethyl bearing one was found to be amorphous [14]. Contrarily, following studies demonstrated that crystallization is only possible for poly(2-alkyl oxazoline)s, if carbon atom in the alkyl group (n) is greater than 3 [15], [16]. Melting transitions were observed around 150 °C for the polymers with –butyl and longer side-chains, and attributed to the side chain crystallization. T_g values was observed to decrease linearly with increasing n [15], [16]. Polymer chain mobility at a given temperature increases with decreasing T_g [169]. T_g of various polymeric systems was reported to decrease with increasing alkyl side chain length [170–172] We have studied the bulk crystallization of polyoxazolines with –methyl, -ethyl, -propyl, -isopropyl, -butyl, and –hexyl side chains to understand the effect of alkyl side chain length on crystallization behavior.

Crystallization rate of polymers depends on both kinetic and thermodynamic factors[173]. Crystal nucleation and growth studies in the temperature range T_g

(glass transition temperature) and T_m (melting temperature) showed that the crystallization kinetics were sensitive to small temperature changes [174]. It is well-known that the crystallization rate of bulk polymers exhibits a bell-shaped curve as a function of temperature between T_g and T_m. The crystallization rate is slow close to T_m because the thermodynamic driving force for crystallization ΔG_{crys} is small. On the other side close to T_g, despite large ΔG_{crys}, the crystallization rate is slow due to rather small chain mobilities and is diffusion-limited. Therefore crystallization of polymers happen in the temperature range between T_g and T_m, and a maximum crystallization rate is observed in the middle of these two temperatures [175].

7.2. Experimental Details

Poly(2-ethyl-2-oxazoline) (PEOX) (M_w ~ 500,000g/mol, and PDI = 3 – 4) was purchased from Aldrich and used without any purification. Poly(2-isopropyl-2-oxazoline) (PIPOX) (M_w ~ 6,800 g/mol), having polydispersity index (PDI) of 1.08, was synthesized by Dr. Helmut Schlaad. Poly(2-methyl-2-oxazoline) (PMOX) (M_w ~ 17,000 g/mol), poly(2-propyl-2-oxazoline) (PPOX) (M_w ~ 22,600 g/mol), poly(2-butyl-2-oxazoline) (PBOX) (M_w ~ 7,600 g/mol), and poly(2-hexyl-2-oxazoline) (PHOX) (M_w ~ 9,300 g/mol), having PDI values in between 1.1 and 1.2 were synthesized by Dr. Richard Hoogenboom.

Crystallization of PAOX, having different molecular weights, were studied by DSC. Aluminum hermetic pans and lids were used. The heating/cooling rate was kept constant at 10 ºC/min under nitrogen flow of 50mL/min. The samples were first heated to 250 °C and kept at that temp for 3 min to ensure complete melting. Then the samples were cooled back to 25 °C. The second heating curves were

presented. For isothermal crystallization experiments, samples were isothermally annealed in DSC for 45 min or longer at various temperatures after second heating/cooling cycle. Resulting exothermic peaks were monitored as a function of time. After that samples were heated up to 250 °C for determination of their melting peaks.

7.3. Results

7.3.1. Attempts to crystallize PMOX, PEOX, and PPOX in bulk

The thermal properties of polyoxazolines having –methyl, -ethyl, -propyl side chains were determined by DSC. Second heating curves obtained with a heating rate of 10 °C/min are shown in figure 7.1.

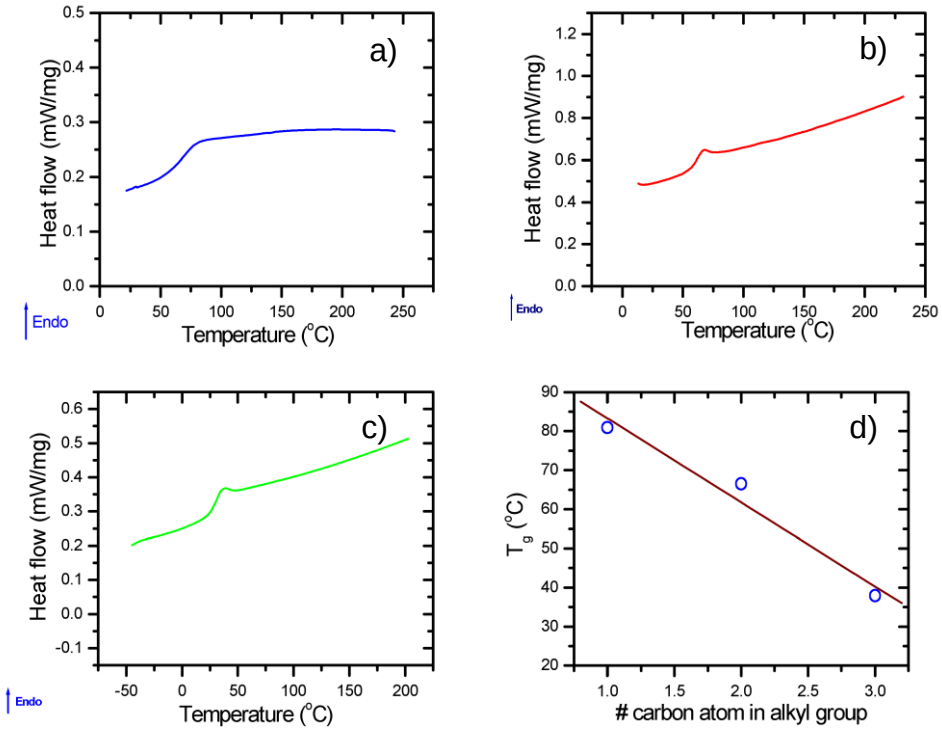

Figure 7. 1 DSC second heating curves obtained for a) PMOX (M_w ~17,000 g/mol), b) PEOX (M_w ~500,000 g/mol), and c) PPOX (M_w ~22,600 g/mol). d) Glass transition temperatures as a function of number of carbon atoms in alkyl side chain.

In figure 7.1 a), b), and c), heat flows are presented as a function of temperature. For all of the samples, only glass transition temperatures were observed, which indicates that the polymers did not crystalline and were in amorphous state. T_g values were assigned from the peak maximum of the curves and are 80, 67, and 38 °C for PMOX, PEOX, and PPOX, respectively. T_g decreased linearly with increasing alkyl side chain length which indicates larger chain mobility as shown in 7.1 d). These results are consistent with previously

reported behavior for PAOX carrying these alkyl groups [15], [16] and indicate that PDI is not a critical factor for our puposes.

Isothermal annealing of polymers were carried out after second heating/cooling cycles by DSC for 100 minutes at 130, 150, and 100 °C for PMOX, PEOX, and PPOX, respectively. Isothermal crystallization rate is maximum in the middle of T_g and T_m, so annealing temperatures were chosen by considering these temperatures. In figure 7.2, DSC heat flows during isothermal annealing are presented as a function of time.

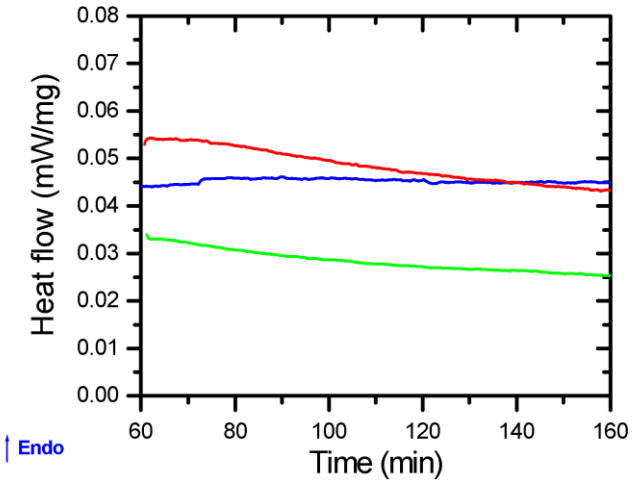

Figure 7. 2 DSC heat flows during isothermal annealingas a function of time (blue curve: PMOX, Red curve: PEOX, and Green curve: PPOX)

Exothermic peaks due to isothermal crystallization were not observed Samples were heated up to 250 °C after isothermal annealing to check the presence of any endothermic peak due to melting. Figure 7.3 shows DSC scans as a function of temperature for all polymers.

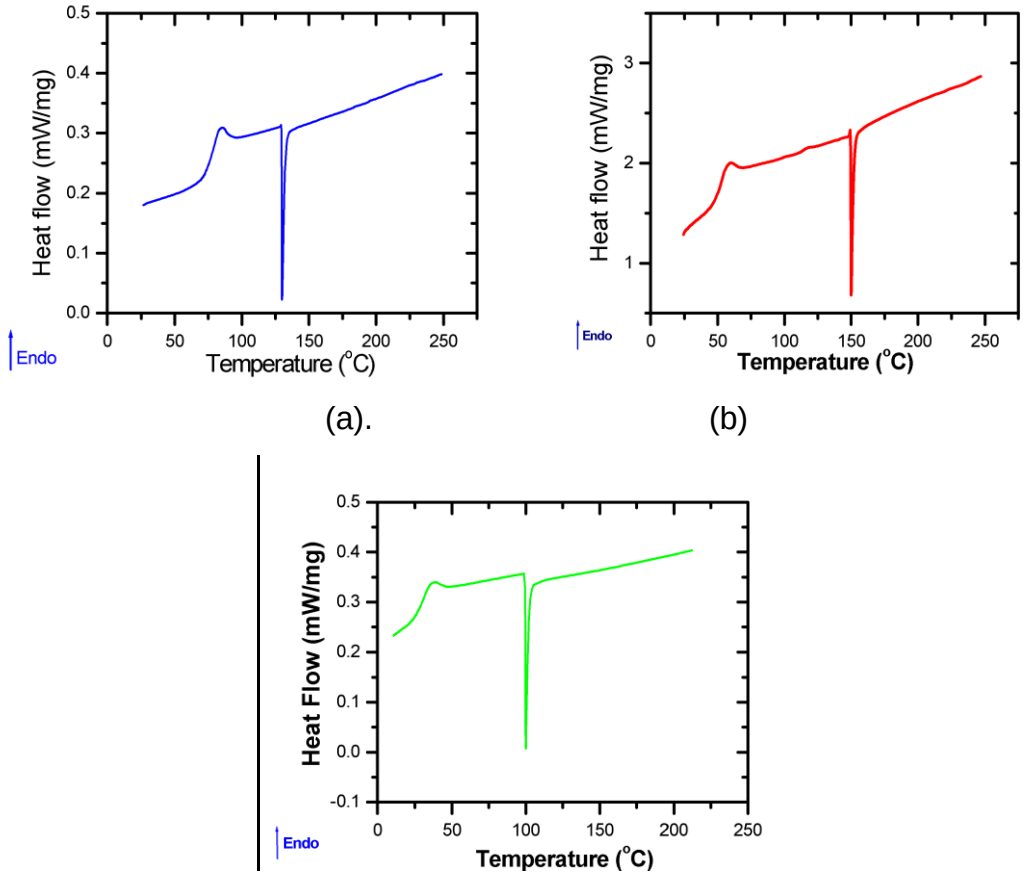

Figure 7. 3 DSC heat flows of a) PMOX, b) PEOX, and c) PPOX as a function of temperature after isothermal annealing.

Glass transition temperatures were observed during heating from room temperature to isothermal crystallization temperatures. After isothermal annealing step, any endothermic transition due to melting was NOT observed during heating process up to 250 °C. Furthermore, isothermal annealing studies of PPOX were done at different temperatures of 50, 65, 80, 95, 110, and 130 °C to check whether

any crystallization and melting could be observed. In figure 7.4, DSC heat flows after isothermal annealing at 50, 65, 80, 95, 110, and 130 °C are shown as a function of temperature.

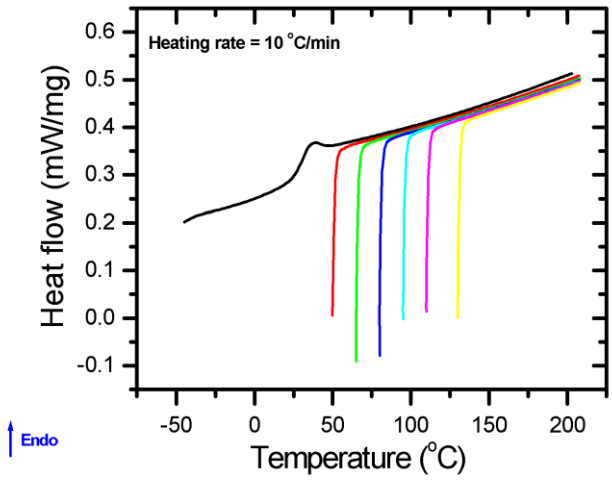

Figure 7. 4 DSC scans of PPOX after isothermal crystallization as a function of temperature. Black curve belongs to second heating without any isothermal annealing. Red, green, blue, cyan, pink, and yellow curves are after isothermal annealing at 50, 65, 80, 95, 110, and 130 °C, respectively .

PPOX sample was first heated up to 200 °C and cooled back to room temperature. In the second heating, only glass transition was observed at 38 °C. Then, sample was cooled back to 50 °C and kept at this temperature for 45 min for crystallization. After that it was heated again up to 200 °C to see any endothermic transition. We could not observe any melting peak during this step. Same process was repeated for different annealing temperatures to crystallize PPOX in bulk but crystallization of PPOX could not be observed.

Polyoxazolines with –methyl, -ethyl, and –propyl side chains were could not crystallized isothermally in DSC. Changing isothermal annealing temperature or increasing annealing time did not cause crystallization. These results are consistent with previous data in literature [14] [15].

7.3.2. Thermal behavior of PBOX and PHOX

PAOXs with the shortest alkyl side chains (-methyl, -ethyl, -propyl) did not crystallize in bulk. Thermal properties of PAOX having (-butyl, and –hexyl) side chains were determined by DSC. In figure 7.5, DSC heating and cooling curves of PBOx, and PHOx are shown.

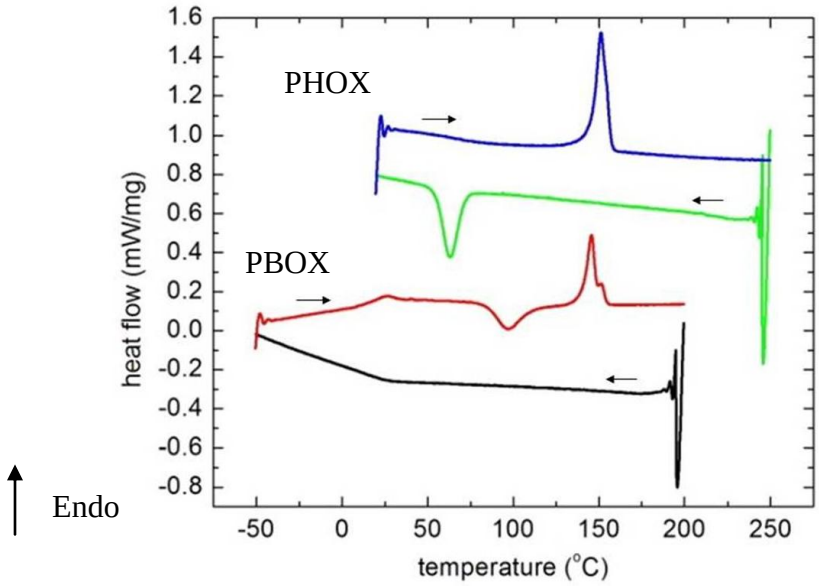

Figure 7. 5 DSC heating/cooling curves of PBOX and PHOX as a function of temperature. Red and Black curves belongs to heating and cooling curves of

PBOX, respectively. Blue and green curves are for heating and cooling curves of PHOX, respectively.

PHOX showed an intense endothermic peak around 150 °C during 2nd heating cycle and crystallized in the cooling cycle. Crystallization peak is around 63 °C. Interestingly, PBOX showed a glass transition, crystallization and melting peaks in its heating curve. It showed glass transition temperature T_g ~ 25 °C , crystallized at 90 °C, and had melting temperature T_m ~ 150 °C. PAOX having -butyl side chains showed cold crystallization (crystallization observed in the heating cycle). The crystallization of PAOXs with longer alkyl side chains changed from cold crystallization (crystallization observed in the heating cycle) to normal crystallization (crystallization observed in the cooling cycle) as the alkyl side chain length increased. We attribute the different crystallization behaviors to the different chain mobilities. When the alkyl group is short, dipolar interactions between different chains will be strong. This strong interaction hinders the chain movement to achieve equilibrium crystal structure.

7.3.3. Isothermal crystallization of PIPOX in DSC

To understand the relation of chain mobilities and different crystallization behavior, isothermal crystallization of poly(2-isopropyl-2-oxazoline) (PIPOX) was studied by DSC at different annealing temperatures. PIPOX was chosen for this study because of its tendency to crystallize easily compared to PPOX due to rather compact isopropyl groups. Results are shown in Figure 7.6.

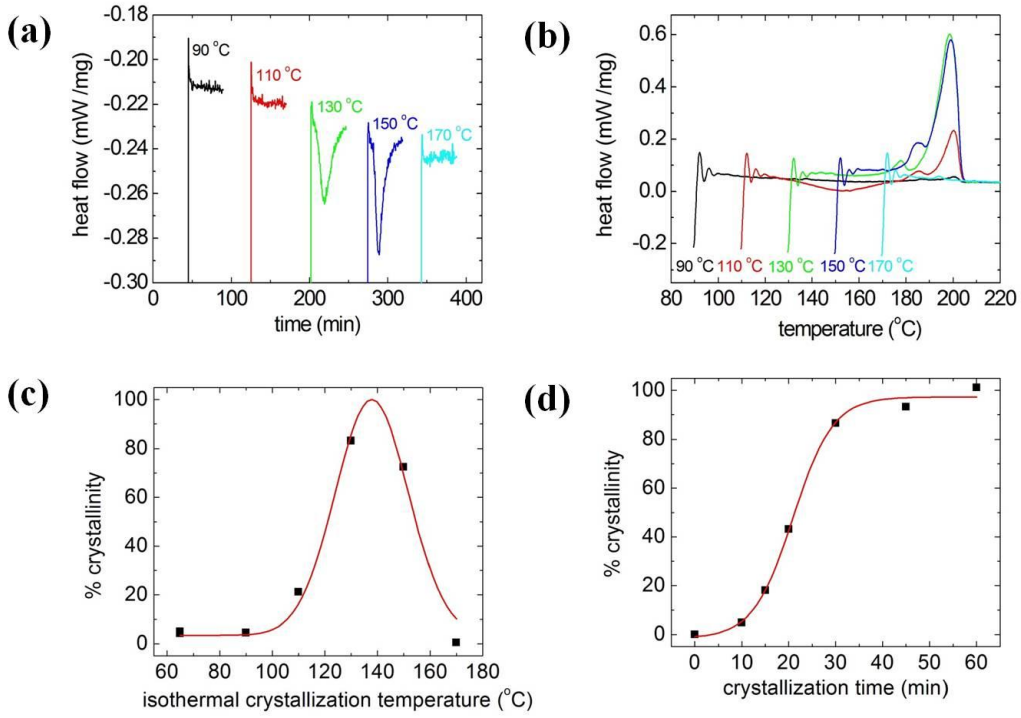

Figure 7. 6. a) DSC of isothermal crystallization of PIPOX at various temperatures. b) Heating curves (10 °C/min) after isothermal crystallization. c) % crystallinity as a function of isothermal crystallization temperature. d) % crystallinity as a function of crystallization time at 130 °C.

Figure 7.6. a) shows the DSC heat flows of PIPOX during 45 min. isothermal crystallization as a function of time at different temperatures. Exothermic peaks due to isothermal crystallization were clearly observed at 130 °C, and 150 °C. The DSC heating curves after isothermal crystallization at a scan rate of 10 °C/min are shown in Figure 7.6. b). Melting peaks were only observed for 110 °C, 130 °C, and 150 °C. At 110 °C, an isothermal crystallization peak was not observed in Figure 7.6. a). During the heating cycle after isothermal annealing, a broad crystallization

peak was first observed ~150 °C followed by a clear melting peak at 198 °C. This indicates the presence of very slow crystallization that started but was not completed within the given time interval of isothermal annealing. Upon heating, the crystallization continued further and resulted in a melting peak at higher temperatures. At 130 °C and 150 °C, crystallization happened isothermally and a larger melting peak was observed upon heating. The area under the melting peaks was defined as % crystallization. The graph of % crystallinity as a function of isothermal crystallization temperature is shown in Figure 7.6. c). Red curve is Gaussian fit to data points. Data was normalized by the peak value after curve was fitted to the data. This approach assumes that at T corresponding to the peak value, the crystallization is completed within the given time interval. At 130 °C and 150 °C, more crystallites were formed within the given time interval due to faster crystallization. At 170 °C, crystals cannot form because the system is too close to T_m and the thermodynamic driving force for crystallization is weak. Figure 7.6. d) shows % crystallinity as a function of time at 130 °C, close to the fastest crystallization temperature. Even at this temperature, there was no significant crystallization in the first 10 min which explains why PIPOX cannot crystallize at a scan rate of 10 °C/min. Then, crystallinity reached 85% within 30 min and 100% within 1 hour.

7.4. Discussions

In thermal analysis of pristine poly(2-alkyloxazoline)s having –methyl, –ethyl or –propyl side chains, only glass transitions were observed. Glass transition temperatures were found to be decreasing with increasing number of carbon atoms in alkyl group. The reason of decrease in T_g with increasing alkyl side chain

length was attributed to the increase in flexibility of the polymer. These results are in agreement with the previously reported data [15], [16]. In these studies longer alkyl side chain length polyoxazolines were shown to be crystalline. However, in that study the observation of crystallinity only for –butyl or longer alkyl groups in side chain was considered as side chain crystallization. We could not crystallize any of the short alkyl side chain polyoxazolines in bulk via isothermal annealing. It was previously reported that poly(2-isopropyl-2-oxazoline), PIPOX, was crystallized isothermally in bulk at 130 °C [12]. Driving mechanism for crystallization was proposed, which involve non-specific hydrophobic interactions, and oriented dipolar interactions together. It is known that dipole moments of the tertiary amides are quite high, and in the order of 3.7 – 3.8 for the dimethyl acetamide and dimethyl formamide respectively [176]. According to the proposed mechanism, nonspecific hydrophobic interactions become dominant with increasing temperature and bring hydrophobic isopropyl groups together. These close distances between the chains allow the amide dipoles of PIPOX to interact and align. By considering this mechanism, the reason of amorphous behavior of PMOX, PEOX, and PPOX can be explained. When alkyl side chains are short, the backbones of polymer chains in the molten state can get closer to each other and the amide dipoles interact strongly. This strong interaction slows down the relaxation of the backbones. The increase in the alkyl side chain length increases the average distance between the amide dipoles of different polymer chains and decreases the average strength of dipolar interactions significantly. Weaker dipolar interactions allow faster relaxation of the backbones to achieve equilibrium crystalline structures.

Cold crystallization was observed for PBOX while PHOX crystallization happened in the cooling cycle. Such cold crystallization is typical for semi-crystalline polymers when cooled down rather fast from molten state to temperatures below T_g or when the polymer chain mobility is rather slow. In case of fast cooling, the time interval that the polymer chains are in between T_m and T_g is short. Within this short time interval, the nucleation and/or growth of crystals cannot happen due to slow dynamics of polymer chains and the polymer goes from a molten to an amorphous solid state. In the heating cycle at the same scan rate, the polymer gets the same time interval between T_g and T_m. Above T_g, crystallization happens and then melting is observed. When the scan rate is decreased or in the case of more mobile polymer chains, the polymer can crystallize partially (crystallinity < 100%) in the cooling cycle because the time between T_m and T_g will now be enough for nucleation and growth of crystals. In the heating cycle the amorphous parts will show T_g and the crystalline parts will show an endothermic melting peak at T_m. The different crystallization behaviors were attributed to different polymer chain mobilities. Decrease in dipolar interaction strength, due to alkyl side chain length increase, allows the system to orient itself to form crystal structure.

Since –propyl and –isopropyl groups are isomers to each other; close physicochemical behaviors could be expected when these three-carbon alkyl substituents are combined to polyoxazolines. Although PIPOX did not show any melting peak at DSC scan rate of 10 °C/min, crystallization behavior was observed in PIPOX by varying isothermal crystallization temperature and time: cold crystallization after 110 °C/45 min isothermal conditions and normal crystallization at optimum temperatures between 130-150 °C. Difference in their behaviors could

be explained with the hindrance of dipolar interactions with the bulky –isopropyl group more compared to –propyl one.

7.5. Conclusions

Polyoxazolines having –methyl, -ethyl, and –propyl side chains were defined to be amorphous in bulk and only showed glass transition in DSC scans. T_g values were found to be decreasing with increasing alkyl side chain length and attributed to the increase in chain mobility. In isothermal annealing studies, heat flows were monitored as a function of time by DSC and any exothermic peaks due to isothermal crystallization were observed. No endothermic peak was observed after isothermal annealing steps too. These results clearly indicate that isothermal crystallization was not observed for PMOX, PEOX, and PPOX. The reason of amorphous behavior of these polymers is thought to be the prevention of backbone relaxations due to strong dipolar interactions between different chains. Increasing alkyl side chain length from propyl to butyl changed the thermal behavior significantly. PBOX showed cold crystallization behavior during heating cycle of the DSC scan. Further increase in alkyl side chain length to -hexyl caused change in crystallization behavior from cold crystallization to normal crystallization. It demonstrates that crystallization of PAOXs is more difficult when alkyl side chain length is small. The increase in the alkyl side chain length increases the average distance between the amide dipoles of different polymer chains and decreases the average strength of dipolar interactions significantly. Although branching side chains decreases the mobility compared to linear analogues, more compact isopropyl groups facilitate their packing into a crystalline structure in PIPOX.

PIPOX was crystallized isothermally in bulk when enough time was given at temperatures between T_g and T_m while linear PPOX was not. Difference could be explained by hindrance of strong dipolar interactions with bulky –isopropyl group.

CHAPTER 8: DURABLE THERMORESPONSIVE AND ANTI-MICROBIAL HYBRID COATINGS OF PEOX

8.1. Overview

Wettability is a fundamental property of a solid surface, which plays important roles in daily life, and industry. Functional surfaces with special wettability have aroused much interest because of their great advantages in applications such as anti-fogging, self-cleaning, and anti-microbial materials [177–179]. Wettability of a surface is simply characterized by measuring the contact angle (CA) of a liquid droplet sitting on the surface. In the case of water droplets, CA less than 90° is indicative of a hydrophilic surface, while CA greater than 90° is hydrophobic [130]. Two extreme cases, superhydrophobic and superhydrophilic surfaces have attracted great attention because of their importance in both fundamental research and practical applications [180], [181].

Smart surfaces with reversibly switchable wettability, especially switching between superhydrophobicity and superhydrophilicity, are of great importance due to their numerous applications such as self-cleaning surfaces and delivery systems [138], [182]. Surfaces with reversible wettability have been achieved by various stimuli, including light irradiation [183], electric field [184], solvent treatments [185], and thermal treatments [186]. Temperature can trigger conformational changes from extended to collapsed structure of thermosensitive polymers, and hence it is considered a promising external stimulus to easily alter the surface wettability. PNIPAM, a common thermoresponsive polymer, has been widely used in

fabrication of surfaces exhibiting reversibly switchable wettability [18], [19], [24]. Despite thermoresponsive behavior is also present in polyoxazolines, carrying short alkyl side chains, switchable wetting of these polymers have not been reported previously.

In addition to switchable wettability, for applications, many other important functions, such as antibacterial or antifungal activity, may be desired. Intensive studies of new antibacterial materials are important because of increase in infections caused by bacteria. Organic antibacterial agents have been broadly utilized. These substances usually have low melting and boiling points; therefore, they have a tendency to evaporate or decompose and lose their toxicity. Previous studies have shown that metal ions such as silver, copper and zinc have antibacterial activity [187]. Among these, silver ions have been shown to have significant effectiveness [188], [189]. Silver nanoparticles also show antibacterial effect [190], [191]. Recently, hybrids of silver nanoparticles with amphiphilic hyperbranched macromolecules were shown to have effective antimicrobial activity [192].

Compared to organic materials, the inorganic–organic hybrids have many advantages, which include chemical durability, thermal resistance and fewer side effects on the human body [193]. Hybrid materials are attractive materials in which the inorganic and the organic components are combined at the molecular level [194]. The sol-gel method is now widely used for the preparation of hybrid material coatings, since it has the advantage of being a low temperature process and potentially giving highly homogeneous coatings [195–197]. Typical precursors are low molecular weight organoalkoxysilanes which undergo various forms of

hydrolysis and polycondensation reactions to form a three dimensional network. The control of the reactivity of organoalkoxyilane is necessary in order to be able to tailor the structure of resulting materials. Most commonly used precursors are tetraethoxysilane (TEOS) and tetramethoxysilane due to their low moisture sensitivity and reactivity [197]. During the formation of silica network, they allow chemical bonding of polymeric/oligomeric materials and also small organic moieties to produce hybrid network. Various hybrid poly-2-methyl-2-oxazoline and poly-2-ethyl-2-oxazoline incorporated silica networks were already explored [198–201]. But, there are very few reports in the literature using these hybrid materials for enhancement of mechanical properties of coatings [202].

Since PEOX is hydrophilic at low temperatures and exhibit hydrophobic behavior above T_c, it has a potential for the production of thermoresponsive surfaces. However, it is already mentioned that PEOX is soluble in water at ambient temperature. That means, in the presence of water physically adsorbed PEOX film will be desorbed from the surface. To change the adhesion of PEOX from physical adsorption to chemical bonding, another component should be added to the coating solution. By this method, thermoresponsive and durable coatings could be produced. In this chapter, we report on functional PEOX coatings. Thermoresponsive and antimicrobial PEOX coatings were prepared on glass or siliconoxide surfaces. Antibacterial activity was provided by addition of synthesized silver nanoparticles. Adhesions of the coatings to solid substrates were improved by addition of silica networks, synthesized by TEOS, to the polymer solutions. Addition of silica network to coatings also inhibited water penetration and increased durability. Synthesis, characterization and antibacterial activity of silver nanoparticles are described in section 8.3.1. Synthesis of the inorganic TEOS sol

and hybrid solution, characterization of interactions in hybrid coating solution, temperature induced surface wettability change of coatings, adhesion and antibacterial properties of coatings are explained in sub-sections of 8.3.2.

8.2. Experimental Details

PEOX (Mw ~ 200,000) was used in all experiments. The sizes of the AgNPs in solutions were measured by DLS at 25 ºC and for each measurement 100 data with 10 s run time were recorded. Since the technique does not give direct information of single particles; a particle size distribution is obtained. AgNPs have significant absorption band around 400 nm [203]. UV-Vis spectra of solutions were recorded between 300-800 nm to monitor synthesis and stability of silver nano-particles. The antimicrobial activity of silver nano-particles was investigated against *E. Coli* as a model for Gram-negative bacteria. Bacteriological tests were performed in both liquid Lactose Broth (LB) medium and also LB medium on solid agar plates. Different volumes of silver nano-particle containing solutions were added to these mediums and bactericidal activities were expressed by optical density measurements and viable colony formation unit (CFU) counts. A Carry 100 Bio model UV–Vis Spectrophotometer was used to measure optical densities of incubated bacteria and to obtain bacterial growth curves.

AgNP containing polymer solutions were dip-coated (or spin coated) on silicon and glass substrates. Spin coatings were performed at the rate of 2000 rpm for 1 min. Film thicknesses were controlled by changing the concentration of solutions. Dip coatings were prepared from specified concentration of the hybrid-coating solution and film thicknesses were controlled by varying the withdrawal rate of the

substrates from solution. FTIR was used to probe interactions of the acid catalyzed tetraethyl orthosilicate (TEOS) sol with PEOX-200K. Film morphologies were mainly studied by atomic force microscopy in tapping mode. Static water contact angle measurements, in the temperature range of 20 °C to 80 °C, were carried out to probe thermoresponsiveness of the coatings.

8.3. Results and discussions

8.3.1. Silver nanoparticles in solutions and their antibacterial activity

8.3.1.1. Synthesis of silver nanoparticles (AgNP)

Synthesis of AgNP's was achieved by reduction of silver ions according to the reaction:

$$2AgNO_3 + 2NaBH_4 \longrightarrow 2Ag + H_2 + B_2H_6 + 2NaNO_3$$

Excess amount of sodium borohydrate (15 ml, 0.001M $NaBH_4$ solution in ethanol) was kept in ice bath to decrease the reaction rate. Silver nitrate solution (5 ml, 0.001M $AgNO_3$ in ethanol) was added to the reaction medium drop by drop to prevent the sudden growth of AgNP's. Experimental set-up is shown in figure 8.1 a).

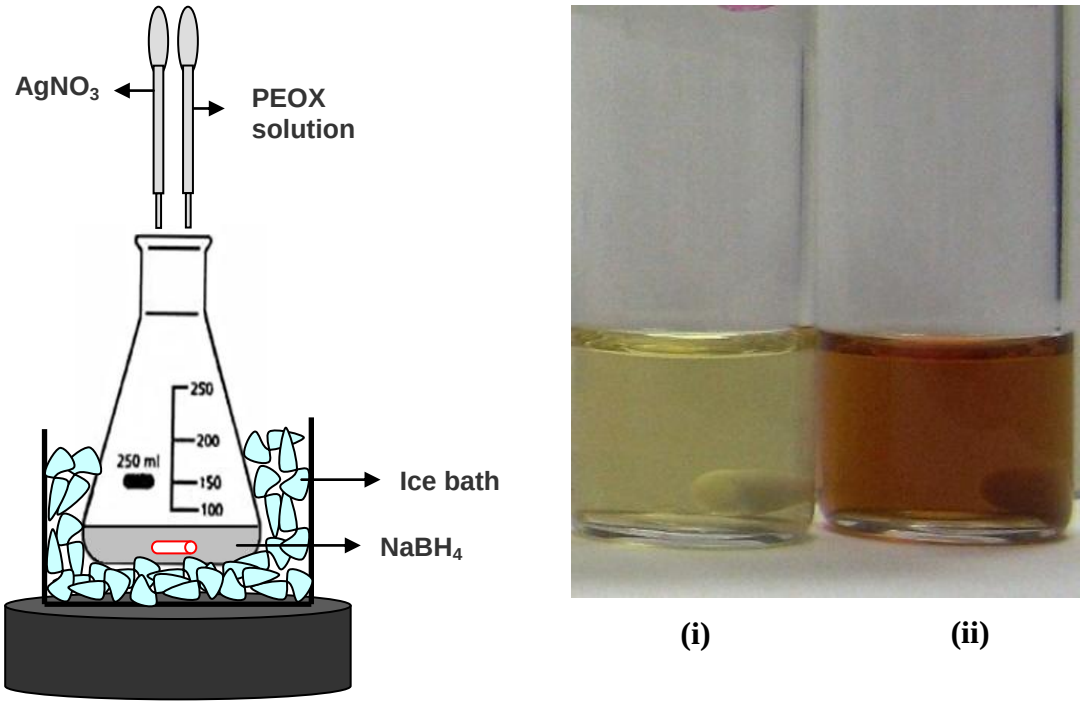

Figure 8. 1a) Experimental set-up used for the synthesis of AgNPs. b) Photograph of AgNP containing solutions with (i) and without (ii) PEOX-200K

It is well known that polymers adsorbed onto particles prevent particle aggregation due to steric hindrance of the adsorbed polymers [204]. During the reaction, 100 mg/ml PEOX-200K solution in ethanol was added simultaneously with $AgNO_3$ solution to isolate formed nano-particles from each other. When solution has been prepared without PEOX-200K, the bright yellow color of the solution was turned to brown due to aggregation and oxidation of silver nano-particles (figure 7.1 b). In addition to increased stability of AgNPs, adsorbed PEOX

chains on AgNPs also helped better miscibility with the matrix of the coatings which is also PEOX.

8.3.1.2. Stability of AgNP's containing PEOX solutions

To control the size of AgNPs and to prevent their aggregation, PEOX-200K was added during the synthesis of AgNPs. Growth of the silver nano-particles was followed by DLS measurements. Figure 8.2 shows the comparison of sizes of AgNPs with and without PEOX addition.

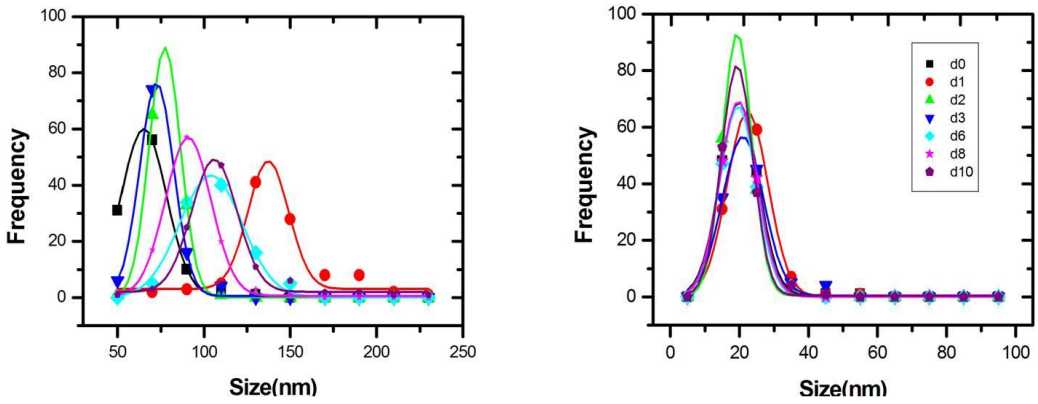

Figure 8. 2 Size of AgNPs a) without and b) with PEOX additions as a function of time: black squares (after synthesis), red circles (1st day), green triangles (2nd day), blue inverse triangles (3rd day), cyan rhombohedrons (6th day), pink stars (8th day), and purple pentagons (10th day).

The size distribution profile of the AgNPs was obtained at 25 ºC as a function of time. Particle sizes were defined as the maximum of the Gaussian curves which were fitted to the frequency count data. In figure 8.2. a) The size of the freshly

synthesized nano-particles was around 54 nm. The size increased with time and finally particles aggregated. This indicates that synthesized AgNPs are not stable in the absence of PEOX in solutions. In figure 8.3 a) size distribution profile of the AgNPs in the presence of PEOX is shown. When PEOX was added during the synthesis of AgNPs to obtain 50 mg/ml final concentration, size of the AgNPs decreased to 22 nm from 54 nm. The size of the particles did not change even 10 days after synthesis. The increase in the frequency of particles in size data demonstrates that during this period new silver nano-particles were formed. This result indicates that PEOX adsorbs on the surface of the particles and prevent aggregation. Stability of AgNPs in solution was also monitored by UV-vis spectroscopy in the wavelength range of 300-800 nm. In figure 8.3 UV-spectra of PEOX-200K containing AgNPs characteristic absorptions are shown as a function of time.

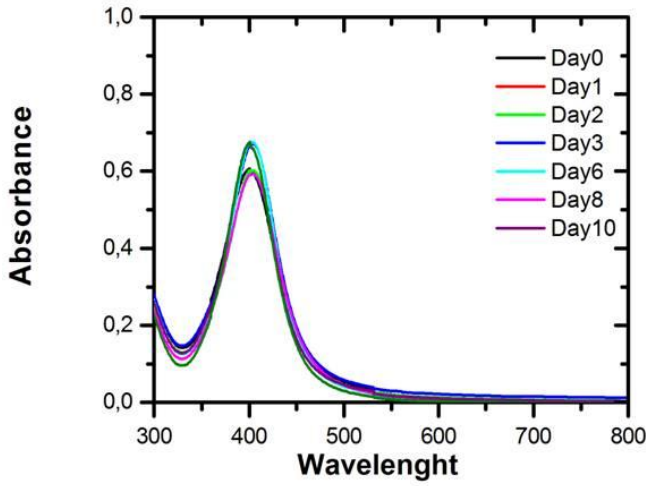

Figure 8. 3 UV-Vis spectra of PEOX-200K containing AgNP solution as a function of time.

AgNPs showed significant absorption band around 400 nm. Position of the peak did not change for 10 days. This indicates that PEOX adsorption on AgNP surfaces was successful in preventing agglomeration.

8.3.1.3. Antibacterial activity of PEOX-AgNP solutions

The antibacterial activity of the silver nano-particles was investigated against gram-negative Escherichia coli. The cells divide at a constant rate depending on the composition of the growth medium and the conditions of incubation, such as temperature and rotation rate. In general, E. coli grows between 5 °C and 46°C with an optimum of 35–40 °C. During the experiments lactose broth (LB) was used as inoculation medium and growth medium temperature was 37 °C and rotation rate is 200 rpm [205]. 4 different solutions were prepared for the investigation of antibacterial activity of AgNPs. These solutions are:

Solution 1. Negative control solution containing 10 ml LB and 200 µl *E. coli* overnight stock solution.
Solution 2. Positive control solution containing 10 ml LB, 200 µl *E. Coli* overnight stock solution and 10 µl antibiotic solution
Solution 3. 10 ml LB, 200 µl *E. Coli* overnight stock solution and 400µl AgNP solution which is not containing PEOX in it
Solution 4. 10 ml LB, 200 µl *E. Coli* overnight stock solution and 400µl PEOX-AgNP solution

UV–Vis Spectrophotometer was used to measure optical densities of incubated bacteria as a function of time to obtain bacterial growth curves. Under favorable

conditions, a growing bacterial population doubles at regular intervals. Transparent liquid solution becomes turbid with time due to increase in bacterial cells in solution. All measurements were done at the wavelength of 550 nm and the results are shown in figure 8.4.

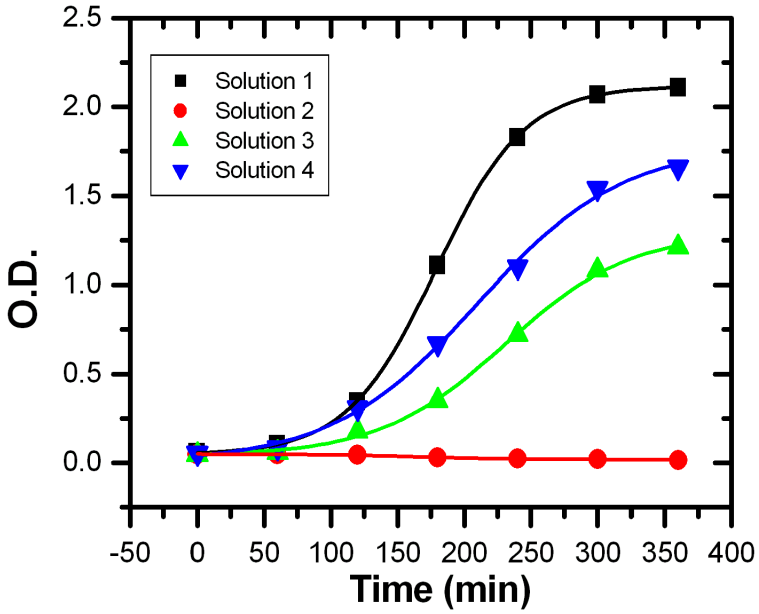

Figure 8. 4 Bacterial growth curves of negative control (black), positive control (red), AgNP solution (blue) and AgNP-PEOX solution (green)

Figure 8.4 shows the optical densities of each solution as a function of time. Each color represents the growth curve of *E coli* in different solutions and curves are sigmoidal fit to the data. Typical sigmoidal growth curves were obtained for all solutions except for solution 2. Ag nano-particles showed slight growth inhibition effect against *E. Coli* compared with the negative control. None of the solution was effective as antibiotic. More concentrated solutions are needed to enhance

antibacterial activity. On coatings, with removal of solvent the concentration of silver nano-particles will increase. This may lead to more effective antibacterial property.

8.3.2. PEOX-AgNP-TEOS hybrid coatings

The sol-gel method is now widely used for the preparation of inorganic-organic hybrid coatings. Most commonly used precursors are tetraethoxysilane (TEOS) and tetramethoxysilane (TMOS). During the formation of silica network, they allow chemical bonding of polymeric materials to produce hybrid network. To obtain durable thermoresponsive coatings on surfaces, silica network was added to PEOX-AgNP solution. TEOS was used as precursor to synthesize desired network by hydrolysis and polycondensation reactions.

8.3.2.1. Synthesis of TEOS sol

TEOS is ideal chemical precursor for sol-gel synthesis because it reacts readily with water. The reaction is called hydrolysis, and shown in figure 8.5.

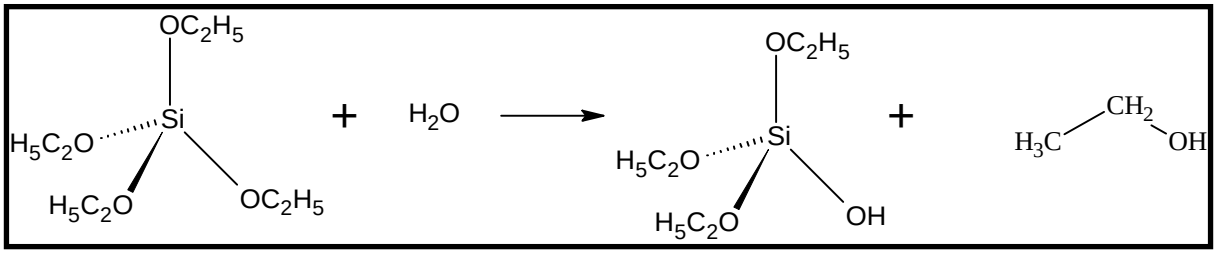

Figure 8. 5 Hydrolysis reaction of TEOS

This reaction proceeds with condensation. By definition, condensation liberates a small molecule, such as water or alcohol (see in figure 8.6).

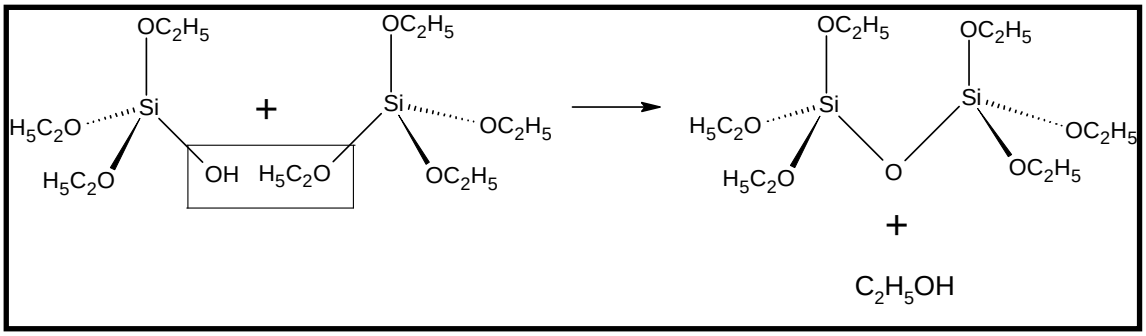

Figure 8. 6 Ethanol condensation reaction

This type of reaction can continue to build larger and larger silicon-containing molecules by the process of polycondensation reactions in acidic conditions. A representative part of such a network can be shown in figure 8.7.

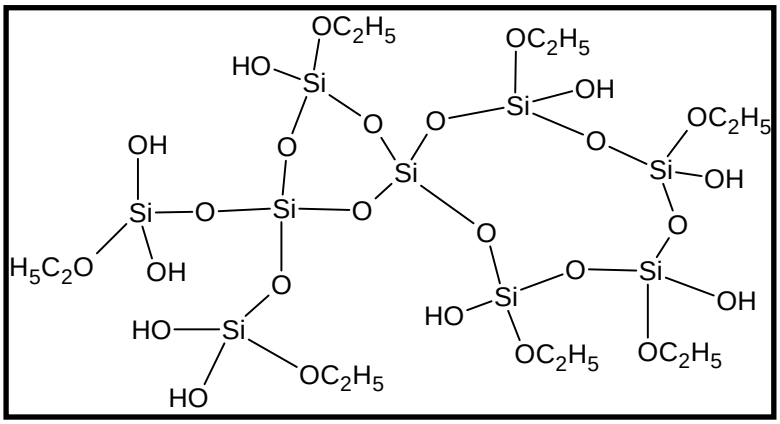

Figure 8. 7 Shematic representation of silica network

The obtained organically modified network was used as the inorganic part of the hybrid coating solution. In this study, the acid-catalyzed solution was prepared from TEOS, ethanol, concentrated nitric acid and distilled water. The TEOS sol was prepared in three steps by mixing constituents separately. After that, the TEOS sol was stirred at room temperature for 12 hours for the formation of network like structure.

8.3.2.2. Synthesis of PEOX-AgNP-TEOS hybrid solutions

PEOX solution containing silver nano-particles was mixed with TEOS sol. Schematic representation of hybrid coating can be seen in figure 8.8.

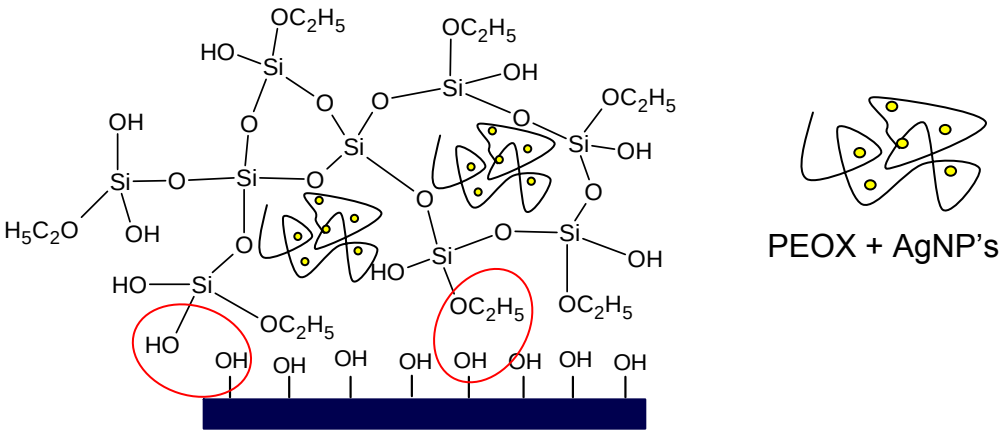

Figure 8. 8 Schematic representation of hybrid coating

In figure 8.8, silver nano-particles are represented as yellow dots and PEOX is shown as rope like structure which was both adsorbed on surfaces of silver nanoparticles and also traped them in its entanglements. These structures are

incorporated in overall hybrid structure by mixing PEOX-AgNP and TEOS sols. Presence of –OR and –OH functionalities in the network structure also thought to enhance adhesion of the coating solution.

8.3.2.3. Characterization of interactions between PEOX and TEOS by FT-IR spectroscopy

Different amount of 50 mg/ml PEOX-200K solution was added to acid catalyzed TEOS solutions in ethanol. Solutions were coated on glass substrates by spin coating and dried coatings were investigated by Fourier transform infrared spectroscopy (FT-IR spectroscopy) (figure 8.9).

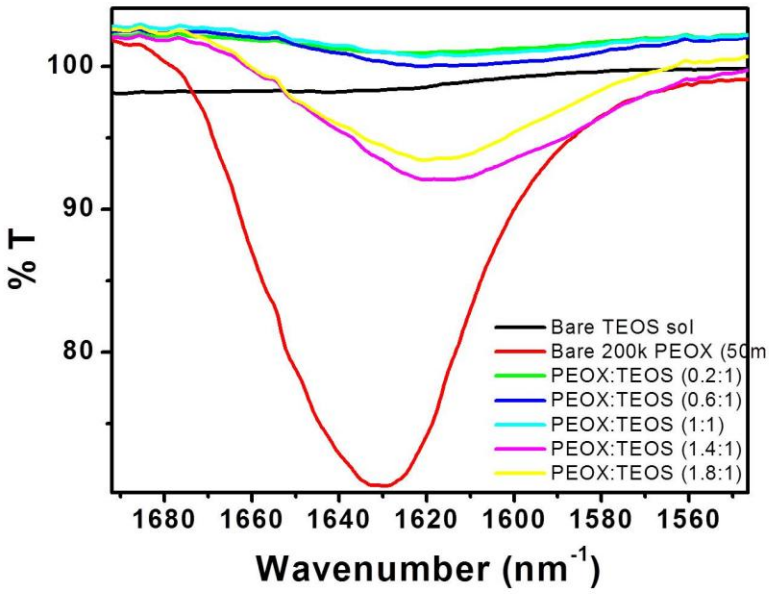

Figure 8. 9 IR analysis of coatings prepared by mixture of different amounts of PEOX-200K in fixed amount of acid catalyzed TEOS sol.

In figure 8.9 FT-IR spectra of the PEOX-TEOS coatings are shown between 1550 to 1700 cm^{-1}, where the intense amide carbonyl peak exists. Increasing amount of PEOX in coating solutions caused shift in the amide carbonyl peak of PEOX from 1630 cm^{-1} to the lower wave numbers. We attributed this shift to the hydrogen bonding interaction between the amide carbonyl group of the PEOX and the –OH functional part of the silica network.

8.3.2.4. Thermoresponsive behavior of hybrid coatings

PEOX-AgNP and different amount of TEOS sol containing PEOX-AgNP-TEOS solutions were dip coated on glass substrates and water contact angles on these films were investigated as a function of temperature. Results are shown in Figure 8.10.

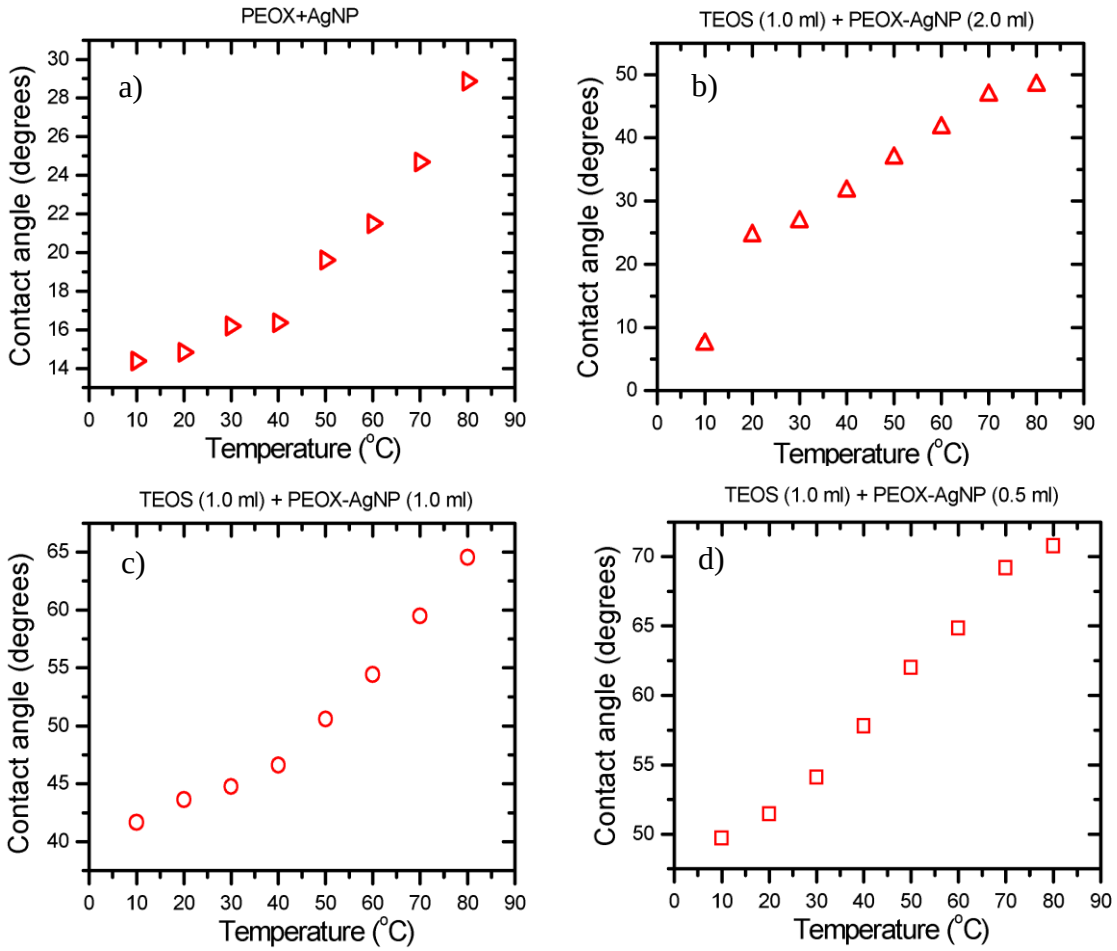

Figure 8. 10 Static water contact angle measurement results of a) PEOX-AgNP coating, b), c) and d) PEOX-AgNP-TEOS coatings including 1 ml of TEOS sol and 2.0 ml, 1.0 ml, and 0.5 ml PEOX-AgNP sol respectively.

In figure 8. 10 a) Static water contact angle (CA) measurement of PEOX-AgNP sol is shown as a function of temperature. CA value was observed to be increasing with increasing temperature from 14 to 29 °. Figure 8.10 b) shows the improvement in the thermoresponsive behavior of the coating with addition of small amount of TEOS sol to the coating solution. Low temperature contact angle value

decreased from 14 to 8 ° and CA increased with temperature up to 50 °. Further increase in the amount of TEOS sol caused increase in CA value to 42 and 50 ° and clearly shown in Figure 8.10 c) and d). Highest CA value ~ 70 ° was obtained when the volume of the TEOS sol in the hybrid solution is more than PEOX sol.

Contact angle above 90 ° (hydrophobic) could not be obtained from any of the coatings but CA values were observed to be increasing with temperature. Increase in amount of PEOX in solutions decreased CA values because of hydrophilic nature of PEOX at low temperatures compared to TEOS network. With PEOX films, switching of surface chemistry is achieved by virtue of a thermally-activated swelling transition in water which occurred gradually.

8.3.2.5. Morphologies of smart coatings before and after water treatments

Stability of the coatings on the surfaces is very important. By addition of different amount of TEOS sols to the PEOX-AgNP sol hybrid coatings were produced to improve adhesion of coatings and prevention of water penetration. Coatings were kept in water around 1 hour and surface morphologies were investigated by AFM both before and after water treatments. In figure 8.11 AFM height images of surfaces are shown.

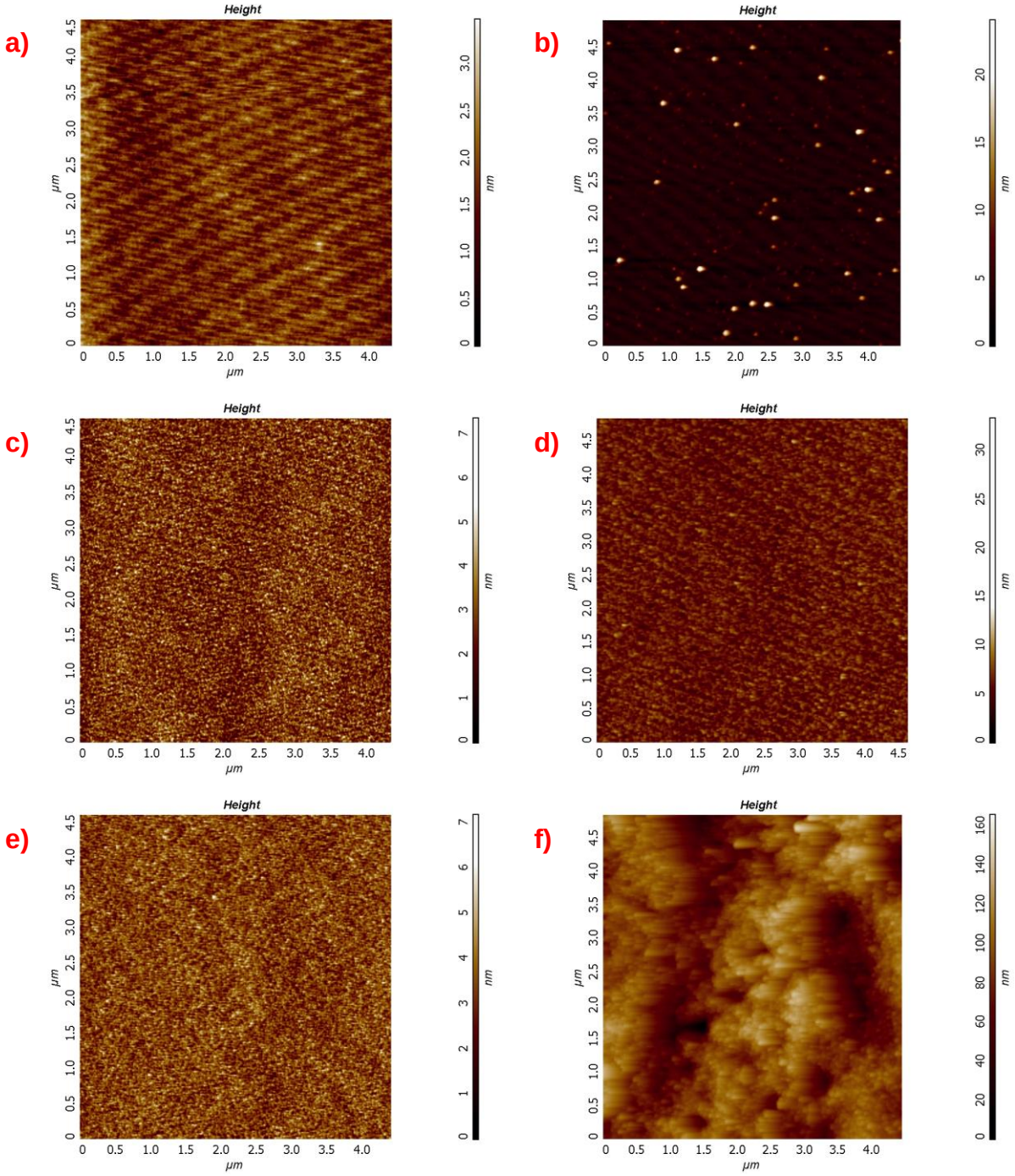
a)
b)
c)
d)
e)
f)
Height
µm
nm

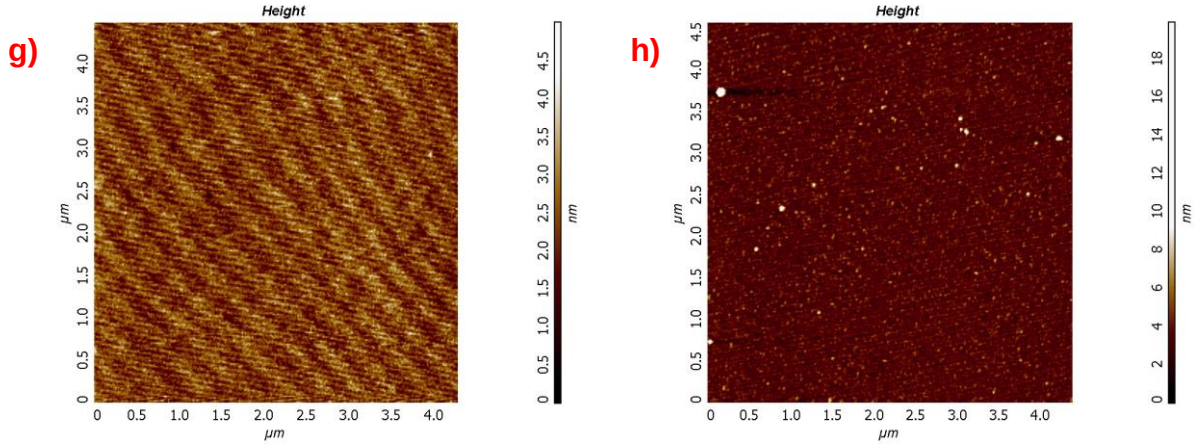

Figure 8. 11 AFM height images of a) and b) PEOX-AgNP solution, c) and d) PEOX-AgNP (0.5 ml)+TEOS sol (1.0 ml) solution, e) and f) PEOX-AgNP (1.0 ml)+TEOS sol (1.0 ml) solution, g) and h) PEOX-AgNP (2.0 ml)+TEOS sol (1.0 ml) before and after water treatments respectively.

The surfaces of the all coatings were quite smooth before water treatments. Root mean square roughness of the surfaces, which were calculated from 5 µm x 5 µm areas, are 0.39 nm, 0.89 nm, 0.82 nm and 0.57 nm for a), c), e) and g), respectively. After water treatment, roughnesses of the surfaces are changed to 3.27 nm, 1.27 nm, 19.41 nm and 0.88 nm for b), d), f) and h), respectively. There is only physical adsorption of coating material to the glass surface in the case of PEOX-AgNP coating. Nearly all the coating was removed from the surface and ~20 nm high islands were formed on the surface. With addition of large volume of TEOS sol into the PEOX-TEOS solution (c and d) coatings gained stability and surface roughness nearly did not change. After water treatment surface roughness stayed nearly unchanged, which indicates successful penetration of water was achieved. Decreased volume of TEOS-sol in hybrid solution (e) did not affect the

surface morphology of the film but after water treatment film was swelled and very high roughness was observed. It is clearly seen in Figure 8.11. f). It indicates that penetration of water molecules to the inside of the coating was enhanced and highly swelled coating showed very rough surface morphology in AFM investigations. When the amount of TEOS was halved (g), coating was dewetted from the surface after water and 15 nm to 20 nm high spherical islands were formed. These islands are shown in Figure 8.11. h). According to these results it can be concluded that most stable film against water was obtained from PEOX-AgNP (0.5 ml) + TEOS sol (1.0 ml) solution.

8.3.2.6. Anti-bacterial activity of coatings

Anti-bacterial activities of the coatings were investigated according to the ASTM E 2180-01 protocol by Arçelik. According to this protocol anti-bacterial activity is classified into 4 different classes according to the decrease in the colony formation units (CFU). If the inhibition is smaller than 10 that means the surface has no bactericidal effect. Inhibition range 10 – 10^2 classified as low bactericide and 10^2 – 10^3 is defined as effective bactericide. Inhibition more than 10^3 is called strong bactericide. AgNP doped PEOX – TEOS hybrid coatings were investigated against gram negative *E. coli* and gram positive *S. aureus*. According to the inhibitions in CFU's, developed coatings have effective anti-bacterial activity against *E. coli* and *S. aureus.*

8.4. Conclusions

Silver nano-particles were synthesized in PEOX containing solution to enhance the colloidal stability of solution. Antibacterial properties of the solutions were investigated against gram negative *E. coli* bacteria and Ag nano-particles showed slight growth inhibition effect. Adhesion properties and durability of the coatings were improved by addition of silica networks to the solutions. FT-IR measurements clearly showed that increasing amount of PEOX in coating solutions caused shift in the amide carbonyl peak of PEOX from 1630 cm^{-1} to the lower wave numbers. We attributed this shift to the hydrogen bonding interaction between the amide carbonyl group of the PEOX and the –OH functional part of the silica network. Switching of surface chemistry of films was achieved by thermally-activated swelling transition of PEOX. Increase in amount of PEOX in coatings caused decrease in contact angle values by incorporating more hydrophilic character to it. Decreasing amount of PEOX in the solutions caused increase in adhesion of coating to the substrate and also prevents the dewetting of the film in water treatments. Effective anti-bacterial activity against gram negative *E. coli* and gram positive *S. aureus* was observed for hybrid coating.

CONCLUSION

Behavior of PEOX in aqueous solutions was thoroughly investigated. T_c of solutions were probed by DLS measurements to understand the effect of different variables on critical solution behavior of PEOX. Influences of PEOX concentration, molecular weight, and series of sodium salts from Hofmeister series were systematically studied. It was found that increasing concentration and molecular weight of the PEOX caused decrease in T_c. For polymers, which have same end-caps in their backbone end, increasing molecular weight cause decrease in effect of end groups on T_c and thus T_c decreases. T_c was observed to be linearly decreasing with increasing kosmotropic salt concentration in aqueous PEOX solutions. T_c showed nonlinear dependence with increasing chaotropic salt concentration. These behaviors were explained by mechanisms containing hydration entropy of anions, surface tension increment, and direct ion binding similar to PNIPAM. However, PEOX T_c was tuned in a very large temperature scale (20 °C to 70 °C) with addition of salts compared to small temperature range of PNIPAM. This difference was attributed to their chemical structure difference. PNIPAM can behave as a hydrogen donor, because of the secondary amide in its structure and needs more ions for dehydration. For divalent kosmotropic anions the dominant mechanism was proposed as the dehydration of PEOX chains. For monovalent kosmotropic anions a combination of dehydration and surface tension mechanisms was responsible for the change of T_c. Chaotropic anions did not show any correlation with hydration entropy and surface tension increments. It indicates that direct ion binding is the dominant mechanism for chaotropic anions.

PEOX is the only polymer which was found to be amorphous in bulk in literature. We have studied on isothermal crystallization of different alkyl side chain length (–methyl, –ethyl, –propyl, –butyl, –hexyl, and –isopropyl) PAOXs. PMOX, PEOX, and PPOX showed only T_g in DSC during heating cycles. We could not crystallize any of them in bulk by isothermal annealing. Cold crystallization was observed for PBOX, and PHOX crystallization happened in the cooling cycle. The different crystallization behaviors were attributed to different polymer chain mobilities. Increase in alkyl side chain length cause increase in chain mobility and also decrease in dipolar interaction strength between different chains. It is known that branching in the alkyl side chain decreases the chain mobility, but we achieved to crystallize PIPOX isothermally in bulk. This crystallinity difference between PPOX and PIPOX was attributed to the decrease in dipolar interaction strength due to hindrance of the interaction by more bulky isopropyl group. It can be concluded that for easy crystallization alkyl side chain length should be long or branched.

PIPOX was found to crystallize upon isothermal treatment in aqueous solutions above the cloud point temperature (T_c) into fibers. The crystal structure (specifically the largest d spacing) and T_m of these crystalline fibers were consistent with those expected from bulk polymers. Such crystallization has not been reported for PEOX in aqueous solution. We observed for the first time self-assemled PEOX fibers above T_c, and rate of aggregation was found to be enhanced with addition of salting-out (NaAc) and salting-in (NaSCN) additives. DSC and XRD investigations confirmed that formed fibers in the presence of salts are crystalline. Also PEOX formed fiber type aggregates when aqueous solutions were kept far below T_c of the solution. Aggregation was observed to be much slower compared to self-assembly

above T_c. Aggregation kinetics were studied by following aggregation stages as a function of PEOX concentration and molecular weight, and sigmoid type growth curves were obtained. This type of curves demonstrates that PEOX followed typical nucleation and growth mechanism for self-assembly. These aggregates are also crystalline like those formed above T_c, and T_m of these crystalline fibers were consistent with those expected from bulk polymers and in agreement with the previously reported data. Crystallinity of PEOX could not be achieved in bulk. Thus, hydrophobic and dipolar interactions are not enough to explain crystallization. One end of the amide dipole is on the backbone of the PEOX, so backbone solvation in aqueous medium was proposed to contribute to the mobility of polymer and leads the system to form well-defined crystals, similar to PIPOX.

Thermoresponsive behaviors of PAOXs in aqueous solutions were thoroughly investigated but on surfaces it has not been reported previously. Anti-bacterial, thermoresponsive, and durable films were prepared by combination of PEOX, AgNPs, and silica network in hybrid coating solution. Each component in solution gave one of the functionality. Switching of surface chemistry of films was achieved by thermally-activated swelling transition of PEOX. Effective anti-bacterial activity against gram negative *E. coli* and gram positive *S. aureus* was observed for hybrid coating due to the presence of AgNPs. Addition of silica network to coatings caused increase in contact angle values, increase in adhesion of coating to the substrate, and prevent the dewetting of the film in water treatments.

BIBLIOGRAPHY

[1] A. Ansari, P. Scaria, and M. Woodle, “Polymers for delivering peptides and small molecules in vivo,” *US Patent 2006/0051315*, 2003.

[2] J. Warchol and C. Walton, “Creping adhesives containing oxazoline polymers and methods of use thereof,” *US Patent 5,980,690*, 1999.

[3] S. Ma and J. Rodriguez-Parada, “Block copolymers of oxazolines and oxazines as pigment dispersants and their use in ink jet inks,” *US Patent 5,854,331*, 1998.

[4] M. a C. Stuart, W. T. S. Huck, J. Genzer, M. Müller, C. Ober, M. Stamm, G. B. Sukhorukov, I. Szleifer, V. V Tsukruk, M. Urban, F. Winnik, S. Zauscher, I. Luzinov, and S. Minko, “Emerging applications of stimuli-responsive polymer materials.,” *Nature materials*, vol. 9, no. 2, pp. 101–13, Feb. 2010.

[5] N. Takeda, E. Nakamura, M. Yokoyama, and T. Okano, “Temperature-responsive polymeric carriers incorporating hydrophobic monomers for effective transfection in small doses.,” *Journal of controlled release : official journal of the Controlled Release Society*, vol. 95, no. 2, pp. 343–55, Mar. 2004.

[6] H. Schild, “Poly (N-isopropylacrylamide): experiment, theory and application,” *Progress in Polymer Science*, vol. 17, pp. 163–249, 1992.

[7] S.-Y. Lin, K.-S. Chen, and R.-C. Liang, “Thermal micro ATR/FT-IR spectroscopic system for quantitative study of the molecular structure of poly(N-isopropylacrylamide) in water,” *Polymer*, vol. 40, no. 10, pp. 2619–2624, May 1999.

[8] H. Inomata, S. Goto, and S. Saito, “Phase transition of N-substituted acrylamide gels,” *Macromolecules*, vol. 23, pp. 4887–4888, 1990.

[9] M. Shibayama, S. Mizutani, and S. Nomura, “Thermal properties of copolymer gels containing N-isopropylacrylamide,” *Macromolecules*, vol. 29, pp. 2019–2024, 1996.

[10] K. Otake, H. Inomata, M. Konno, and S. Saito, “Thermal analysis of the volume phase transition with N-isopropylacrylamide gels,” *Macromolecules*, vol. 23, no. 1, pp. 283–289, Jan. 1990.

[11] P. Lin, C. Clash, and E. Pearce, “Solubility and miscibility of poly (ethyl oxazoline),” *Journal of Polymer …*, vol. 26, pp. 603–619, 1988.

[12] A. L. Demirel, M. Meyer, and H. Schlaad, “Formation of polyamide nanofibers by directional crystallization in aqueous solution.,” *Angewandte Chemie (International ed. in English)*, vol. 46, no. 45, pp. 8622–4, Jan. 2007.

[13] M. Meyer, M. Antonietti, and H. Schlaad, “Unexpected thermal characteristics of aqueous solutions of poly(2-isopropyl-2-oxazoline),” *Soft Matter*, vol. 3, no. 4, p. 430, 2007.

[14] M. Litt, F. Rahl, and L. Roldan, “Polymerization of cyclic imino ethers. VI. X-ray study of some polyaziridines,” *Journal of Polymer Science Part A-2*, vol. 7, pp. 463–473, 1969.

[15] R. Hoogenboom, M. W. M. Fijten, H. M. L. Thijs, B. M. van Lankvelt, and U. S. Schubert, “Microwave-assisted synthesis and properties of a series of poly(2-alkyl-2-oxazoline)s,” *Designed Monomers & Polymers*, vol. 8, no. 6, pp. 659–671, Dec. 2005.

[16] E. F.-J. Rettler, J. M. Kranenburg, H. M. L. Lambermont-Thijs, R. Hoogenboom, and U. S. Schubert, “Thermal, Mechanical, and Surface Properties of Poly(2-N-alkyl-2-oxazoline)s,” *Macromolecular Chemistry and Physics*, vol. 211, no. 22, pp. 2443–2448, Nov. 2010.

[17] T. Yakushiji, K. Sakai, A. Kikuchi, and T. Aoyagi, “Graft architectural effects on thermoresponsive wettability changes of poly (N-isopropylacrylamide)-modified surfaces,” *Langmuir*, vol. 14, pp. 4657–4662, 1998.

[18] L. Liang, P. Rieke, and G. Fryxell, “Temperature-sensitive surfaces prepared by UV photografting reaction of photosensitizer and N-isopropylacrylamide,” *The journal of physical chemistry. B*, vol. 104, pp. 11667–11673, 2000.

[19] E. Burdukova, H. Li, N. Ishida, J.-P. O’Shea, and G. V Franks, “Temperature controlled surface hydrophobicity and interaction forces induced by poly (N-isopropylacrylamide).,” *Journal of colloid and interface science*, vol. 342, no. 2, pp. 586–92, Feb. 2010.

[20] A. S. Hoffman, “The origins and evolution of ‘controlled’ drug delivery systems.,” *Journal of controlled release : official journal of the Controlled Release Society*, vol. 132, no. 3, pp. 153–63, Dec. 2008.

[21] Z. Liu and P. Calvert, “Multilayer Hydrogels as Muscle-Like Actuators,” *Advanced Materials*, vol. 12, no. 4, pp. 288–291, Feb. 2000.

[22] M. Motornov, S. Minko, and K. Eichhorn, “Reversible tuning of wetting behavior of polymer surface with responsive polymer brushes,” *Langmuir*, vol. 10, no. 9, pp. 8077–8085, 2003.

[23] P. M. Mendes, “Stimuli-responsive surfaces for bio-applications.,” *Chemical Society reviews*, vol. 37, no. 11, pp. 2512–29, Nov. 2008.

[24] A. Kikuchi and T. Okano, “Intelligent thermoresponsive polymeric stationary phases for aqueous chromatography of biological compounds,” *Progress in Polymer Science*, vol. 27, no. 6, pp. 1165–1193, Jul. 2002.

[25] B. Jeong and A. Gutowska, “Lessons from nature: stimuli-responsive polymers and their biomedical applications.,” *Trends in biotechnology*, vol. 20, no. 7, pp. 305–11, Jul. 2002.

[26] I. Galaev and B. Mattiasson, “‘Smart’polymers and what they could do in biotechnology and medicine,” *Trends in biotechnology*, vol. 17, pp. 335–340, 1999.

[27] A. Hoffman and P. Stayton, “Really smart bioconjugates of smart polymers and receptor proteins,” *Journal of Biomedical Materials Research*, vol. 52, no. 4, pp. 577–586, 2000.

[28] Y. Qiu and K. Park, “Environment-sensitive hydrogels for drug delivery.,” *Advanced drug delivery reviews*, vol. 53, no. 3, pp. 321–39, Dec. 2001.

[29] K. Nakajima, S. Honda, Y. Nakamura, F. López-Redondo, S. Kohsaka, M. Yamato, a Kikuchi, and T. Okano, “Intact microglia are cultured and non-invasively harvested without pathological activation using a novel cultured cell recovery method.,” *Biomaterials*, vol. 22, no. 11, pp. 1213–23, Jun. 2001.

[30] D. Meyer, G. Kong, and M. Dewhirst, “Targeting a genetically engineered elastin-like polypeptide to solid tumors by local hyperthermia,” *Cancer research*, vol. 61, pp. 1548–1554, 2001.

[31] D. Roy, W. L. a Brooks, and B. S. Sumerlin, “New directions in thermoresponsive polymers.,” *Chemical Society reviews*, vol. 42, no. 17, pp. 7214–43, Sep. 2013.

[32] a Durand and D. Hourdet, “Thermoassociative graft copolymers based on poly(N-isopropylacrylamide): effect of added co-solutes on the rheological behaviour,” *Polymer*, vol. 41, no. 2, pp. 545–557, Jan. 2000.

[33] C. Pietsch, R. Hoogenboom, and U. S. Schubert, “PMMA based soluble polymeric temperature sensors based on UCST transition and solvatochromic dyes,” *Polymer Chemistry*, vol. 1, no. 7, p. 1005, 2010.

[34] E. a. Clark and J. E. G. Lipson, “LCST and UCST behavior in polymer solutions and blends,” *Polymer*, vol. 53, no. 2, pp. 536–545, Jan. 2012.

[35] G. Karlström, “A new model for upper and lower critical solution temperatures in poly (ethylene oxide) solutions,” *The Journal of Physical Chemistry*, vol. 89, pp. 4962–4964, 1985.

[36] H. Feil, Y. H. Bae, J. Feijen, and S. W. Kim, “Effect of comonomer hydrophilicity and ionization on the lower critical solution temperature of N-isopropylacrylamide copolymers,” *Macromolecules*, vol. 26, no. 10, pp. 2496–2500, May 1993.

[37] G. Ten Brinke and F. Karasz, “Lower critical solution temperature behavior in polymer blends: compressibility and directional-specific interactions,” *Macromolecules*, vol. 17, pp. 815–820, 1984.

[38] N. Southall, K. Dill, and A. Haymet, “A view of the hydrophobic effect,” *The Journal of Physical …*, vol. 106, pp. 521–533, 2002.

[39] F. Liu, J. Seuring, and S. Agarwal, “Controlled radical polymerization of N -acryloylglycinamide and UCST-type phase transition of the polymers,” *Journal of Polymer Science Part A: Polymer Chemistry*, vol. 50, pp. 4920–4928, Dec. 2012.

[40] W. Jackson and J. Brandts, “of protein denaturation. Calorimetric study of the reversible denaturation of chymotrypsinogen and conclusions regarding the accuracy of the two-state approximation,” *Biochemistry*, vol. 9, pp. 2294–2301, 1970.

[41] E. Tiktopulo, V. Uversky, and V. Lushchik, “‘ Domain’ Coil-Globule Transition in Homopolymers,” *Macromolecules*, vol. 28, pp. 7519–7524, 1995.

[42] J. Seuring and S. Agarwal, “Polymers with Upper Critical Solution Temperature in Aqueous Solution: Unexpected Properties from Known Building Blocks,” *ACS Macro Letters*, vol. 2, no. 7, pp. 597–600, Jul. 2013.

[43] H. Schild and D. Tirrell, “Microcalorimetric detection of lower critical solution temperatures in aqueous polymer solutions,” *Journal of Physical Chemistry*, vol. 94, pp. 4352–4356, 1990.

[44] P. Painter, Y. Park, and M. Coleman, “Thermodynamics of hydrogen bonding in polymer blends. 2. Phase behavior,” *Macromolecules*, vol. 22, pp. 580–585, 1989.

[45] F. Winnik, “Fluorescence studies of aqueous solutions of poly (N-isopropylacrylamide) below and above their LCST,” *Macromolecules*, vol. 242, no. 7, pp. 233–242, 1990.

[46] A. R. Shultz and P. J. Flory, “Phase Equilibria in Polymer—Solvent Systems,” *Journal of the American Chemical Society*, vol. 74, no. 19, pp. 4760–4767, Oct. 1952.

[47] R. . Horne, “Macromolecule hydration and the effect of solutes on the cloud point of aqueous solutions of polyvinyl methyl ether: A possible model for protein denaturation and temperature control in homeothermic animals,” *Journal of Colloid and Interface Science*, vol. 35, pp. 77–84, 1971.

[48] G. Némethy, “Structure of Water and Hydrophobic Bonding in Proteins. I. A Model for the Thermodynamic Properties of Liquid Water,” *Journal of Chemical Physics*, vol. 36, pp. 3401–3417, 1962.

[49] F. Zeng, Z. Tong, and H. Feng, “NMR investigation of phase separation in poly (N-isopropyl acrylamide)/water solutions,” *Polymer*, vol. 38, no. 22, pp. 5539–5544, 1997.

[50] A. Lele, M. Hirve, M. Badiger, and R. Mashelkar, “Predictions of bound water content in poly (N-isopropylacrylamide) gel,” *Macromolecules*, vol. 30, pp. 157–159, 1997.

[51] T. Hino and J. Prausnitz, “Molecular thermodynamics for volume-change transitions in temperature-sensitive polymer gels,” *Polymer*, vol. 39, no. 14, pp. 3279–3283, 1998.

[52] Y. Bae, S. Lambert, D. Soane, and J. Prausnitz, “Cloud-point curves of polymer solutions from thermooptical measurements,” *Macromolecules*, vol. 24, pp. 4403–4407, 1991.

[53] E. E. Dormidontova, “Role of Competitive PEO−Water and Water−Water Hydrogen Bonding in Aqueous Solution PEO Behavior,” *Macromolecules*, vol. 35, no. 3, pp. 987–1001, Jan. 2002.

[54] G. Van Assche, B. Van Mele, T. Li, and E. Nies, “Adjacent UCST Phase Behavior in Aqueous Solutions of Poly(vinyl methyl ether): Detection of a Narrow Low Temperature UCST in the Lower Concentration Range,” *Macromolecules*, vol. 44, no. 4, pp. 993–998, Feb. 2011.

[55] K. Van Durme, G. Van Assche, E. Nies, and B. Van Mele, “Phase transformations in aqueous low molar mass poly(vinyl methyl ether) solutions: theoretical prediction and experimental validation of the peculiar

solvent melting line, bimodal LCST, and (adjacent) UCST miscibility gaps.," *The journal of physical chemistry. B*, vol. 111, no. 6, pp. 1288–95, Feb. 2007.

[56] M. B. Huglin and M. A. Radwan, "Unperturbed dimensions of a zwitterionic polymethacrylate," *Polymer International*, vol. 26, no. 2, pp. 97–104, Jan. 1991.

[57] X. Jia, D. Chen, and M. Jiang, "Preparation of PEO-b-P2VPH+-S2O8(2-) micelles in water and their reversible UCST and redox-responsive behavior.," *Chemical communications (Cambridge, England)*, no. 16, pp. 1736–8, Apr. 2006.

[58] R. Buscall, "The phase-separation behaviour of aqueous solutions of polyacrylic acid and its partial sodium salts in the presence of sodium chloride," *European Polymer Journal*, vol. 18, no. 11, pp. 967–974, 1982.

[59] S. Fujishige, K. Kubota, and I. Ando, "Phase transition of aqueous solutions of poly (N-isopropylacrylamide) and poly (N-isopropylmethacrylamide)," *The Journal of Physical Chemistry*, vol. 93, pp. 3311–3313, 1989.

[60] S. Ito, "Phase transition of aqueous solution of poly (N-alkylacrylamide) derivatives-effects of side chain structure," *Kobunshi Ronbunshu*, vol. 46, no. 7, pp. 437–443, 1989.

[61] C. Wu and S. Zhou, "Thermodynamically stable globule state of a single poly (N-isopropylacrylamide) chain in water," *Macromolecules*, vol. 28, pp. 5388–5390, 1995.

[62] M. Ward and T. Georgiou, “Thermoresponsive terpolymers based on methacrylate monomers: Effect of architecture and composition,” *Journal of Polymer Science Part A: …*, vol. 48, pp. 775–783, 2010.

[63] C. Kojima and K. Yoshimura, “Temperature-sensitive hyperbranched poly (glycidol) s with oligo (ethylene glycol) monoethers,” *Journal of Polymer …*, vol. 48, pp. 4047–4054, 2010.

[64] C. Wu and S. Zhou, “Laser light scattering study of the phase transition of poly (N-isopropylacrylamide) in water. 1. Single chain,” *Macromolecules*, vol. 28, pp. 8381–8387, 1995.

[65] C. Wu and X. Wang, “Globule-to-Coil Transition of a Single Homopolymer Chain in Solution,” *Physical Review Letters*, vol. 80, no. 18, pp. 4092–4094, May 1998.

[66] F. Ganachaud and M. Monteiro, “Molecular weight characterization of poly (N-isopropylacrylamide) prepared by living free-radical polymerization,” *Macromolecules*, vol. 33, pp. 6738–6745, 2000.

[67] C. Schilli, M. Lanzendörfer, and A. Müller, “Benzyl and cumyl dithiocarbamates as chain transfer agents in the RAFT polymerization of N-isopropylacrylamide. In situ FT-NIR and MALDI-TOF MS investigation,” *Macromolecules*, vol. 35, pp. 6819–6827, 2002.

[68] A. Convertine, N. Ayres, and C. Scales, “Facile, controlled, room-temperature RAFT polymerization of N-isopropylacrylamide,” *Biomacromolecules*, vol. 5, pp. 1177–1180, 2004.

[69] C. J. Hawker, a W. Bosman, and E. Harth, “New polymer synthesis by nitroxide mediated living radical polymerizations.,” *Chemical reviews*, vol. 101, no. 12, pp. 3661–88, Dec. 2001.

[70] M. Kamigaito, T. Ando, and M. Sawamoto, “Metal-catalyzed living radical polymerization.,” *Chemical reviews*, vol. 101, pp. 3689–746, Dec. 2001.

[71] Z. Tong, F. Zeng, X. Zheng, and T. Sato, “Inverse Molecular Weight Dependence of Cloud Points for Aqueous Poly(N -isopropylacrylamide) Solutions,” *Macromolecules*, vol. 32, no. 13, pp. 4488–4490, Jun. 1999.

[72] F. Winnik, H. Ringsdorf, and J. Venzmer, “Methanol-water as a co-nonsolvent system for poly (N-isopropylacrylamide),” *Macromolecules*, vol. 23, pp. 2415–2416, 1990.

[73] K. Otake, R. Karaki, and T. Ebina, “Pressure effects on the aggregation of poly (N-isopropylacrylamide) and poly (N-isopropylacrylamide-co-acrylic acid) in aqueous solutions,” *Macromolecules*, vol. 26, pp. 2194–2197, 1993.

[74] L. Lee and B. Cabane, “Effects of surfactants on thermally collapsed poly (N-isopropylacrylamide) macromolecules,” *Macromolecules*, vol. 30, pp. 6559–6566, 1997.

[75] H. Schlaad, C. Diehl, A. Gress, M. Meyer, a L. Demirel, Y. Nur, and A. Bertin, “Poly(2-oxazoline)s as Smart Bioinspired Polymers.,” *Macromolecular rapid communications*, vol. 31, no. 6, pp. 511–25, Mar. 2010.

[76] C. Diehl and H. Schlaad, “Thermo-responsive polyoxazolines with widely tuneable LCST.,” *Macromolecular Bioscience*, vol. 9, no. 2, pp. 157–161, 2009.

[77] K. Aoi, H. Suzuki, and M. Okada, “Architectural control of sugar-containing polymers by living polymerization: ring-opening polymerization of 2-oxazolines initiated with carbohydrate derivatives,” *Macromolecules*, vol. 25, pp. 7073–7075, 1992.

[78] W. Seeliger, E. Aufderhaar, W. Diepers, R. Feinauer, R. Nehring, W. Thier, and H. Hellmann, “Neuere Synthesen und Reaktionen cyclischer Imidsäureester,” *Angewandte Chemie*, vol. 78, no. 20, pp. 913–927, Oct. 1966.

[79] T. Kagiya, S. Narisawa, T. Maeda, and K. Fukui, “Ring-opening polymerization of 2-substituted 2-oxazolines,” *Journal of Polymer Science Part B: Polymer Letters*, vol. 4, no. 7, pp. 441–445, Jul. 1966.

[80] D. A. Tomalia and D. P. Sheetz, “Homopolymerization of 2-alkyl- and 2-aryl-2-oxazolines,” *Journal of Polymer Science Part A-1: Polymer Chemistry*, vol. 4, no. 9, pp. 2253–2265, Sep. 1966.

[81] T. G. Bassiri, A. Levy, and M. Litt, “Polymerization of cyclic imino ethers. I. Oxazolines,” *Journal of Polymer Science Part B: Polymer Letters*, vol. 5, no. 9, pp. 871–879, Sep. 1967.

[82] K. Aoi, “Polymerization of oxazolines,” *Progress in Polymer Science*, vol. 21, no. 1, pp. 151–208, 1996.

[83] B. M. Culbertson, “Cyclic imino ethers in step-growth polymerizations,” *Progress in Polymer Science*, vol. 27, no. 3, pp. 579–626, Apr. 2002.

[84] S. Kobayashi, M. Kaku, S. Sawada, and T. Saegusa, “Synthesis of poly (2-methyl-2-oxazoline) macromers,” *Polymer Bulletin*, vol. 13, pp. 447–451, 1985.

[85] T. Gant and A. Meyers, “The chemistry of 2-oxazolines (1985–present),” *Tetrahedron*, vol. 50, no. 8, pp. 2297–2360, 1994.

[86] S. Kobayashi and H. Uyama, “Polymerization of cyclic imino ethers: From its discovery to the present state of the art,” *Journal of Polymer Science Part A: Polymer Chemistry*, vol. 40, no. 2, pp. 192–209, Jan. 2002.

[87] R. BRINKHUIS and G. Hendrikus, “Hyperbranched Esteroxazolines Polymers,” 2003.

[88] R. Hoogenboom, “Poly(2-oxazoline)s: a polymer class with numerous potential applications.,” *Angewandte Chemie (International ed. in English)*, vol. 48, no. 43, pp. 7978–94, Jan. 2009.

[89] F. Wiesbrock, R. Hoogenboom, C. H. Abeln, and U. S. Schubert, “Single-Mode Microwave Ovens as New Reaction Devices: Accelerating the Living Polymerization of 2-Ethyl-2-Oxazoline,” *Macromolecular Rapid Communications*, vol. 25, no. 22, pp. 1895–1899, Nov. 2004.

[90] N. Adams and U. S. Schubert, “Poly(2-oxazolines) in biological and biomedical application contexts.,” *Advanced drug delivery reviews*, vol. 59, no. 15, pp. 1504–20, Dec. 2007.

[91] K. Kempe, M. Lobert, R. Hoogenboom, and U. S. Schubert, “Screening the synthesis of 2-substituted-2-oxazolines.,” *Journal of combinatorial chemistry*, vol. 11, no. 2, pp. 274–80, Mar. 2009.

[92] N. Hadjichristidis, M. Pitsikalis, S. Pispas, and H. Iatrou, “Polymers with complex architecture by living anionic polymerization.,” *Chemical reviews*, vol. 101, no. 12, pp. 3747–92, Dec. 2001.

[93] K. Matyjaszewski and J. Xia, “Atom Transfer Radical Polymerization,” *Chemical Reviews*, vol. 101, no. 9, pp. 2921–2990, Sep. 2001.

[94] G.-H. Hsiue, H.-Z. Chiang, C.-H. Wang, and T.-M. Juang, “Nonviral gene carriers based on diblock copolymers of poly(2-ethyl-2-oxazoline) and linear polyethylenimine.,” *Bioconjugate chemistry*, vol. 17, no. 3, pp. 781–6, 2006.

[95] G. V. N. Rathna, “Gelatin hydrogels: enhanced biocompatibility, drug release and cell viability.,” *Journal of materials science. Materials in medicine*, vol. 19, no. 6, pp. 2351–8, Jun. 2008.

[96] C. J. Waschinski and J. C. Tiller, “Poly(oxazoline)s with telechelic antimicrobial functions.,” *Biomacromolecules*, vol. 6, no. 1, pp. 235–43, 2005.

[97] R. Hoogenboom and H. Schlaad, “Bioinspired Poly(2-oxazoline)s,” *Polymers*, vol. 3, no. 4, pp. 467–488, Feb. 2011.

[98] J.-S. Park and K. Kataoka, “Comprehensive and Accurate Control of Thermosensitivity of Poly(2-alkyl-2-oxazoline)s via Well-Defined Gradient or

Random Copolymerization," *Macromolecules*, vol. 40, no. 10, pp. 3599–3609, May 2007.

[99] N. Morimoto, R. Obeid, S. Yamane, F. M. Winnik, and K. Akiyoshi, "Composite nanomaterials by self-assembly and controlled crystallization of poly(2-isopropyl-2-oxazoline)-grafted polysaccharides," *Soft Matter*, vol. 5, no. 8, p. 1597, 2009.

[100] H. Uyama and S. Kobayashi, "A novel thermo-sensitive polymer. Poly (2-isopropyl-2-oxazoline)," *Chemistry Letters*, pp. 1643–1646, 1992.

[101] J.-S. Park, Y. Akiyama, F. M. Winnik, and K. Kataoka, "Versatile Synthesis of End-Functionalized Thermosensitive Poly(2-isopropyl-2-oxazolines)," *Macromolecules*, vol. 37, no. 18, pp. 6786–6792, Sep. 2004.

[102] C. Diab, Y. Akiyama, and K. Kataoka, "Microcalorimetric Study of the Temperature-Induced Phase Separation in Aqueous Solutions of Poly (2-isopropyl-2-oxazolines)," *Macromolecules*, vol. 37, no. 7, pp. 2556–2562, 2004.

[103] R. Luxenhofer and R. Jordan, "Click Chemistry with Poly(2-oxazoline)s," *Macromolecules*, vol. 39, no. 10, pp. 3509–3516, May 2006.

[104] K. Kempe and M. Lobert, "Synthesis and characterization of a series of diverse poly (2-oxazoline) s," *Journal of Polymer …*, vol. 47, pp. 3829–3838, 2009.

[105] J.-S. Park and K. Kataoka, "Precise Control of Lower Critical Solution Temperature of Thermosensitive Poly(2-isopropyl-2-oxazoline) via Gradient

Copolymerization with 2-Ethyl-2-oxazoline as a Hydrophilic Comonomer," *Macromolecules*, vol. 39, no. 19, pp. 6622–6630, Sep. 2006.

[106] J. Zhao, R. Hoogenboom, G. Van Assche, and B. Van Mele, "Demixing and Remixing Kinetics of Poly(2-isopropyl-2-oxazoline) (PIPOZ) Aqueous Solutions Studied by Modulated Temperature Differential Scanning Calorimetry," *Macromolecules*, vol. 43, no. 16, pp. 6853–6860, Aug. 2010.

[107] R. Obeid, F. Tanaka, and F. M. Winnik, "Heat-Induced Phase Transition and Crystallization of Hydrophobically End-Capped Poly(2-isopropyl-2-oxazoline)s in Water," *Macromolecules*, vol. 42, no. 15, pp. 5818–5828, Aug. 2009.

[108] R. Hoogenboom, H. M. L. Thijs, M. J. H. C. Jochems, B. M. van Lankvelt, M. W. M. Fijten, and U. S. Schubert, "Tuning the LCST of poly(2-oxazoline)s by varying composition and molecular weight: alternatives to poly(N-isopropylacrylamide)?," *Chemical communications (Cambridge, England)*, pp. 5758–60, Nov. 2008.

[109] H. M. L. Lambermont-Thijs, H. P. C. Van Kuringen, J. P. W. Van Der Put, U. S. Schubert, and R. Hoogenboom, "Temperature Induced Solubility Transitions of Various Poly(2-oxazoline)s in Ethanol-Water Solvent Mixtures," *Polymers*, vol. 2, no. 3, pp. 188–199, Aug. 2010.

[110] H. M. L. Lambermont-Thijs, R. Hoogenboom, C.-A. Fustin, C. Bomal-D'Haese, J.-F. Gohy, and U. S. Schubert, "Solubility behavior of amphiphilic block and random copolymers based on 2-ethyl-2-oxazoline and 2-nonyl-2-

oxazoline in binary water–ethanol mixtures," *Journal of Polymer Science Part A: Polymer Chemistry*, vol. 47, no. 2, pp. 515–522, Jan. 2009.

[111] M. M. Bloksma, D. J. Bakker, C. Weber, R. Hoogenboom, and U. S. Schubert, "The Effect of Hofmeister Salts on the LCST Transition of Poly(2-oxazoline)s with Varying Hydrophilicity.," *Macromolecular rapid communications*, vol. 31, no. 8, pp. 724–8, Apr. 2010.

[112] S. Huber and R. Jordan, "Modulation of the lower critical solution temperature of 2-Alkyl-2-oxazoline copolymers," *Colloid and Polymer Science*, vol. 286, pp. 395–402, Nov. 2007.

[113] S. Huber, N. Hutter, and R. Jordan, "Effect of end group polarity upon the lower critical solution temperature of poly(2-isopropyl-2-oxazoline)," *Colloid and Polymer Science*, vol. 286, pp. 1653–1661, Oct. 2008.

[114] W. Kunz, J. Henle, and B. W. Ninham, "'Zur Lehre von der Wirkung der Salze' (about the science of the effect of salts): Franz Hofmeister's historical papers," *Current Opinion in Colloid & Interface Science*, vol. 9, no. 1–2, pp. 19–37, Aug. 2004.

[115] W. Kunz, P. Lo Nostro, and B. W. Ninham, "The present state of affairs with Hofmeister effects," *Current Opinion in Colloid & Interface Science*, vol. 9, no. 1–2, pp. 1–18, Aug. 2004.

[116] Y. Zhang and P. S. Cremer, "Interactions between macromolecules and ions: The Hofmeister series.," *Current opinion in chemical biology*, vol. 10, no. 6, pp. 658–63, Dec. 2006.

[117] M. Dragusin and D. Ionescu, “The influence of the hofmeister series of anions on the BSA-HYP complex interaction with artificial lipid membranes.,” *Romanian Journal of Biophysics*, vol. 19, no. 3, pp. 199–210, 2009.

[118] A. W. Omta, M. F. Kropman, S. Woutersen, and H. J. Bakker, “Negligible effect of ions on the hydrogen-bond structure in liquid water.,” *Science (New York, N.Y.)*, vol. 301, pp. 347–9, Jul. 2003.

[119] J. D. Smith, R. J. Saykally, and P. L. Geissler, “The effects of dissolved halide anions on hydrogen bonding in liquid water.,” *Journal of the American Chemical Society*, vol. 129, no. 45, pp. 13847–56, Nov. 2007.

[120] K. D. Collins, G. W. Neilson, and J. E. Enderby, “Ions in water: characterizing the forces that control chemical processes and biological structure.,” *Biophysical chemistry*, vol. 128, pp. 95–104, Jul. 2007.

[121] J. Song, R. Ryoo, and M. Jhon, “Anion binding properties of poly (vinylpyrrolidone) in aqueous solution studied by halide NMR spectroscopy,” *Macromolecules*, vol. 24, pp. 1727–1730, 1991.

[122] M. Boström, D. Williams, and B. Ninham, “Specific Ion Effects: Why DLVO Theory Fails for Biology and Colloid Systems,” *Physical Review Letters*, vol. 87, no. 16, p. 168103, Oct. 2001.

[123] M. Boström, D. R. M. Williams, and B. W. Ninham, “Specific ion effects: why the properties of lysozyme in salt solutions follow a Hofmeister series.,” *Biophysical journal*, vol. 85, no. 2, pp. 686–94, Aug. 2003.

[124] Y. Zhang, S. Furyk, D. E. Bergbreiter, and P. S. Cremer, “Specific ion effects on the water solubility of macromolecules: PNIPAM and the Hofmeister series.,” *Journal of the American Chemical Society*, vol. 127, no. 41, pp. 14505–10, Oct. 2005.

[125] J. Wang, D. Gan, L. a Lyon, and M. a El-Sayed, “Temperature-jump investigations of the kinetics of hydrogel nanoparticle volume phase transitions.,” *Journal of the American Chemical Society*, vol. 123, no. 45, pp. 11284–9, Nov. 2001.

[126] X. Wang, X. Qiu, and C. Wu, “Comparison of the Coil-to-Globule and the Globule-to-Coil Transitions of a Single Poly(N -isopropylacrylamide) Homopolymer Chain in Water,” *Macromolecules*, vol. 31, no. 9, pp. 2972–2976, May 1998.

[127] V. Aseyev, H. Tenhu, and F. Winnik, “Non-ionic thermoresponsive polymers in water,” *Advanced Polymer Science*, vol. 242, pp. 29–89, 2011.

[128] X. Qiu, M. Li, C. Kwan, and C. Wu, “Light-scattering study of the coil-to-globule transition of linear poly (N-isopropylacrylamide) ionomers in water,” *Journal of Polymer …*, vol. 36, pp. 1501–1506, 1998.

[129] H. Cheng, L. Shen, and C. Wu, “LLS and FTIR Studies on the Hysteresis in Association and Dissociation of Poly(N- isopropylacrylamide) Chains in Water,” *Macromolecules*, vol. 39, no. 6, pp. 2325–2329, Mar. 2006.

[130] G. R. Strobl, *The Physics of Polymers*. Berlin, Heidelberg: Springer Berlin Heidelberg, 1996.

[131] D. Chandler, “Interfaces and the driving force of hydrophobic assembly.,” *Nature*, vol. 437, pp. 640–647, Sep. 2005.

[132] C. Diehl, P. Černoch, I. Zenke, H. Runge, R. Pitschke, J. Hartmann, B. Tiersch, and H. Schlaad, “Mechanistic study of the phase separation/crystallization process of poly(2-isopropyl-2-oxazoline) in hot water,” *Soft Matter*, vol. 6, no. 16, p. 3784, 2010.

[133] C. Diehl, I. Dambowsky, R. Hoogenboom, and H. Schlaad, “Self-assembly of poly(2-alkyl-2-oxazoline)s by crystallization in ethanol-water mixtures below the upper critical solution temperature.,” *Macromolecular rapid communications*, vol. 32, no. 21, pp. 1753–8, Nov. 2011.

[134] A. Gress, B. Smarsly, and H. Schlaad, “Formation of Glycopolyamide Nanofibers,” *Macromolecular Rapid Communications*, vol. 29, no. 4, pp. 304–308, Feb. 2008.

[135] Y. Katsumoto, A. Tsuchiizu, X. Qiu, and F. M. Winnik, “Dissecting the Mechanism of the Heat-Induced Phase Separation and Crystallization of Poly(2-isopropyl-2-oxazoline) in Water through Vibrational Spectroscopy and Molecular Orbital Calculations,” *Macromolecules*, vol. 45, no. 8, pp. 3531–3541, Apr. 2012.

[136] G. D. Crevoisier, “Switchable Tackiness and Wettability of a Liquid Crystalline Polymer,” *Science*, vol. 285, pp. 1246–1249, Aug. 1999.

[137] M. Callies and D. Quéré, “On water repellency,” *Soft Matter*, vol. 1, no. 1, p. 55, 2005.

[138] T. P. Russell, “Surface-responsive materials.,” *Science (New York, N.Y.)*, vol. 297, no. 5583, pp. 964–7, Aug. 2002.

[139] S. Milner, T. Witten, and M. Cates, “Theory of the grafted polymer brush,” *Macromolecules*, vol. 21, pp. 2610–2619, 1988.

[140] J. a. Howarter and J. P. Youngblood, “Self-Cleaning and Anti-Fog Surfaces via Stimuli-Responsive Polymer Brushes,” *Advanced Materials*, vol. 19, no. 22, pp. 3838–3843, Nov. 2007.

[141] Y. G. Takei, T. Aoki, K. Sanui, N. Ogata, Y. Sakurai, and T. Okano, “Dynamic Contact Angle Measurement of Temperature-Responsive Surface Properties for Poly(N-isopropylacrylamide) Grafted Surfaces,” *Macromolecules*, vol. 27, no. 21, pp. 6163–6166, Oct. 1994.

[142] T. Yakushiji, K. Sakai, A. Kikuchi, T. Aoyagi, Y. Sakurai, and T. Okano, “Effects of Cross-Linked Structure on Temperature-Responsive Hydrophobic Interaction of Poly(N -isopropylacrylamide) Hydrogel-Modified Surfaces with Steroids,” *Analytical Chemistry*, vol. 71, no. 6, pp. 1125–1130, Mar. 1999.

[143] J. E. Chung, M. Yokoyama, and T. Okano, “Inner core segment design for drug delivery control of thermo-responsive polymeric micelles.,” *Journal of controlled release : official journal of the Controlled Release Society*, vol. 65, no. 1–2, pp. 93–103, Mar. 2000.

[144] I. Dimitrov, B. Trzebicka, A. H. E. Müller, A. Dworak, and C. B. Tsvetanov, “Thermosensitive water-soluble copolymers with doubly responsive

reversibly interacting entities," *Progress in Polymer Science*, vol. 32, no. 11, pp. 1275–1343, Nov. 2007.

[145] Y. Pan, R. Wesley, and R. Luginbuhl, "Plasma polymerized N-isopropylacrylamide: synthesis and characterization of a smart thermally responsive coating," *Biomacromolecules*, vol. 2, pp. 32–36, 2001.

[146] Malvern Instruments, *Zetasizer Nano Series User Manual*, no. 2. 2004.

[147] A. Einstein, *Investigations on the Theory of the Brownian Movement*. Dover Publications, 1956.

[148] P. C. Hiemenz and R. Rajagopalan, *Principles of colloid and surface chemistry*, vol. 70, no. 2. Marcel Dekker, 1997.

[149] Anton Paar, *Automated Viscosimeter Instruction Manual*. 2008.

[150] K. M. Ravikumar and W. Hwang, "Region-specific role of water in collagen unwinding and assembly.," *Proteins*, vol. 72, no. 4, pp. 1320–32, Sep. 2008.

[151] C. A. Naumann, C. F. Brooks, G. G. Fuller, T. Lehmann, J. Ru, W. Knoll, P. Kuhn, O. Nuyken, and C. W. Frank, "Two-Dimensional Physical Networks of Lipopolymers at the Air / Water Interface : Correlation of Molecular Structure and Surface Rheological Behavior," *Langmuir*, vol. 17, no. 9, pp. 2801–2806, 2001.

[152] Nanomagnetics Instruments, *Multimode Atomic Force Microscope User Manual*. 2007.

[153] T. Young, “An Essay on the Cohesion of Fluids,” *Philosophical Transactions of the Royal Society of London*, vol. 95, no. 65–87, 1805.

[154] E. Kokufuta, Y. Zhang, T. Tanaka, and A. Mamada, “Effects of surfactants on the phase transition of poly (N-isopropylacrylamide) gel,” *Macromolecules*, vol. 26, pp. 1053–1059, 1993.

[155] S. Beltran, J. Baker, and H. Hooper, “Swelling equilibria for weakly ionizable, temperature-sensitive hydrogels,” *Macromolecules*, vol. 24, pp. 549–551, 1991.

[156] H. Schild and D. Tirrell, “Sodium 2-(N-dodecylamino) naphthalene-6-sulfonate as a probe of polymer-surfactant interaction,” *Langmuir*, no. 6, pp. 1676–1679, 1990.

[157] H. I. Naozumi Wada, Yoshinori Kajima, Yasuhiko Yagi and S. Saito, “Effect of surfactant on the phase transition of n-alkylacrylmide gels,” *Langmuir*, vol. 9, pp. 46–49, 1993.

[158] H. Ringsdorf, J. Venzmer, and F. M. Winnik, “Fluorescence Studies of Hydrophobically Modified,” *Macromolecules*, vol. 24, no. 7, pp. 1678–1686, 1991.

[159] Y. Zhang, S. Furyk, L. B. Sagle, Y. Cho, D. E. Bergbreiter, and P. S. Cremer, “Effects of Hofmeister Anions on the LCST of PNIPAM as a Function of Molecular Weight.,” *The journal of physical chemistry. C, Nanomaterials and interfaces*, vol. 111, no. 25, pp. 8916–8924, Jan. 2007.

[160] M. Boström, D. Williams, and B. Ninham, “Surface tension of electrolytes: specific ion effects explained by dispersion forces,” *Langmuir*, vol. 17, pp. 4475–4478, 2001.

[161] P. Tatar Güner and a L. Demirel, “Effect of anions on the cloud point temperature of aqueous poly(2-ethyl-2-oxazoline) solutions.,” *The journal of physical chemistry. B*, vol. 116, no. 49, pp. 14510–4, Dec. 2012.

[162] L. C. Palmer and S. I. Stupp, “Molecular self-assembly into one-dimensional nanostructures.,” *Accounts of chemical research*, vol. 41, no. 12, pp. 1674–84, Dec. 2008.

[163] A. Shpigelman and I. Portnaya, “Saccharide structure effects on poly N-isopropylacrylamide phase transition in aqueous media; Reflections on protein stability,” *Journal of Polymer …*, pp. 2307–2318, 2008.

[164] S. Zhang, “Fabrication of novel biomaterials through molecular self-assembly.,” *Nature Biotechnology*, vol. 21, no. 10, pp. 1171–1178, 2003.

[165] M. Muthukumar, C. K. Ober, and E. L. Thomas, “Competing interactions and levels of ordering in self-organizing polymeric materials,” *Science*, vol. 277, no. 5330, pp. 1225–1232, 1997.

[166] P. T. Güner, A. Mikó, F. F. Schweinberger, and a. L. Demirel, “Self-assembled poly(2-ethyl-2-oxazoline) fibers in aqueous solutions,” *Polymer Chemistry*, vol. 3, no. 2, p. 322, 2012.

[167] L. Mandelkern, “Crystallization kinetics of homopolymers: overall crystallization: a review,” *Biophysical Chemistry*, vol. 112, no. 2–3, pp. 109–116, Dec. 2004.

[168] L. F. Filobelo, O. Galkin, and P. G. Vekilov, “Spinodal for the solution-to-crystal phase transformation.,” *The Journal of chemical physics*, vol. 123, no. 1, p. 014904, 2005.

[169] V. Causin, C. Marega, A. Marigo, L. Valentini, and J. M. Kenny, “Crystallization and Melting Behavior of Poly(3-butylthiophene), Poly(3-octylthiophene), and Poly(3-dodecylthiophene),” *Macromolecules*, vol. 38, no. 2, pp. 409–415, Jan. 2005.

[170] J. M. G. Cowie, Z. Haq, I. J. McEwen, and J. Velićkovič, “Poly(alkyl itaconates): 8. Observations of dual glass transitions and crystallinity in the dialkyl ester series diheptyl to di-eicosyl,” *Polymer*, vol. 22, no. 3, pp. 327–332, 1981.

[171] K. W. McCreight, J. J. Ge, M. Guo, I. Mann, F. Li, Z. Shen, X. Jin, F. W. Harris, and S. Z. D. Cheng, “Phase structures and transition behaviors in polymers containing rigid rodlike backbones with flexible side chains. V. Methylene side-chain effects on structure and molecular motion in a series of polyimides,” *Journal of Polymer Science Part B: Polymer Physics*, vol. 37, no. 14, pp. 1633–1646, Jul. 1999.

[172] X. He, J. Wu, G. Huang, and X. Wang, “Effect of Alkyl Side Chain Length on Relaxation Behaviors in Poly(n-alkyl Acrylates) and Poly(n-alkyl

Methacrylates),” *Journal of Macromolecular Science, Part B*, vol. 50, no. 1, pp. 188–200, Nov. 2010.

[173] J. Doye and D. Frenkel, “Kinetic Monte Carlo simulations of the growth of polymer crystals,” *The Journal of chemical physics*, vol. 110, pp. 2692–2702, 1999.

[174] R. J. Ciora and J. H. Magill, “A Study of the Isothermal Crystallization Kinetics of Polyphosphazene Polymers. 2. Poly[bis(trifluoroethoxy) phosphazene],” *Macromolecules*, vol. 23, pp. 2350–2359, 1990.

[175] G. Madras and B. J. McCoy, “Temperature effects on the transition from nucleation and growth to Ostwald ripening,” *Chemical Engineering Science*, vol. 59, no. 13, pp. 2753–2765, Jul. 2004.

[176] W. Xie, J. Pu, A. MacKerell, and J. Gao, “Development of a polarizable intermolecular potential function (PIPF) for liquid amides and alkanes,” *Journal of chemical theory and …*, vol. 3, pp. 1878–1889, 2007.

[177] P. Kurt, L. Wood, D. Ohman, and K. Wynne, “Highly effective contact antimicrobial surfaces via polymer surface modifiers,” *Langmuir*, vol. 23, pp. 4719–4723, 2007.

[178] R. Wang, K. Hashimoto, and A. Fujishima, “Light-induced amphiphilic surfaces,” *Nature*, vol. 388, pp. 431–432, 1997.

[179] H. Erbil, A. Demirel, Y. Avcı, and O. Mert, “Transformation of a simple plastic into a superhydrophobic surface,” *Science*, vol. 299, pp. 1377–1380, 2003.

[180] X. Feng and L. Jiang, “Design and creation of superwetting/antiwetting surfaces,” *Advanced Materials*, vol. 18, pp. 3063–3078, 2006.

[181] G. Kumar and K. N. Prabhu, “Review of non-reactive and reactive wetting of liquids on surfaces.,” *Advances in colloid and interface science*, vol. 133, no. 2, pp. 61–89, Jun. 2007.

[182] C. Feng, Y. Zhang, J. Jin, Y. Song, and L. Xie, “Reversible wettability of photoresponsive fluorine-containing azobenzene polymer in Langmuir-Blodgett films,” *Langmuir*, vol. 17, no. 15, pp. 4593–4597, 2001.

[183] S. Abbott, J. Ralston, G. Reynolds, and R. Hayes, “Reversible Wettability of Photoresponsive Pyrimidine-Coated Surfaces,” *Langmuir*, vol. 15, no. 26, pp. 8923–8928, Dec. 1999.

[184] J. Lahann, S. Mitragotri, T.-N. Tran, H. Kaido, J. Sundaram, I. S. Choi, S. Hoffer, G. a Somorjai, and R. Langer, “A reversibly switching surface.,” *Science (New York, N.Y.)*, vol. 299, no. 5605, pp. 371–4, Jan. 2003.

[185] S. H. Anastasiadis, H. Retsos, S. Pispas, N. Hadjichristidis, and S. Neophytides, “Smart Polymer Surfaces,” *Macromolecules*, vol. 36, no. 6, pp. 1994–1999, Mar. 2003.

[186] D. Jones and J. Smith, “micropatterned thermoresponsive polymer brushes: AFM investigations of poly (N-isopropylacrylamide) brushes prepared by surface-initiated polymerizations,” *Advanced …*, vol. 14, no. 16, pp. 1130–1134, 2002.

[187] T. N. Kim, Q. L. Feng, J. O. Kim, J. Wu, H. Wang, G. C. Chen, and F. Z. Cui, “Antimicrobial effects of metal ions (Ag+, Cu2+, Zn2+) in hydroxyapatite.,” *Journal of materials science. Materials in medicine*, vol. 9, no. 3, pp. 129–34, Mar. 1998.

[188] H. Jeon, S. Yi, and S. Oh, “Preparation and antibacterial effects of Ag–SiO 2 thin films by sol–gel method,” *Biomaterials*, vol. 24, pp. 4921–4928, 2003.

[189] G. Zhao and S. E. Stevens, “Multiple parameters for the comprehensive evaluation of the susceptibility of Escherichia coli to the silver ion.,” *Biometals : an international journal on the role of metal ions in biology, biochemistry, and medicine*, vol. 11, no. 1, pp. 27–32, Jan. 1998.

[190] I. Sondi, D. V Goia, and E. Matijević, “Preparation of highly concentrated stable dispersions of uniform silver nanoparticles,” *Journal of Colloid and Interface Science*, vol. 260, no. 1, pp. 75–81, Apr. 2003.

[191] I. Sondi and B. Salopek-Sondi, “Silver nanoparticles as antimicrobial agent: a case study on E. coli as a model for Gram-negative bacteria.,” *Journal of colloid and interface science*, vol. 275, no. 1, pp. 177–82, Jul. 2004.

[192] C. Aymonier and U. Schlotterbeck, “Hybrids of silver nanoparticles with amphiphilic hyperbranched macromolecules exhibiting antimicrobial properties,” *Chemical …*, pp. 3018–3019, 2002.

[193] J. Schierholz, L. Lucas, A. Rump, and G. Pulverer, “Efficacy of silver-coated medical devices,” *Journal of Hospital Infection*, vol. 40, pp. 257–262, 1998.

[194] U. Schubert, N. Huesing, and A. Lorenz, “Hybrid inorganic-organic materials by sol-gel processing of organofunctional metal alkoxides,” *Chemistry of materials*, vol. 7, pp. 2010–2027, 1995.

[195] S. Yano, K. Iwata, and K. Kurita, “Physical properties and structure of organic-inorganic hybrid materials produced by sol-gel process,” *Materials Science and Engineering: C*, vol. 6, no. 2–3, pp. 75–90, Nov. 1998.

[196] Z. Grubisic-Gallot, F. Schosseler, P. Lixon, and B. Cabane, “Size distribution of polymers in sol-gel condensation,” *Macromolecules*, vol. 25, no. 14, pp. 3733–3738, Jul. 1992.

[197] H. Schmidt and G. Jonschker, “The sol-gel process as a basic technology for nanoparticle-dispersed inorganic-organic composites,” *Journal of Sol-Gel Science and Technology*, vol. 19, pp. 39–51, 2000.

[198] Y. Chujo, E. Ihara, S. Kure, K. Suzuki, and T. Saegusa, “Block copolymer of 2-methyl-2-oxazoline with silica gel an organic-inorganic hybrid polymer,” *Makromolekulare Chemie. Macromolecular Symposia*, vol. 42–43, no. 1, pp. 303–312, Mar. 1991.

[199] T. Ogoshi and Y. Chujo, “Synthesis of colloidal polyoxazoline/silica hybrids prepared in an aqueous solution,” *Polymer*, vol. 47, no. 11, pp. 4036–4041, May 2006.

[200] K.-M. Kim, D.-K. Keum, and Y. Chujo, “Organic−Inorganic Polymer Hybrids Using Polyoxazoline Initiated by Functionalized Silsesquioxane,” *Macromolecules*, vol. 36, no. 3, pp. 867–875, Feb. 2003.

[201] Y. Chujo, E. Ihara, S. Kure, and T. Saegusa, “Synthesis of triethoxysilyl-terminated polyoxazolines and their cohydrolysis polymerization with tetraethoxysilane,” *Macromolecules*, vol. 26, no. 7, pp. 5681–5686, 1993.

[202] C. Alexis, C. Charnay, V. Lapinte, and J. Robin, “Hydrophilization by coating of silylated polyoxazoline using sol–gel process,” *Progress in Organic Coatings*, vol. 76, pp. 519–524, 2012.

[203] N. T. Binh, D. T. Ly, N. T. Hue, and L. T. Quyen, “Silver nanoparticles prepared by laser ablation and their optical characteristics,” *Journal of Science, Mathematics - Physics*, vol. 24, pp. 1–5, 2008.

[204] G. Volet and C. Amiel, “Polyoxazoline adsorption on silica nanoparticles mediated by host-guest interactions.,” *Colloids and surfaces. B, Biointerfaces*, vol. 91, pp. 269–73, Mar. 2012.

[205] P. Tatar, N. Kiraz, M. Asiltürk, F. Sayılkan, H. Sayılkan, and E. Arpaç, “Antibacterial Thin Films on Glass Substrate by Sol–Gel Process,” *Journal of Inorganic and Organometallic Polymers and Materials*, vol. 17, no. 3, pp. 525–533, Mar. 2007.

VITA

EDUCATION

Ph.D. Koç University, Istanbul, Turkey
PhD in Materials Science and Engineering Program (August, 2013)
Thesis title: Physico-chemical Characterization and Self-assembly of Poly(2-ethyl-2-oxazoline)s in Aqueous Solutions

M.S. Akdeniz University, Antalya, Turkey
MS in Chemistry (June, 2007)
Thesis title: Antibacterial Coatings

B.S. Hacettepe University, Ankara, Turkey
Chemistry (June, 2003)

RESEARCH EXPERIENCE

Graduate research and teaching assistant (September, 2008 – present)

- Study on the effect of a series of sodium salts on cloud point temperature (T_c) of aqueous PEOX solutions

- Investigation on the self-assembly of PEOX into crystalline nanofibers both above and below T_c.

- Isothermal crystallization studies on series of poly(2-alkyl-2-oxazoline)s in bulk.

- Synthesis of stable silver nano-particle colloidal solutions

- Fabrication of anti-bacterial, thermoresponsive, and durable films on glass and silicon wafer substrates

- Participation in industrial project titled “Anti-fogging, anti-microbial, and easy-to-clean functional surfaces” as a research assistant, funded by Arçelik A.Ş. and The Scientific and Technological Research Council of Turkey (TUBITAK).

Graduate research and teaching assistant (September, 2004 – June, 2007)

- Synthesis of the silver-N-(2-aminoethyl)-3-aminopropyltrimethoxysilane complexes.

- Studies on hydrothermal synthesis of high temperature resistant Ag_3PO_4 and nano-sized anatase TiO_2.

- Production of organofunctional silane based thin films on glass substrates via sol-gel method with addition of silver complexes and nano-sized anatase TiO_2 particles.

- Manufacture of Ag_3PO_4 containing antimicrobial ceramics.

- Investigation of antibacterial activity of coatings and ceramics against *E. coli*, and *S. aureus*.

- Participation in industrial project titled “Synthesis of transparent hydrophobic coatings and their applications on glass substrates” as a research assistant, funded by Şişe Cam A.Ş. and TUBITAK.

- Participation in industrial project titled “Coating of polyvinylchloride surfaces” as a research assistant, funded by Adopen A.Ş. and TUBITAK.

- Participation in industrial project titled “Antibacterial coatings” as a research assistant, funded by Serel Seramik A.Ş. and T.R. Prime Ministry State Planning Organization (DPT).

- Participation in industrial project titled “Photocatalytic transparent coatings which include nano-TiO2” as a research assistant, funded by Şişe Cam A.Ş. and DPT.

PEER REVIEWED RESEARCH PUBLICATIONS

- Demirel A.L., **Tatar-Guner P.**, Schlaad H., Schubert U.S., Hoogenboom R., Revisiting the Crystallization of Poly(2-alkyl-2-oxazoline)s, submitted, **2013**.

- **Tatar-Guner P.**, Demirel A.L., Effect of Anions on the Cloud Point Temperature of Aqueous Poly(2-ethyl-2-oxazoline) Solutions, *Journal of Physical Chemistry B*, **2012**, 14510.

- Ates S., **Tatar-Guner P.,** Yagci Y., Demirel A.L., Synthesis and Characterization of polysulfone-g-poly(2-alkyl-2-oxazoline)s, *Designed Monomers and Polymers*, **2012**, 1.

- Yılmaz G., Kumbaracı V., Talinli N., **Tatar P.**, Demirel A.L., Yagci Y., Photoinduced Grafting of Polystyrene onto Silica Particles by Ketene Chemistry, *Journal of Polymer Science Part A: Polymer Chemistry*, **2012**, 2517.

- **Tatar-Guner P**, Miko A., Schweinberger F.F., Demirel A.L., Self-assembled poly(2-ethyl-2-oxazoline) fibers in aqueous solutions, Polymer Chemistry, **2012**, 322.

- Tasdelen M.A., Beyazit S., Gunes D., Bicak N., **Tatar P.**, Demirel A.L., Yagci Y., Poly(p-phenylene-methylene)-Based Block Copolymers by Mechanistic Transformation, *Journal of Polymer Science Part A: Polymer Chemistry*, **2011**, 4021.

- Sayilkan F., Asilturk M., **Tatar P.**, Kiraz N., Sener S., Arpac E., Sayilkan H., Photocatalytic Performance of Sn-doped TiO2 nanostructured thin films for photocatalytic degradation of malachite green dye under UV and Vis-Lights, *Materials Research Bulletin*, **2008**, 127.

- **Tatar P.**, Kiraz N., Asilturk M, Sayilkan F., Sayilkan H., Arpac E., Antibacterial thin films on glass substrate by sol-gel process, *Journal of inorganic and organometallic polymers and materials*, **2007**, 525.

- Arpac E., Sayilkan F., Asilturk M., **Tatar P.**, Kiraz N., Sayilkan H., Photocatalytic performance of Sn-doped and undoped TiO_2 nanostructured thin films under UV and VIS-lights, *Journal of Hazardous Materials*, **2007**, 69.

- Sayilkan F., Asilturk M., **Tatar P.**, Kiraz N., Arpac E., Sayilkan H., Photocatalytic performance of Sn-doped TiO_2 nanostructured mono and double layer thin films for malachite green dye degradation under UV and VIS-lights, *Journal of Hazardous Materials*, **2007**, 140.

- Sayilkan F., Asilturk M., **Tatar P.**, Kiraz N., Arpac E., Sayilkan H., Preparation of re-usable photocatalytic filter for degradation of Malachite green dye under UV and VIS-irradiation, *Journal of Hazardous Materials*, **2007**, 735.

CONFERENCE PRESENTATIONS

- *American Chemical Society Spring 2012 National Meeting & Exposition, San Diego CA/ USA **2012**, Oral Presentation*
  "Formation of Poly(2-ethyl-2-oxazoline) Fibers in Aqueous Solutions"

- *The 7th International Syposium: Molecular Mobility and Order in Polymer Systems, St. Petersburg/RUSSIA **2011**, Oral Presentation*
  "Self-organization of poly(2-ethyl-2-oxazoline)s in Aqueous Solutions"

- *Summer School on Nanoscale Science of Biological Interfaces, University of California Santa Barbara CA/USA 2010, Poster Presentation*
  "Self-assembly of poly(2-alkyl-2-oxazoline)s in Aqueous Solutions"

- *16th Statistical Physics Days, Istanbul/TURKEY 2009, Oral Presentation*
  "Self-organization of poly(2-alkyl-2-oxazoline)s in Aqueous Solutions"

- *21st National Chemistry Congress, Malatya/TURKEY 2007, Poster Presentation*
  "Synthesis Characterization and Determination of Antibacterial Activity of Ceramics"

- *21st National Chemistry Congress, Malatya/TURKEY 2007, Poster Presentation*
  "Cleaning of pool water via filters coated by nano-Sn doped TiO2; determination of Antibacterial and photpcatalytic activity of filters"

- 6th International Paint, Varnish, Ink and Auxiliary Products Industry Congress & Exhibition, Istanbul/TURKEY 2006, Oral Presentation
  "Sol-gel Antibacterial Coatings"

TEACHING EXPERIENCE

- General Chemistry I & II Laboratory Instructor, Fall 2012 and Spring 2013

- General Chemistry I, Problem Session Teaching Assistant, and Thermomechanical Properties of Materials, Homework and Quiz evaluation assistant, Physical Chemistry II, Laboratory assistant, Fall 2011 and Spring 2012, Koc University

- Physical Chemistry I, Problem Session Teaching Assistant, and Thermomechanical Properties of Materials, Homework and Quiz evaluation assistant, Fall 2010 and Spring 2011, Koc University

- Physical Chemistry I & II, Problem Session Teaching Assistant, Fall 2009 and Spring 2010, Koc University

- Physical Chemistry I & II, Problem Session Teaching Assistant, Fall 2008 and Spring 2009, Koc University

- Inorganic Chemistry I & II, Organic Chemistry I & II Laboratory Assistant, Inorganic Chemistry I & II, PS session Teaching Assistant, Fall 2006 and Spring 2007, Akdeniz University

- Inorganic Chemistry I & II, Analytical Chemistry I & II, Laboratory Assistant Inorganic Chemistry I & II PS session Teaching Assistant, Fall 2005 and Spring 2006, Akdeniz University

- General Chemistry I & II, Analytical Chemistry I & II, Inorganic Chemistry I & II, Laboratory Assistant, Fall 2004 and Spring 2005, Akdeniz University

- General Chemistry I & II, Inorganic Chemistry I & II, Laboratory Assistant, Fall 2003 and Spring 2004, Akdeniz University